E.O. Paton Electric Welding Institute of the National Academy of Sciences of Ukraine

International Scientific-Technical and Production Journal

The Paton WELDING JOURNAL

June 2013
No.6

Published since 2000

English translation of the monthly «Avtomaticheskaya Svarka» (Automatic Welding) journal published in Russian since 1948

Founders
E.O. Paton Electric Welding Institute
of the NAS of Ukraine,
International Association «Welding»

Publisher
International Association «Welding»

Translators:
A.A.Fomin, O.S.Kurochko,
I.N.Kutianova, T.K.Vasilenko
Editor
N.A.Dmitrieva
Electron galley
D.I.Sereda, T.Yu.Snegiryova

Address
E.O. Paton Electric Welding Institute,
International Association «Welding»
11, Bozhenko Str., 03680, Kyiv, Ukraine
Tel.: (38044) 200 60 16, 200 82 77
Fax: (38044) 200 82 77, 200 81 45
E-mail: journal@paton.kiev.ua
www.patonpublishinghouse.com
URL: www.rucont.ru

State Registration Certificate
KV 4790 of 09.01.2001
ISSN 0957-798X

Subscriptions
$348, 12 issues per year,
air postage and packaging included.
Back issues available.

CONTENTS

«The Paton Welding Journal» abstracted and indexed in Ukrainian refereed journal «Source», RJ VINITI «Welding» (Russia), INSPEC, «Welding Abstracts», ProQuest (UK), EBSCO Research Database, CSA Materials Research Database with METADEX (USA), Questel Orbit Inc. Weldasearch Select (France); presented in Russian Science Citation Index & «Google Scholar»; abstracted in «Welding Institute Bulletin» (Poland) & «Rivista Italiana della Saldatura» (Italy); covered in the review of the Japanese journals «Journal of Light Metal Welding», «Journal of the Japan Welding Society», «Quarterly Journal of the Japan Welding Society», «Journal of Japan Institute of Metals», «Welding Technology».

EFFECT OF NON-METALLIC INCLUSIONS ON FORMATION OF STRUCTURE OF THE WELD METAL IN HIGH-STRENGTH LOW-ALLOY STEELS

V.V. GOLOVKO and **I.K. POKHODNYA**
E.O. Paton Electric Welding Institute, NASU,
11 Bozhenko Str., 03680, Kiev, Ukraine. E-mail: office@paton.kiev.ua

Investigated was the possibility of using the oxide metallurgy approaches providing for control of the amount, distribution and morphology of the inclusions in metal melts, which affect conditions for formation of microstructure of the weld metal. It was shown that increase in the content of the fine-grained secondary phase can be achieved by varying the content of the fine carbide phase in structure of the weld metal. A high density of distribution of the 0.3–1.0 μm inclusions containing titanium or zirconium oxides leads to formation of the bainitic structure, whereas the decreased content of carbon in metal and narrowing of the range of bainitic transformations limit the probability of formation of the upper bainite microstructure. It was found that to provide the microstructure characterised by a combination of high values of strength, ductility and toughness it is necessary to form inclusions of a certain composition, size and distribution density in the weld metal. This can be achieved by using the oxide metallurgy methods, which provide for addition of a certain amount of refractory inclusions to the weld pool, limitation of its oxygen content and selection of the deoxidation system, as well as of the required temperature range of intermediate transformations based on the TTT-diagrams and welding thermal cycle. 12 Ref., 9 Tables, 13 Figures.

Keywords: *welding, low-alloy steels, oxide metallurgy, welds, non-metallic inclusions, alloying, microstructure, mechanical properties*

High-strength low-alloy (HSLA) steels have been receiving an increasingly wider acceptance in fabrication of metal structures during the last decades. Along with expansion of the scopes of consumption of this class of steels, we can note increasing requirements to the level of their mechanical properties, brittle fracture resistance and cost effectiveness. For example, a growing consumption of the natural gas by developed countries dictates increase in the working pressure of a transported gas from 55–75 to 100 or more, the growth of which in pipelines made from steels of strength category K60 (X70) leads to increase in metal intensity and specific costs. This is accompanied by increase in the level of requirements to operating safety, reliability and service life of pipelines, which in turn requires increase in impact toughness and brittle fracture resistance, as well as improvement of weldability of the said steels.

Transition from steels of strength categories K60 (X70) to steels K65 (X80) and stronger required revision of the principles of alloying and microalloying them from the metal science standpoints. Providing the required level of strength of sheet and plate products in a combination with other most important indices of mechanical properties ($\delta_5 > 22$ %, $KCV > 130$ J/cm^2, and content of tough components in fractures of drop-weight test specimens > 95 % at –20 °C) is possible only in transition from the ferritic-pearlitic structure to the other structural state of a material, i.e. steels with the fine ferritic-bainitic structure [1, 2].

To ensure the required level of performance of welded metal structures, chemical and structural compositions, as well as mechanical properties of the weld metal should correspond to those of the base metal. The problem of formation of the weld metal with the ferritic-bainitic structure can be solved by using the possibilities offered by oxide metallurgy [3, 4].

The necessary condition for formation of the high-toughness fine structure of the type of acicular ferrite is the presence of a certain amount of non-metallic inclusions (NMI) in the weld metal [5, 6]. It should be noted that inclusions up to 1 μm in size, which contain titanium compounds, are most efficient in this respect [7–9].

The use of the oxide metallurgy approaches allows affecting the processes of initiation and growth of structural components by varying the composition, content and sizes of NMI [10, 11]. Investigation of the effect of NMI on the secondary microstructure was carried out on specimens of the weld metal of low-alloy steel of strength category K60 alloyed with carbon, manganese and silicon, with an adjustable content of oxygen and microalloyed with titanium. The welds were

Table 1. Chemical composition of metal of the investigated welds, wt.%

Weld designation	C	Si	Mn	Ni	Mo	Ti	Cr	Al	S	P	O
Ti-1	0.078	0.437	0.43	0.22	0.19	0.027	0.24	0.012	0.008	0.009	0.101
Ti-2	0.073	0.227	0.48	0.24	0.19	0.084	0.25	0.019	0.007	0.010	0.054
Ti-3	0.075	0.181	0.54	0.23	0.19	0.127	0.25	0.028	0.006	0.009	0.032
Ti-4	0.125	0.557	0.47	0.22	0.17	0.130	0.23	0.029	0.011	0.008	0.102
Ti-5	0.083	0.389	0.51	0.24	0.18	0.244	0.26	0.039	0.008	0.010	0.030
Ti-6	0.118	0.217	0.52	0.21	0.16	0.297	0.22	0.054	0.007	0.008	0.022

Table 2. Mechanical properties of metal of the investigated welds

Weld designation	σ_t, MPa	$\sigma_{0.2}$, MPa	δ_5, %	ψ, %	KCV, J/cm^2, at T, °C		
					20	0	−20
Ti-1	597.5	437.7	23.15	58.8	62.4	42.9	23.7
Ti-2	603.5	443.4	23.5	67.7	64.3	40.8	19.0
Ti-3	665.9	527.2	18.8	66.9	43.3	20.9	13.8
Ti-4	807.3	664.2	17.6	66.0	22.2	16.7	13.0
Ti-5	769.0	673.3	17.5	68.9	28.5	13.8	16.0
Ti-6	634.0	488.9	20.6	59.8	49.6	18.3	13.9

made by the method of submerged-arc welding (welding heat input — about 33.4 kJ/cm). In this case the main part of oxygen transfers to the weld pool through the slag phase, as the distribution of oxygen between the slag and pool is determined by a ratio of the activity of oxygen in the slag (a_O) to the activity of oxygen in the weld pool metal [a_O]. Considering that the content of oxygen in metal is low and the [a_O] value is close to one, the transition of oxygen depends only on (a_O).

Chemical composition of metal of the investigated welds is given in Table 1, and its mechanical properties are given in Table 2.

Results of dilatometric investigations of the weld metal conducted by using the «Gleeble» high-speed dilatometer are shown in Figure 1. Composition of the microstructure components and their sizes were determined by using optical microscope «Neophot 30» (Table 3).

It was found that growth of the content of titanium in the weld metal is accompanied by increase in temperature of the finish of bainitic transformation B_f and decrease in the $\gamma \rightarrow \alpha$ transformation temperature range. Proportion of the titanium and oxygen in the weld metal affects the balance between the content of the inclusions above 1 μm in size consisting primarily of oxides (Figure 2)*, and that of the inclusions less than 1 μm in size consisting of carbides (Figure 3). Increase in the content of fine carbides leads to increase in the content of upper bainite in the secondary structure of the weld metal (see Table 3). This causes increase in strength and decrease in impact toughness of the weld metal (see Table 2) due to an increased brittleness of the given structural component.

Alloying of the weld metal with titanium allows the size of the ferritic grains to be substan-

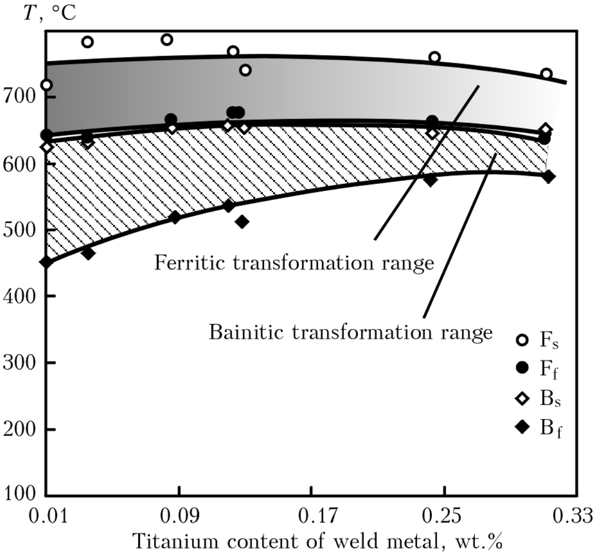

Figure 1. Dependence of temperature range of structural transformations in metal of the investigated welds on the titanium content: F_s, F_f — start and finish of ferritic transformation; B_s, B_f — start and finish of bainitic transformation

*The pictures in Figures 2 and 3 were obtained by Prof. V.N. Tkach by using scanning electron microscope EVO-50.

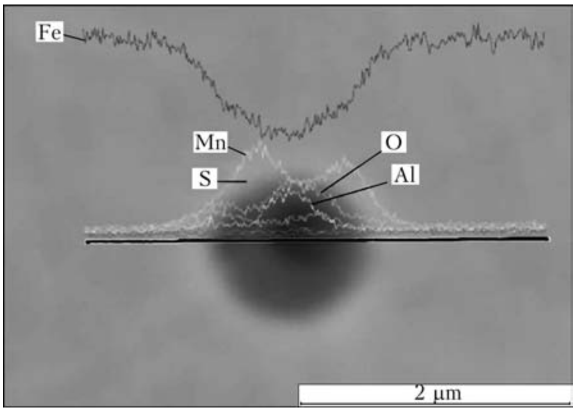

Figure 2. Morphology and composition of NMI more than 1.5 μm in size

tially decreased (see Table 3). Increasing the content of the fine carbide phase in the weld metal alloyed with titanium leads to growth of the α-phase nucleation centres and refining of the ferritic grains, on the one hand, and to enhancement of the effect of precipitation hardening on the formation of mechanical properties of the weld metal, on the other hand (Table 4). The effect of solid solution hardening of ferrite substantially increased in the Ti-6 weld metal.

Fine inclusions up to 1 μm in size have a core consisting of aluminium and titanium oxides, as well as an external cubic fringe with a high content of titanium nitrides (see Figure 3). Coarser inclusions consist of complex-composition oxides with manganese sulphide precipitates located on their surfaces (see Figure 2).

Increase in the content of carbide inclusions in the weld metal led to refining of ferritic grains and increase in the density of distribution of the grain boundaries. In this case it is the grain boundaries that acted as the most probable, in terms of energy, centres of growth of the ferritic structure. However, a high content of NMI above

Element	Content, wt.%
C	1.49
N	3.35
O	39.51
Al	28.41
Si	0.06
P	0.02
S	0.08
Ti	15.71
Mn	0.15
Fe	9.91

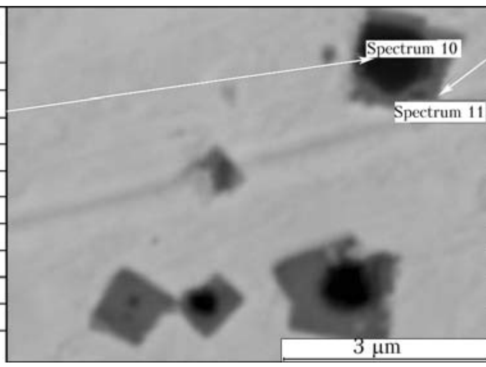

Element	Content, wt.%
C	3.01
N	10.67
O	9.15
Al	2.61
Si	0.15
P	0.03
S	0.04
Ti	47.43
Mn	0.29
Fe	25.41

Figure 3. Morphology and composition of NMI less than 1.5 μm in size

Table 3. Amount of microstructure components (%) and mean size of ferritic grain in metal of the investigated welds

Weld designation	Acicular ferrite	Polygonal ferrite	Lower bainite	Upper bainite	Polyhedral ferrite	Ferritic grain size, μm
Ti-1	23.5	10.5	21.5	25.5	19	150
Ti-2	10	20	30	20	20	120
Ti-3	6	3.7	35	28	27.3	70
Ti-4	7	9	41	19.6	23.4	100
Ti-5	–	5.7	36.7	23.6	34	70
Ti-6	–	2	25.3	71.7	1	50

Table 4. Volume content of NMI, their size distribution, and results of calculation of distance between the λ particles

Weld designation	Volume content of inclusions, %	Content (%)/quantity (pcs) of inclusions in size ranges, μm					λ, μm
		< 0.3	0.5–1	1.25–2	2.25–3	> 3	
Ti-1	0.40	25/243	51/490	17/159	5/45	3/26	3.96
Ti-2	0.24	53/647	37/458	8/94	2/21	0.25/3	2.99
Ti-3	0.12	33/233	52/360	11/79	3/21	0.6/4	1.89
Ti-4	0.65	53/408	33/258	10/75	3/21	1.5/12	1.89
Ti-5	0.35	56/315	35/197	2/10	1.5/8	1.5/8	1.80
Ti-6	0.23	62/386	30/189	6/36	2/11	0.16/1	1.61

Table 5. Chemical composition of metal of the investigated welds, wt.%

Weld designation	C	Si	Mn	Ni	Mo	Ti	Zr	Al	S	P	O
Zr-1	0.055	0.480	1.53	0.31	0.38	0.022	0.001	0.013	0.013	0.016	0.035
Zr-2	0.054	0.522	1.67	0.30	0.37	0.015	0.007	0.014	0.014	0.018	0.037

Table 6. Mechanical properties of metal of the investigated welds

Weld designation	σ_t, MPa	$\sigma_{0.2}$, MPa	δ_5, %	ψ, %	KCV, J/cm^2, at T, °C				
					20	−20	−40	−60	−70
Zr-1	736.6	667.0	20.8	61.6	181.3	147.9	96.7	65.9	54.8
Zr-2	740.7	650.2	20.2	62.3	198.8	141.7	94.2	87.5	80.6

1.5 μm in size along the grain boundaries shifts transformations to a high-temperature range. Therefore, mostly polygonal ferrite precipitated in the Ti-1 and Ti-2 weld metals (see Table 3), whereas the content of polyhedral ferrite was higher in structure of the Ti-3, Ti-4, Ti-5 and Ti-6 welds, where the content of oxide inclusions was lower.

Analysis of the obtained data allows a conclusion that increase in the content of the fine-grained structure can be achieved by varying the content of the fine carbide phase in structure of the weld metal (due to control of the metallurgical processes occurring in the slag–metal system). However, the welds have a low level of toughness because of formation of high-temperature morphological types of bainitic ferrite. To increase toughness and ductility of the weld metal it is necessary to achieve an increased content of the low-temperature types of ferrite in their structure due to refining of grains in the primary structure.

To refine the primary structure the weld pool should contain (by the beginning of solidification) refractory NMI in the form of a crystalline phase, which can serve as the γ-phase nucleation centres. Zirconium oxide (T_{melt} = 2715 °C) was added to the weld pool for this purpose. To increase stability of the austenitic phase, the welds were additionally alloyed with manganese. Chemical composition of the weld metal is given in Table 5, and mechanical properties — in Table 6.

Table 7 gives the data on composition of microstructure of the weld metal, which were obtained as a result of metallographic examinations, and Table 8 — the results of evaluation of microhardness of these structural components. Figure 4 shows histograms of the size distribution of NMI, and Table 9 gives the integrated chemical composition of NMI and amount of the 0.3–1.0 μm inclusions contained in them. It can be seen from analysis of the data that the character

Table 7. Amount of microstructure components (%) and mean size of ferritic grain in metal of the investigated welds

Weld designation	Martensite	Polygonal ferrite	Upper bainite	Lower bainite	MAC-phase	Ferritic grain size, μm
Zr-1	17	2	20	60	1	55
Zr-2	15	2	30	50	3	35

Table 8. Microhardness of structural components in metal of the investigated welds

Weld designation	Structural components	$HV1$, MPa	
		Unit values	Mean value
Zr-1	Lower bainite	205; 180; 187	190.7
	Upper bainite	232; 236; 254	241.2
	Martensite	490; 521; 545	519
Zr-2	Lower bainite	208; 187; 185	193.3
	Upper bainite	254; 236; 260	244
	Martensite	450; 457; 476	461

Table 9. Chemical composition, total content of NMI V_{NMI}, and content of fine inclusions $V_{0.3-1.0}$ in metal of the investigated welds

Weld designation	Chemical composition of NMI, wt.%							V_{NMI}, %	$V_{0.3-1.0}$, %
	O	Al	Si	S	Ti	Zr	Mn		
Zr-1	35.05	6.61	8.15	1.83	13.05	Traces	35.30	0.41	19.89
Zr-2	28.44	6.62	9.56	3.34	5.47	9.23	37.33	0.45	19.13

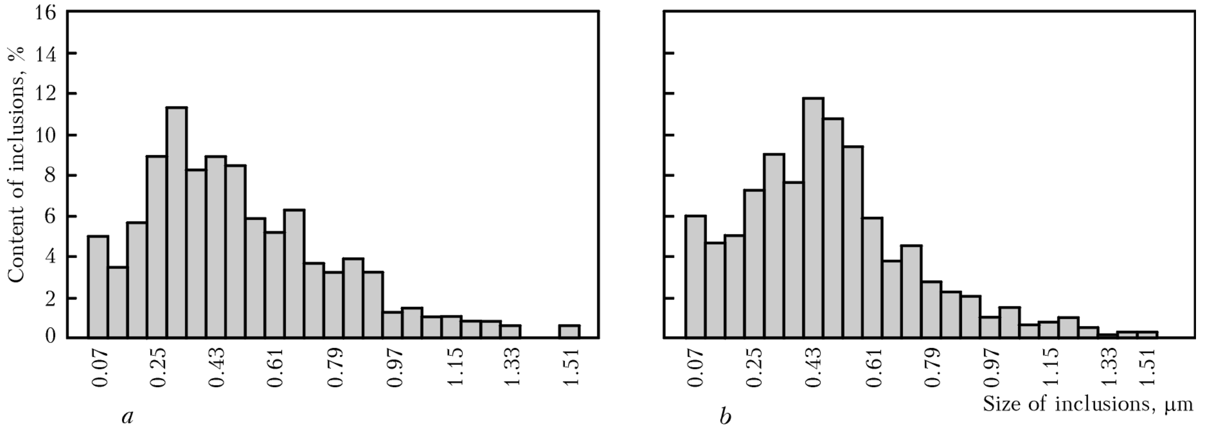

Figure 4. Size distribution of NMI in weld metals: *a* — Zr-1; *b* — Zr-2

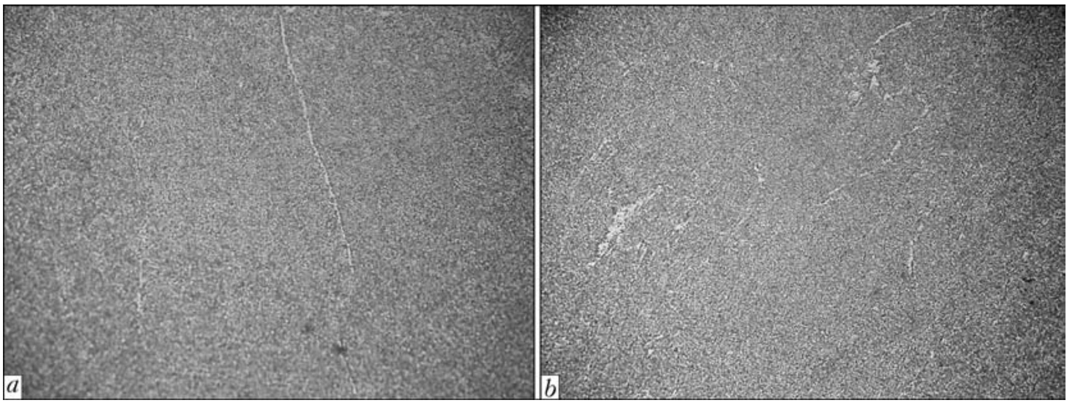

Figure 5. Microstructure (×200) of weld metal: *a* — Zr-1; *b* — Zr-2

of the size and chemical composition distribution of NMI in the Zr-1 and Zr-2 weld metals is similar and differs only in the titanium and zirconium contents. Metallographic examinations by using optical (Figure 5) and electron (Figure 6) microscopy were carried out to reveal the effect of such differences on the peculiarities of formation of microstructure of the weld metal.

As to the level of mechanical properties, the Zr-2 weld metal is characterised by a higher value of impact toughness at low temperatures, compared to the Zr-1 weld metal. This is provided by a combination of such hard component as lath martensite and a relatively soft phase presented by lower bainite contained in its structure.

It can be concluded from the results of measurement of microhardness of the structural components (see Table 8) that the low content of carbon in the Zr-1 and Zr-2 weld metals leads to decrease in its content in the lower bainite microstructure.

Sizes and numeric values of density of the inclusions in the microstructure of the weld metal were determined in the course of metallographic examinations. Each weld analysed to determine the content of the inclusions was examined by the optical and electron microscopy methods. 12 micrographs (frames) as a minimum were obtained at a magnification from 500 to 6000. The mean size of oxide inclusions and numeric values of the density were in a range of about 250 to 650 nm and about $1.5\cdot10^{10}$ to $10.5\cdot10^{10}$ m^{-2}, respectively. In some cases, the mean size ranged from about 250 to about 550 nm.

Microstructure of the Zr-1 and Zr-2 weld metals contains oxide inclusions with a mean size of less than 1 μm. This distribution of the inclusions is achieved due to the presence of the oxide nuclei with a size of no more than 300 nm, which contain about 50 % of zirconium, titanium or their mixture, as well as due to the low content of oxygen. Formation of the sufficient amount of nuclei of the bainitic phase, fixation of the grain boundaries and deoxidation of the weld pool are provided by the corresponding contents of titanium and zirconium oxides, as well as deoxidisers in a composition of the welding flux.

The selected alloying system combined with a certain thermal cycle allows formation of the weld metal with a structure of the bainitic-martensitic type. It can be seen from comparison of the data shown in Figures 5 and 6 that structure of the Zr-1 and Zr-2 weld metals is in a range of the optimal compositions, which is marked in Figure 7.

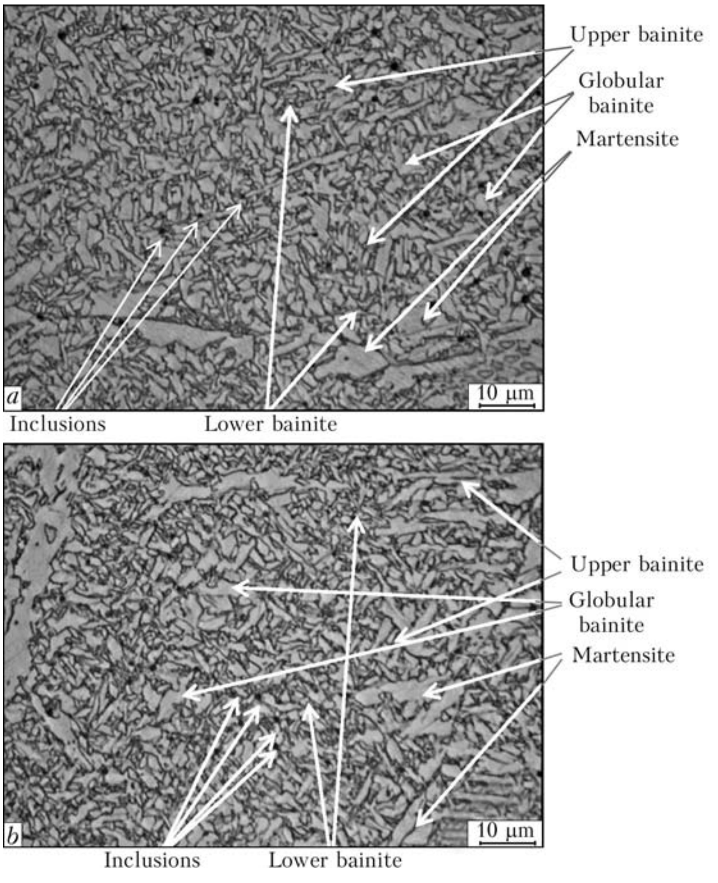

Figure 6. Microstructure of weld metal: *a* — Zr-1; *b* — Zr-2

The presence of martensite in the structure provides high strength properties of the weld metal. The values of ductility and toughness of metal depend on the content and morphology of such structural components as lower bainite and globular bainite.

Formation of lower bainite depends not only on the chemical composition of the weld metal and its cooling rate, but also on the chemical composition, size and value of the density of distribution of oxide inclusions in its composition. Application of the oxide metallurgy methods favours formation of a certain morphology of lower bainite and is a necessary condition for formation of microstructure of the weld metal on HSLA steels.

It was noted that the oxide inclusions more than 1 μm in diameter are inefficient for formation of lower bainite. Based on these results, the weld metal chemical composition and thermal welding cycle were selected so that they minimised formation of coarse oxide inclusions. Adding the certain amount of zirconium and titanium oxides to the weld pool exerts a marked effect on regulation of the size of the inclusions. This is also promoted by the limitation of the oxygen content of the weld metal to a level of less than 0.04 %, as well as by the use of strong deoxidisers, such as aluminium and silicon. Moreover, to limit growth of the oxide inclusions, the value of the welding heat input should be chosen on the basis of a permissible range of metal cooling rates v_{cool} (see Figure 7). The mean size of the oxide inclusions under these conditions ranges from 250 to 500 nm.

The high density of distribution of the 0.3–1.0 μm inclusions containing titanium or zirconium oxides leads to formation of the bainitic structure, whereas the decreased content of carb-

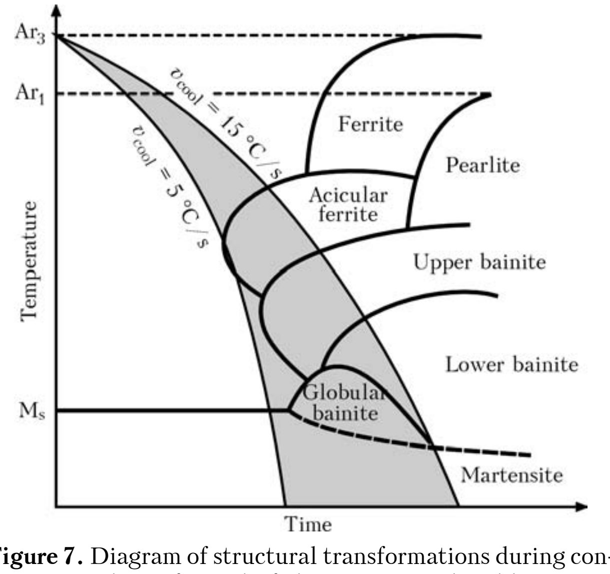

Figure 7. Diagram of structural transformations during continuous cooling of metal of the investigated welds

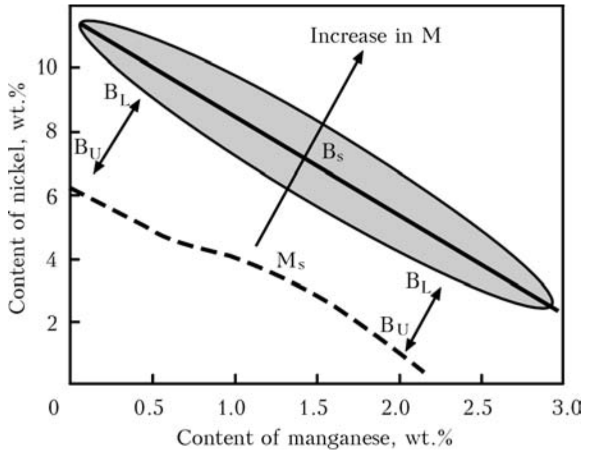

Figure 8. Diagram of the effect of alloying on the temperature of start of bainitic B_S and martensitic M_S transformations, and range of formation of upper B_U and lower B_L bainite and martensite M in microstructure of HSLA steels [12]

on in metal and the narrow range of bainitic transformations, which is determined by the value of the B_s–M_s temperature range (Figure 8), limit the probability of formation of the upper bainite microstructure.

In a general case, the solid oxides are worse wetted with metal than the liquid ones. Hence, they can be more readily entrapped by growing dendrites. It is this fact that can explain behaviour of the oxide inclusions containing titanium or zirconium.

By analysing the results of metallographic examinations, we can note differences in morphology of these inclusions. While the inclusions containing titanium oxides have a rounded shape (Figure 9), the inclusions containing zirconium oxides have an irregular shape formation in their inner part (Figure 10). This confirms an assumption that at the moment of growth of dendrites the inclusions are in the form of a solid phase.

The inclusions containing titanium compounds have, as a rule, manganese and silicon oxides in their composition. It can be seen from the constitutional diagram of the $MnO{\cdot}SiO_2$–$MnO{\cdot}TiO_2$ system (Figure 11) that the melting temperature of such inclusions is lower than the temperature of solidification of low-alloy steels. The constitutional diagram of the MnO–SiO_2–ZrO_2 system (Figure 12) shows that even at a content of up to 50 % of manganese silicates in the oxide phase, a non-metallic inclusion containing zirconium oxide can remain solid at temperatures above 1500 °C. Such inclusions are capable of blocking the growth of dendrites and affecting the grain size in the primary structure of the weld metal.

Fine refractory zirconium oxides up to 500 nm in size are sorbed by the boundaries of growing

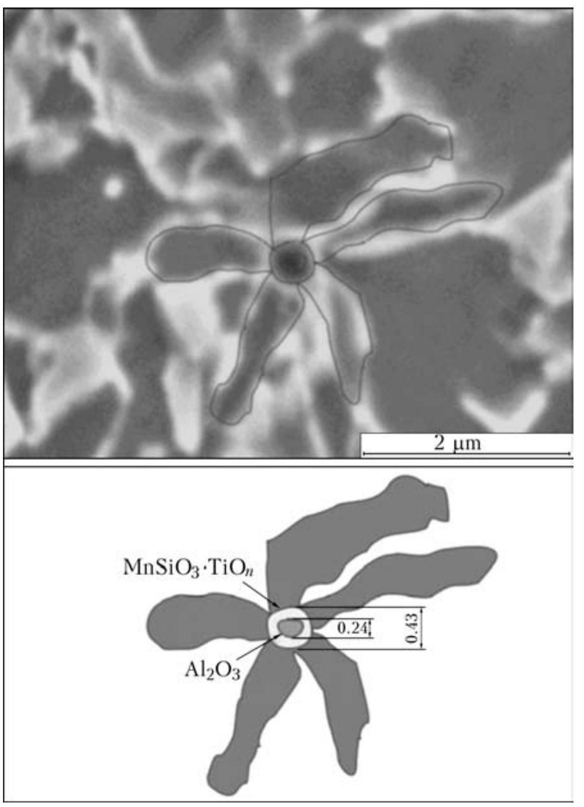

Figure 9. Morphology of non-metallic inclusion containing titanium oxide

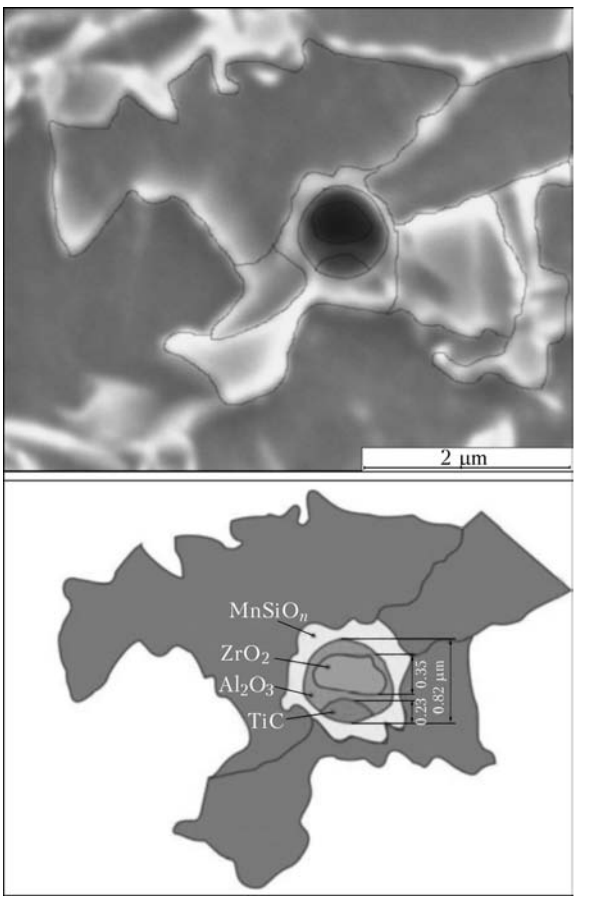

Figure 10. Morphology of zirconium oxide based non-metallic inclusion

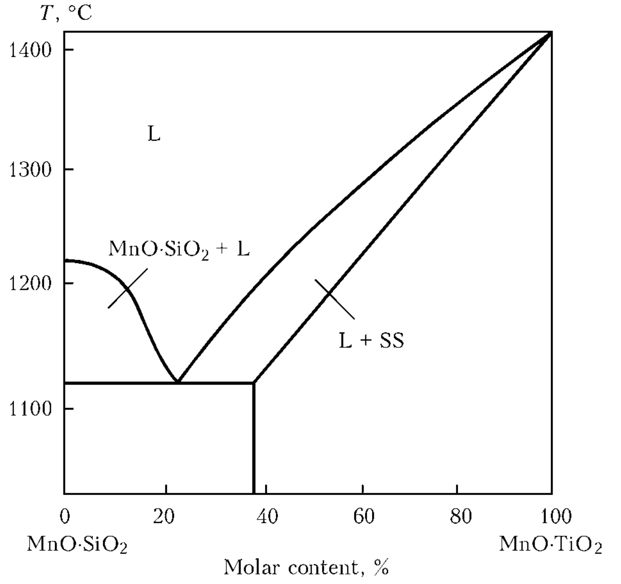

Figure 11. Constitutional diagram of the $MnO \cdot SiO_2$–$MnO \cdot TiO_2$ system

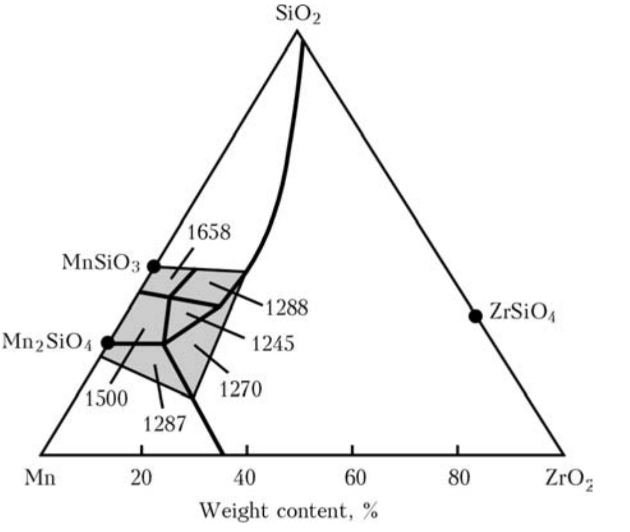

Figure 12. Constitutional diagram of the MnO–SiO_2–ZrO_2 system (numbers in the diagram — values of melting temperatures of the compounds)

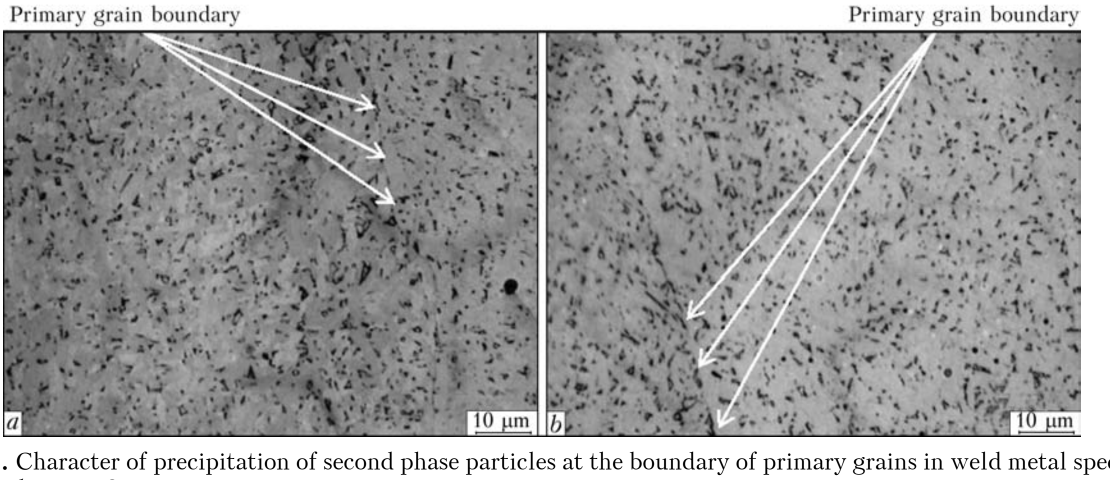

Figure 12. Character of precipitation of second phase particles at the boundary of primary grains in weld metal specimens: *a* — Zr-1; *b* — Zr-2

crystals, this leading to fixation of the grain boundaries. The inclusions exerting this effect are very fine and, therefore, are not the efficient centres of initiation of fracture in the inter-phase plane.

To check this assumption, additional metallographic examinations of specimens of the Zr-1 and Zr-2 weld metals were carried out in order to reveal the primary structure grain boundaries. Transverse sections of the welded joints were etched in a boiling solution of sodium picrate, and then examined by using optical microscope «Neophot 30». Figure 13, *a*, presents a photo of the typical structures, which shows precipitates of the second phase particles at the primary grain boundary in the Zr-1 weld metal in the form of a continuous chain. The second phase particles precipitate also along the primary grain boundary in structure of the Zr-2 weld metal (Figure 13, *b*), but these precipitates do not have a character of the continuous chain. Differences in the character of precipitation of the second phase at the boundary of growing dendrites affect the size of the secondary structure grains (see Table 7) and mechanical properties of the weld metal (see Table 6).

It can be seen from the examination data that NMI are a necessary component of the weld metal in welding of HSLA steels. To provide the microstructure characterised by a combination of high values of strength, ductility and toughness, it is necessary to form inclusions of a certain composition, size and distribution density in the weld metal.

Conclusions

1. The possibility of using oxide metallurgy approaches was investigated, providing for control of the amount, distribution and morphology of the inclusions in metal melts affecting the conditions of formation of the weld metal microstructure.

2. The presence of the NMI up to 1 μm in size containing titanium oxides in the weld metal on HSLA steels provides formation of a tough ferritic-bainitic structure with an increased content of acicular ferrite.

3. The content of the fine secondary structure can be increased by varying the content of the fine carbide phase in structure of the weld metal. However, because of formation of high-temperature morphological types of bainitic ferrite, the welds in this case have a low level of toughness.

4. The high density of distribution of the 0.3–1.0 μm inclusions containing titanium or zirconium oxides leads to formation of the bainitic structure, whereas the decreased content of carbon in metal and narrowing of the bainitic transformation range limit the probability of formation of the upper bainite microstructure.

5. Fine refractory zirconium oxides up to 500 nm in size are sorbed at the boundaries of growing crystals, this leading to fixation of the grain boundaries. The differences in the character of precipitation of the second phase at the boundary of growing dendrites affect the size of the secondary structure grains and mechanical properties of the weld metal.

6. To provide the microstructure characterised by a combination of high values of strength, ductility and toughness, it is necessary to form inclusions of a certain composition, size and distribution density in the weld metal. This can be achieved by using the oxide metallurgy methods providing for addition of a certain amount of refractory inclusions into the weld pool, limitation of the content of oxygen in it, and selection of the deoxidation system, as well as determination of the required temperature range of intermediate transformations based on the TTT-diagrams and welding thermal cycle.

1. Fairchild, D.P., Macia, M.L. (2003) Girth welding development for X120 linepipe. In: *Proc. of 13th Int. Offshore and Polar Engineering Conf*. (Honolulu, Hawaii, 25–30 May, 2003), 26–35.
2. Dhua, S.K., Mukerjee, D., Sarma, D.S. (2002) Weldability and microstructural aspects of shielded metal arc welded HSLA-100 steel plates. *ISIJ Int*., 42(**3**), 290–298.
3. Grong, O., Kolbeinsen, L., van der Eijk, C. et al. (2006) Microstructure control of steels through dispersoid metallurgy using novel grain refining alloys. *Ibid*., **46**, 824–831.
4. Takamura, J., Mizoguchi, S. (1990) Roles of oxides in steels performance — Metallurgy of oxides in steels. *Ibid*., **1**, 591–597.
5. Lee, T.K., Kim, H.J., Kang, B.Y. et al. (2000) Effect of inclusion size on nucleation of acicular ferrite in welds. *Ibid*., 40(**1**), 1260–1268.
6. Pokhodnya, I.K., Golovko, V.V., Denisenko, A.V. et al. (1999) Effect of oxygen on formation of acicular ferrite in low-alloy weld metal (Review). *Avtomatich. Svarka*, **2**, 3–10, 20.
7. Li, H.G., Zheng, S.B., Xie, S.J. et al. (2009) Influence of liquid steel cooling rate during directional solidification on titanium oxide precipitation. *Ironmaking and Steelmaking*, 36(**1**), 29–32.
8. Kikuchi, N., Nabeshima, S., Yamashita, T. et al. (2011) Microstructure refinement in low carbon high manganese steels through Ti-deoxidation, characterization and effect of secondary deoxidation particles. *ISIJ Int*., 51(**12**), 2019–2028.
9. Sarma, D.S., Karasev, A.V., Jonsson, P.G. (2009) On role of non-metallic inclusions in the nucleation of acicular ferrite in steels. *Ibid*., 46(**6**), 1063–1074.
10. Grigorenko, G.M., Golovko, V.V., Kostin, V.A. et al. (2005) Effect of microstructural factors on sensitivity of welds with ultra-low carbon content to brittle fracture. *The Paton Welding J*., **2**, 2–10.
11. Golovko, V.V., Kostin, V.A., Grigorenko, G.M. (2011) Peculiarities of the influence of complex alloying on structure formation and mechanical properties of welds on low-alloyed high-strength steels. *The Paton Welding J*., **7**, 11–17.
12. Keehan, E., Karlsson, L., Andren, H.-O. et al. (2006) New developments with C–Mn–Ni high-strength steel weld metals. Pt A: Microstructure. *Welding J*., **9**, 200–210.

Received 27.03.2013

DETERMINATION OF CONTACT PRESSURE OF REINFORCING SLEEVE IN REPAIR OF PIPELINES WITH SURFACE DEFECTS

V.I. MAKHNENKO, O.I. OLEJNIK and **V.M. SHEKERA**
E.O. Paton Electric Welding Institute, NASU
11 Bozhenko Str., 03680, Kiev, Ukraine. E-mail: office@paton.kiev.ua

An important step of maintaining the operability of main land pipelines is periodical technical diagnostics and, if required, repair operations in the sections with detected inadmissible defects. One of the promising methods to restore the load-carrying capacity of the wall with typical defects (in particular, thinning of main pipeline wall as a result of local corrosion loss of metal) is mounting reinforcing structures of the type of welded bands and leak-tight sleeves. This enables redistribution of stresses from service load between pipe walls and repair structure so that the detected defect was admissible in the working conditions. In order to do it, it is necessary to guarantee sufficient efficiency of repair, in particular, ensure the required contact pressure in the area of surface interaction of the pipe and reinforcing structures. For this purpose, a numerical-experimental procedure has been developed for assessment of the value of contact pressure at mechanical interference of the repair structure (mounting in the defective section of the main pipeline), and methods of numerical assessment of the nature of load redistribution in «pipeline–repair structure» contact pair were proposed, which allow analyzing the influence of repair parameters on the degree of restoration of load-carrying capacity of a pipeline with specific defect. In addition, a test sample of mechanical deformometer was developed, with a design adapted to measurement of circumferential displacements in the wall of reinforcing structure at its mounting on the pipeline. Preliminary laboratory investigations confirmed the effectiveness of the proposed procedure that allows recommending it for application at repair of operating main pipelines. 11 Ref., 1 Table, 5 Figures.

Keywords: *pipeline, thinning defect, repair, reinforcing welded structure, contact pressure, circumferential deformations, mechanical deformometer*

Maintaining the operability of main pipeline systems is an important and urgent task for Ukrainian economy. Periodical technical diagnostics of pipeline condition is performed to ensure their safe service, in particular, to detect service defects and assess the admissibility of the defective section condition. In the case of inadmissible shortening of safe residual operating life of the main pipelines (MP) with the known extent of damage, required repair operations are performed to restore the load-carrying capacity of the pipeline in the area of detected defects. At present methods of MP repair without taking them out of service are becoming ever wider applied, that allows avoiding product transportation during repair-reconditioning operations, reducing labour consumption and adverse influence on the environment [1–3]. In particular, various techniques of reinforcement of pipeline defective sections by reinforcing welded structures (RWS) of the type of bands and leak-tight sleeves are widely applied in Ukraine. This allows redistribution of stresses induced by operating pressure in MP between pipe walls and RWS and lowering the stress level in the defect area, bringing it into an admissible state.

According to normative-technical documentation [4, 5], before RWS mounting and welding, it is necessary to lower the pressure in the pipeline from working pressure P to the level of $P_{rep} = 0.7P$, as well as ensure tight contact between the surfaces of the pipe and RWS due to creation of contact pressure (interference) ΔP_{in}, which forms at structure assembly and at increase of inner pressure up to working pressure after repair (Figure 1). Value of contact pressure essentially influences lowering of stresses in the pipe wall with surface defects and largely determines reinforcement effectiveness and structure operability after repair, so that determination and monitoring of development of contact interaction of MP and RWS is an important task. Currently available design procedures for ΔP_{in} determination are rather cumbersome and require a number of difficult-to-determine values that limits their application in repair practice [6]. This work presents numerical-experimental procedure developed by the authors for monitoring the value of contact pressure at MP repair by its reinforcement by welded sleeves (bands).

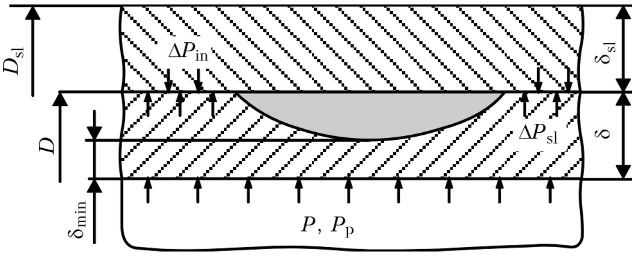

Figure 1. Schematic of redistribution of inner pressure after reinforcement of pipe defective section by a sleeve: D, D_{sl} — outer diameters of pipe and reinforcing structure, respectively; δ, δ_{sl} — wall thicknesses of pipe and reinforcing structure, respectively; δ_{min} — minimum residual wall thickness in the defect location; P_p, ΔP_{sl} — parts of pressure P taken up by walls of pipe and reinforcing structure; ΔP_{in} — contact pressure on reinforcing structure on pipe

In the approximation of uniform distribution of contact between the surfaces of «pipeline–reinforcing structure» contact pair working pressure in MP after mounting the repair structure can be presented by the following dependence:

$$P = P_p + \Delta P_{sl} + \Delta P_{in}, \tag{1}$$

where P_p, ΔP_{sl} is the part of working load taken up by the pipeline and repair structure, respectively.

Work [7] gives graphic dependencies, which characterize the degree of stress redistribution after MP repair by reinforcement at ideal fit of RWS to the pipeline. For this case part of pressure P, which will be taken up by RWS wall, can be described by the dependence

$$\Delta P_{sl} = (P - P_{rep})\chi_1, \tag{2}$$

where $\chi_1 = \left(1 + \dfrac{(0.5D_{sl})^2\,\delta}{(0.5D)^2\delta_{sl}}\right)^{-1}$.

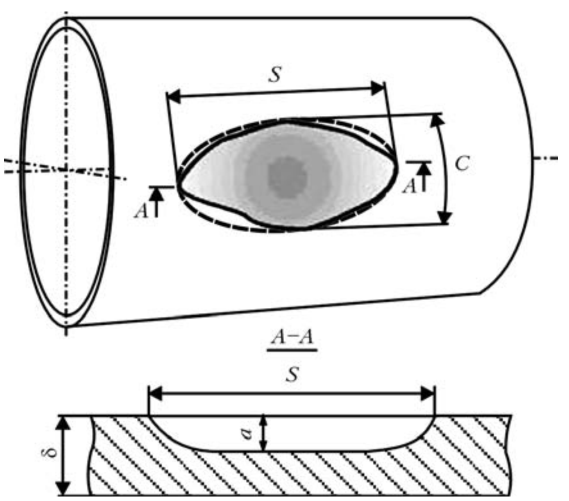

Figure 2. Schematic of thinning of pipe wall of the type of local corrosion metal loss: S — length; C — width; a — depth of defect

Formula (2) does not allow for contact pressure ($\Delta P_{in} = 0$) created during RWS mounting, welding of longitudinal welds and pressure increase up to working pressure. If at pressure in the pipeline $[P]$, pipe wall defects become admissible, then to ensure long-term operating reliability of pipeline section with the mounted repair structure the following condition should be satisfied:

$$P_p \le [P]. \tag{3}$$

Respectively, from (1)–(3) it follows that

$$P - (P - P_{rep})\chi_1 - \Delta P_{in} \le [P]. \tag{4}$$

Hence, pressure in the pipeline P_{rep}, at which RWS should be mounted, is as follows:

$$P_{rep} \le \frac{[P] - P(1 - \chi_1) + \Delta P_{in}}{\chi_1} \text{ at } \Delta P_{in} > 0. \tag{5}$$

Thus, criterion for selection of the required contact pressure value follows from (5)

$$\Delta P_{in} \ge P - [P] - \chi_1(P - P_{rep}). \tag{6}$$

Determination of maximum pressure $[P]$, at which the detected defects are admissible, is based on the requirements of the respective specified norms and standards, depending on operating conditions of a specific MP section and nature of damage [8, 9]. In particular, a typical MP defect is thinning of its wall of the type of local corrosion at metal loss (Figure 2). Admissibility of the state of MP defective section is assessed by numerical evaluation of reference stresses in the area of geometrical anomaly. Accordingly, allowing for additional influence of the characteristic force impact of the repair structure allows reducing the problem of restoration of pipe load-carrying capacity to selection of the balance of load redistribution between the walls of the pipeline and RWS. Substantiation of required ΔP_{in} value requires knowledge of admissible linear defects (Figure 3), which allow making a conclusion about admissibility of detected defects under the conditions of contact unloading [10].

As an example of application of the above methodology, given below are the results of calculation of repair characteristics of a pipe wall with surface thinning of an ellipsoidal shape of the following geometrical dimensions, mm: S = = 600, C = 550, a = 3.5 (Figure 4). The pipe is made from low-alloyed steel X60 (yield point σ_y = 420 MPa, admissible stresses $[\sigma]$ = 286 MPa, D = 1020 mm, δ = 10 mm), and operates at P = = 5.5 MPa. One can see from the diagram (see Figure 3) that this defect is admissible in the case, when inner pressure is equal to $[P] \approx$

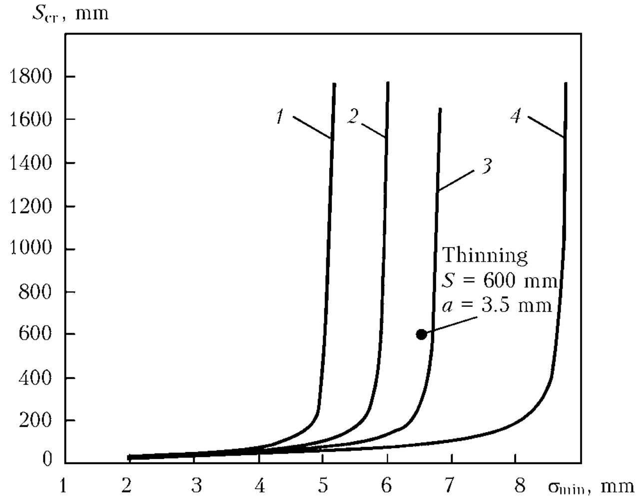

Figure 3. Diagram of admissible linear dimensions of pipe wall thinning S_{cr} depending on minimum thickness of pipe wall δ_{min} for pipeline of 1020 × 10 mm size from X60 steel with maximum service load P = 5.5 MPa at different inner pressures: *1* — 0.6P; *2* — 0.7P; *3* — 0.8P; 4 — P

≈ 0.77P. The Table gives the results of calculation of minimum required ΔP_{in}, depending on RWS wall thickness δ_{sl}, made according to (6).

Calculation results lead to the conclusion that to satisfy condition (3) it is possible to vary sleeve wall thickness δ_{sl} and contact pressure ΔP_{in}. Correct determination of ΔP_{in}, particularly for the case of $P_{rep} \to P$, is the most significant for ensuring the operability of a section repaired using the sleeve. Interference at mounting RWS on pipeline defective section can be controlled using the method of experimental measurement of circumferential displacements of RWS wall, due to elastic deformation at mechanical interference. In this case, ΔP_{in} calculation in RWS wall is performed by determination of Δl — variation of length l of the selected basic section of the structure, as a result of interference, compared to unloaded state and subsequent calculation by the formula

$$\Delta P_{in} = \frac{\Delta l}{l} E \frac{2\delta_{sl}}{D + 2\delta_{sl}}, \qquad (7)$$

where E is the steel modulus of elasticity.

In order to follow Δl variation under field conditions at repair-reconditioning operations on an operating pipeline, the currently operating

Results of calculation of required ΔP_{in} at repair of pipeline of 1020 × 10 mm size from X60 steel with wall thinning of S = = 600 mm, C = 550 mm, a = 3.5 mm

P, MPa	[P]	P_{rep}	δ, mm	δ_{sl}, mm	ΔP_{in}
5.5	~0.77P	0.7P	10	10	0.083P
				15	0.054P
				20	0.035P

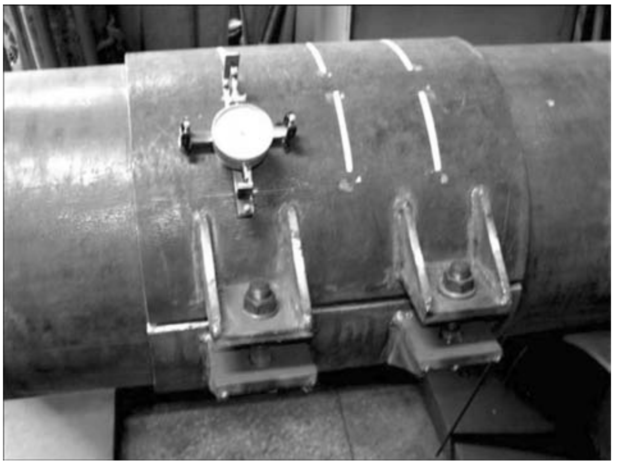

Figure 4. Experimental facility with mechanical deformometer for contact pressure determination

strain gauges and deformometers [11] were used as a basis to develop a new modification of a mechanical deformometer with base $l \approx 100$ mm, the appearance and schematic of which are given in Figure 5. The instrument allows measurement of circumferential deformations on cylindrical surfaces of 380 mm and greater diameter by the results of direct measurement of reciprocal motion of a pair of depressions, made on the sleeve surface by punching.

Measurement principle consists in transferring the displacements in the structure from contact points through reinforcing lever *1* with 1:5 arm ratio to clock-type indicator *2*. Transverse rack *4* with two assemblies for magnetic pressing

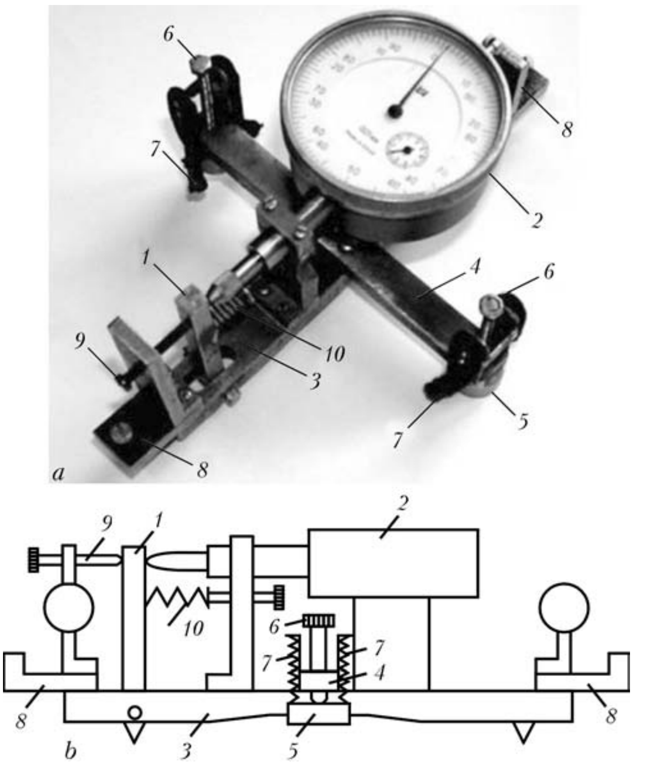

Figure 5. Appearance (*a*) and schematic (*b*) of mechanical deformometer: (for designations see the text)

of the deformometer to RWS is fastened in the middle part of base *3* for a stable fastening of deformometer to cylindrical surface. Each assembly located at rack end faces, consists of yoke *5* with caulked-in magnet, governing screw *6* and springs *7*, balancing pressing-down. In the case of insufficient pressing of the instrument to the metal, links *8* are provided on the band lower half for deformometer fastening. The links allow, by placing circumferential safety straps on them, avoiding accidental disconnection and falling down of the instrument. Holding assembly (screw *9* with spring *10*) is provided for fastening of the rod and lever (instrument mounting and transportation).

To ensure complete control of uniform clamping of the pipe, several deformometers can be used, which are mounted in the characteristic points of the repair structure.

Preliminary laboratory testing of the deformometer in a special facility (see Figure 5) consisting of a pipe section from steel 09G2S of 377 × × 11 mm size, 1000 mm length and 400 mm long band with 11 mm wall thickness, confirmed sufficient accuracy (approximately 1 μm) and effectiveness of the developed deformometer that allows recommending it for application in repair-restoration work in operating MP.

Conclusions

1. Numerical-experimental procedure was developed to assess the contact pressure between pipeline walls and RWS in terms of effectiveness of restoration of load-carrying capacity of pipeline wall with typical service defects. Numerical algorithm was proposed for assessment of load redistribution at contract interaction of structural elements and influence of reinforcement on admissibility of pipeline operation. The case of a typical thinning defect of the type of metal loss is used to show the essential influence of the value of RWS mechanical interference at its mounting on repair effectiveness.

2. Pilot sample of mechanical deformometer was developed with its design adapted to measurement of circumferential displacements in the wall of the reinforcing structure at its mounting on the pipeline. Proceeding from the results of laboratory tests, it was established that the accuracy of measurement of displacements in the wall of the reinforcing structure using this deformometer (approximately 1 μm) is sufficient for assessment of the magnitude of mechanical interference and confirmation of the effectiveness of repair of defective sections of the pipeline.

1. La Morte, C.R., Boring, M., Porter, N. (2007) *Advanced welding repair and remediation methods for in-service pipelines*: Final report. Columbus: EWI.
2. Kiefner, J.F. (1977) Repair of line pipe defects by full-encirclement sleeves. *Welding J.*, **6**, 26–34.
3. Kiefner, J.F., Bruce, W.A., Stephens, D.R. (1994) *Pipeline repair manual*. Houston: Techn. Toolboxes.
4. *VBN V.3.1-00013741-07:2007*: Main oil pipelines. Methods of repair of defective sections. Introd. 01.01.2007. Kiev: Ministry of Fuel and Energy of Ukraine.
5. *GBN V.3.1-00013741-12:2011*: Main gas pipelines. Repair by arc welding in service conditions. Introd. 09.06.2011. Kiev: Ministry of Fuel and Energy of Ukraine.
6. Kryzhanivsky, E.I., Palijchuk, I.I. (2008) Method of calculation of contact pressure for sleeve and pipe joined with interference. *Naftogaz. Energetyka*, **1**, 78–82.
7. Makhnenko, V.I., But, V.S., Kozlitina, S.S. et al. (2010) Optimal reduction of working pressure in pipelines for repair of thinning regions by surfacing. *The Paton Welding J.*, **10**, 6–9.
8. *DSTU-NBV.2.3.-21:2008*: Directive. Determination of residual strength of main pipelines with defects. Kyiv: Minregionbud Ukrainy.
9. (2000) *Fitness-for-service*. American Petroleum Institute Recommended Practice 579. 1st ed.
10. Olejnik, O.I., But, V.S. (2010) Computational methods in development of technologies of main pipeline repair by welding under pressure. In: *Proc. of 5th Int. Conf. on Mathematical Modelling and Information Technologies in Welding and Related Processes* (25–28 May, 2010, Katsiveli, Ukraine). Kiev: PWI, 177–182.
11. Kasatkin, B.S., Kudrin, A.B., Lobanov, L.M. et al. (1981) *Experimental methods of study of strains and stresses*. Kiev: Naukova Dumka.

Received 26.02.2013

GASOABRASIVE WEAR RESISTANCE AT ELEVATED TEMPERATURES OF COATINGS PRODUCED BY THERMAL SPRAYING

V.I. POKHMURSKY[1], **M.M. STUDENT**[1], **A.V. POKHMURSKAYA**[2], **I.A. RYABTSEV**[3], **V.M. GVOZDETSKY**[1] and **T.R. STUPNITSKY**[1]

[1]H.V. Karpenko Physico-Mechanical Institute, NASU
5 Nauchnaya Str., 79601, Lvov, Ukraine. E-mail: pokhmurs@ipm.lviv.ua
[2]Chemnitz University of Technology, Institute of Composite Materials and Surface Technology
73 Erfenschlager Str., 09105, Chemnitz, Germany. E-mail: hanna.pokhmurska@mb.tu-chemnitz.de
[3]E.O. Paton Electric Welding Institute, NASU
11 Bozhenko Str., 03680, Kiev, Ukraine. E-mail: office@paton.kiev.ua

Thermal spraying is becoming ever wider accepted to produce reconditioning and protective coatings for various functional purposes. However, service life of such coatings has not been studied well-enough so far. This work is a study of the mechanism of formation of electric arc sprayed coatings from flux-cored wires of Fe–Cr–B–Al alloying system. It is found that gasoabrasive wear resistance of coatings from flux-cored wires depends on coating hardness, stresses of the first kind in the coating and on composition of oxide films, which form at spraying and at elevated temperatures during gasoabrasive wear testing. Oxide films initially form on the drop surface during spraying. In addition, in air the porous electric arc sprayed coatings are found to have oxidation on the surface and inside the coating (interlamellar oxidation) and oxidation on the boundary between the coating and steel base. It is shown that the high resistance to gasoabrasive wear is observed in coating, in which tensile stresses are transformed into compressive stresses as a result of the process of inner interlamellar oxidation during isothermal soaking at testing temperature of 400–600 °C, leading to increase of coating volume and improvement of its cohesion strength as a result of its reinforcement by interlamellar films of 100–150 nm thickness. Optimum content of alloying elements and their influence on gasoabrasive wear resistance of coatings are determined. Positive influence of residual compressive stresses in the coatings on gasoabrasive wear is shown. Proposed coatings will become applied in power engineering enterprises. 13 Ref., 1 Table, 12 Figures.

Keywords: *thermal spraying, coatings, flux-cored wires, gasoabrasive wear*

Electric spraying process is a sufficiently simple and inexpensive one among thermal spraying methods [1]. Recent introduction of electrodes in the form of flux-cored wires (FCW) for thermal spraying enabled widening the field of application of this method and producing reconditioning and protective coatings for various functional purposes [2–5], in particular for protection from corrosion and gasoabrasive wear of heating elements of thermal electric power stations [6–12]. However, service life of such coatings has not yet been well enough studied that restrains wide-scale application of this method.

The paper is devoted to investigation of the influence of alloying elements on coating structure, their mechanical characteristics, wear resistance at gasoabrasive wear and gas corrosion resistance at higher temperature.

Experimental procedure and studied materials. Coatings were applied by thermal spraying with EM-14 metallizer, spraying FCW of 1.8 mm diameter. Powders of boron-containing compounds (ferrochromium boron FKhB-2 and boron carbide), pure metals (chromium, tungsten and aluminium), as well as aluminium-magnesium alloys were used as charge components. Developed FCW were compared with those of foreign companies (Table), which are used for part protection from gasoabrasive wear. Strip from steel 08kp (rimmed) of 0.4 mm thickness and 10 mm width was used as wire sheath. Coefficient of FCW filling with the charge was 22–35 wt.%. Modes of coating deposition were as follows: I = 150–160 A, U_a = 32–34 V. FCW was sprayed by an air jet under the pressure of 0.60–0.65 MPa with 140–150 mm spraying distance. Coating phase composition was studied in DRON-3 diffractometer with computer recording of diffractograms. CuK_α-radiation was used at U = 32 V and I = = 15 mA. Scanning step was 0.05.

Coating structure and chemical composition after spraying and oxidation were studied in the Carl Zeiss scanning microscope EVO-40 XVP

Calculated FCW composition, wt.%

FCW grade	B	Cr	Al	W	Mo	Si	Other	Fe	Wire trade mark
PP-Kh6R3Yu2	3	6	2	–	–	–	–	Base	FMI
PP-Kh6R3Yu6	3	6	6	–	–	–	–	Same	FMI-2
PP-Kh6R3Yu14	3	6	14	–	–	–	–	»	FMI-11
PP-70Kh6R3Yu6	3	6	6	–	–	–	–	»	FMI
ПП-70V6R3Yu6	3	–	6	–	–	–	–	»	FMI-7
PP-500Kh20R5M10 V10B10G5S2	5	20	–	10	10	2	10Nb	»	EndoTec DO 390N
PP-Kh30M15Yu4	–	22	5	–	–	–	–	»	EuTronic Arc 509
PP-Kh29R4S2G2	4	29	–	–	–	2	2Mn	»	Praxair and TAFA 95MXC

with microanalysis system EVO-4XVP. Microhardness was determined in PMT-3 hardness meter.

In confidence interval of 0.95 and with minimum experiment number (four) relative error of determination of cohesive and adhesive strength and wear resistance parameters did not exceed 5 %.

Samples of electric arc sprayed coating material for determination of the modulus of elasticity by the method of three-point bending were prepared as follows. One surface (of 100 × 20 mm size) of 100 × 20 × 6 mm samples from steel 20 was coated with tin 2 of 40–50 μm thickness and subjected to jet treatment with corundum for preparation of tinned surface for spraying.

Six samples were fastened on the forming surface of a hexagon and 1.5 mm coating from FCW was deposited. Spray-deposited plates were ground from end faces and over the sprayed side down to coating thickness of 1 mm. Prepared samples were placed into a heated furnace, where the temperature was 50 °C higher than tin melting temperature. At heating of coated steel plates the tin layer melted and coating spalled spontaneously due to internal stresses. As a result, beam-type samples of 100 × 20 × 1 mm size from coating material were made. Modulus of elasticity of electric arc sprayed coatings was determined by bending method, and calculation was performed as follows [13]:

$$E = \frac{L_v^3(P_2 - P_1)}{4bh^3(Z_2 - Z_1)},$$

where L_v is the distance between base cutters, mm; P_1, P_2 is the magnitude of first and second load, g; b is the plate width, mm; h is the plate thickness, mm; Z_1, Z_2 are the indicator readings at the first and second loading, mm.

Investigation of gasoabrasive wear at elevated temperatures (up to 600 °C) was conducted in a laboratory unit with application of mechanical acceleration of abrasive (in particular, quartz sand < 200 μm) with particle velocity of 10–40 m/s, and 30° angle of incidence.

Figure 1 gives the schematic of a unit for testing coatings for gasoabrasive wear at higher temperature.

The unit consists of electric furnace *1* (temperature is regulated with accuracy of ±2 °C), abrasive feeding device *2*, DC electric motor *3*, module of adjustment of engine revolutions *4*. To eliminate the edge effects resulting from coating tearing off by abrasive jet on sample edges, they were tightly fastened to each other on the inner side of ring *5* (Figure 1, *a*).

Assembly of abrasive feeding and acceleration (Figure 1, *b*, *c*) consists of inner pipe fixed rigidly, through which the abrasive is uniformly supplied to abrasive acceleration assembly. External pipe, which is fixed on bearings in the case, is designed to transfer the torque to abrasive acceleration assembly. Bearings are air-cooled.

Samples were made from steel 12Kh1MF of 20 × 40 × 6 mm size, and 10 μm of nickel was deposited on all the sample surfaces by galvanizing to eliminate the uncontrolled increase of sample weight, because of oxidation of their unsprayed surfaces at elevated temperatures. Nickel layer was removed by machining from one side of the sample (20 × 40 mm). This surface was subjected to corundum jet treatment and electric arc coating of 1000 μm thickness was deposited layer-by-layer in six passes.

Sprayed surface of samples was ground to 700 μm thickness. Experimental investigations were conducted at 30° angle of abrasive attack and abrasive velocity of 36 m/s, which was set by varying the speed of revolution of DC electric motor *3* from adjustment module *4* (see Figure 1, *a*). Wear resistance of coated samples was determined by their weight loss with up to 0.0002 g accuracy.

Experimental results and their discussion. *Influence of FCW charge composition on coating*

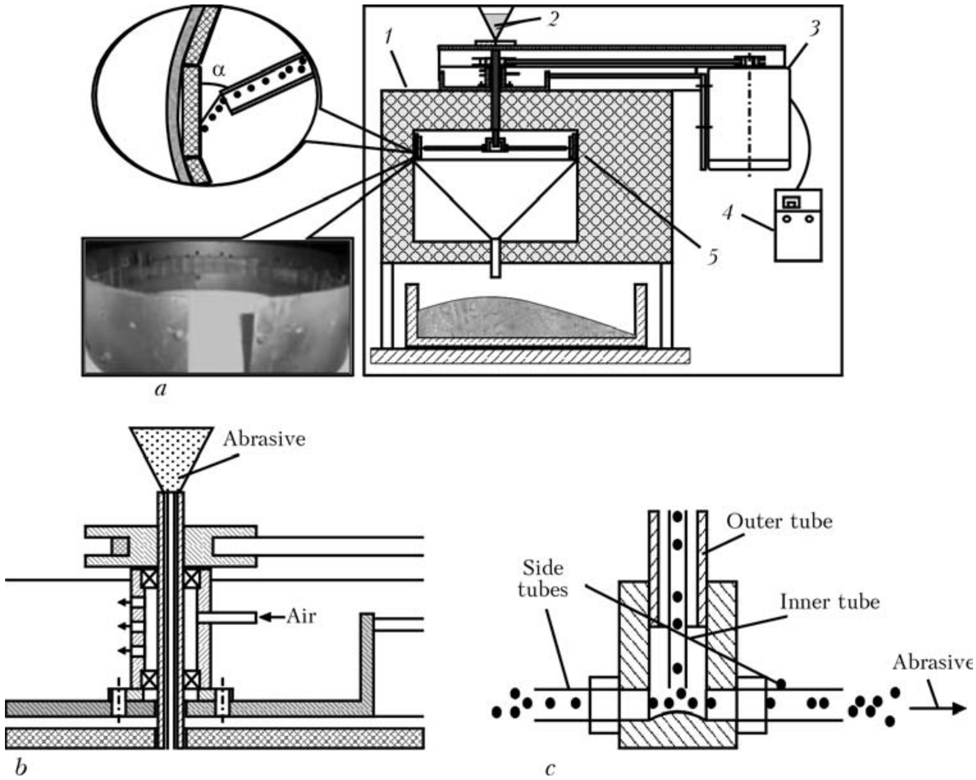

Figure 1. Schematic of unit for gasoabrasive wear testing of coatings at elevated temperature (*a*), and assemblies for abrasive feeding (*b*) and acceleration (*c*) (for designations see the text)

structure. To study the composition of the drops formed at FCW spraying by an air jet, they were trapped in a snow target, and the cuts on sections were studied. It is established that minimum drop size was 15 μm, and maximum was 400 μm. Fraction of 18–50 μm size amounted to 50 wt.%, 50–150 μm size to 40 wt.%, and amount of drops larger than 150 μm was small at 10 wt.%. During spraying of FCW of Fe–Cr–B–Al alloying system, the charge and sheath do not have enough time to fuse completely because of the transiency of melting processes, so that a heterogeneous melt and drops of three types form:

- drops of metal melt, based on Fe alloyed with 3–5 % Cr, 6–14 % Al and B, are surrounded by Al_2O_3 oxide, the particles of which grow as round islets on drop periphery (Figure 2, *a*);
- drops of metal melt, based on Fe alloyed with 3–5 % Cr, 2–4 % Al and B, are surrounded by an oxide film $(FeCr)_2O_3$, which is located between ferrochrome dendrites (Figure 2, *b*);
- round drops of pure oxide Al_2O_3 $(FeAlCr)_2O_3$ and $(FeCr)_2O_3$ (Figure 2, *c*).

When hitting the spraying surface, molten drops are badly deformed and solidify in layers as lamels, separated by oxide films (Figure 3, *a*). Phase analysis of electric arc sprayed coatings revealed that at formation of coatings using FCW with B_4C + Fe charge, coating matrix phase is Fe_α with inclusions of Fe_3C ferric carbide and free B (Figure 3, *b*, *c*). In this case, interaction of boron carbide with iron melt at spray-deposition of coatings runs by the following reaction: $Fe + 1/3B_4C = 1/3Fe_3C + 4/3B$. Adding Cr-containing elements to FCW charge promotes disappearance of free B in the coating structure, whereas interaction of boron carbide with Cr proceeds by the following reaction: $Cr + 2/7B_4C = 4/7CrB_2 + 1/7Cr_3C_2$.

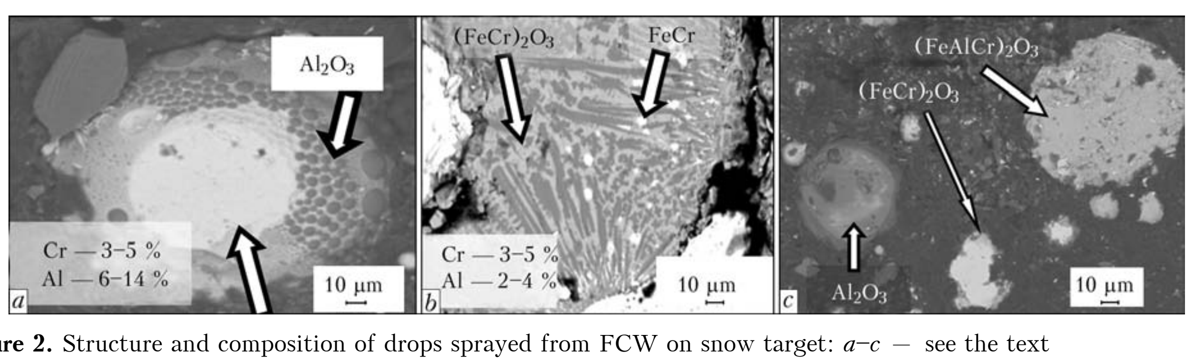

Figure 2. Structure and composition of drops sprayed from FCW on snow target: *a*–*c* — see the text

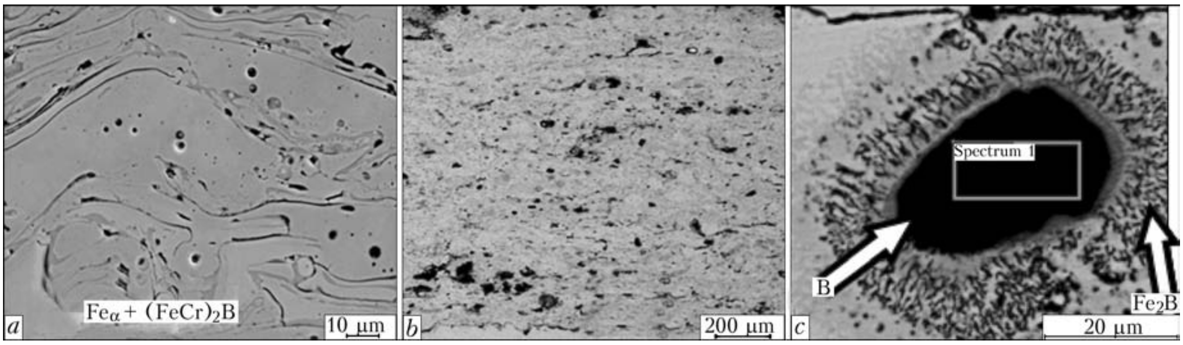

Figure 3. Structure of electric arc sprayed coatings: *a* — FCW with $(FeCr)_2B$ + Fe charge; *b* — FCW with B_4C + Fe charge; *c* — same, boron inclusions in the coating

Coating structure at elevated temperatures. Unlike solid materials in porous electric arc sprayed coatings oxidation in air at elevated temperatures occu both on coating surface and inside it (interlamellar oxidation) (Figure 4, *a*, *b*). In addition, oxidation occurs on the boundary between the coating and steel base (Figure 4, *c*). As a result of 8–10 % porosity of the coatings oxygen penetrates into the steel base even at coating thickness of 0.5–0.8 μm. Total oxygen content in the initial coating is equal to 2.5–3.0 wt.%. After soaking for 100 h at 550 °C oxygen content in the coating rises up to 4–5 wt.%, at 100 h soaking at 700 °C — up to 8.0–9.5 wt.%. Here coating oxidation rate is 10–30 times lower than that of steel.

At the temperature of 600–700 °C oxide films of hematite Fe_2O_3 form on steel surface, growing in the form of needle-like projections 100–200 nm thick (Figure 5, *a*). On coatings with not more than 2 % Al (PP-Kh6R3Yu2) oxide films of hematite alloyed by chromium and aluminium $(FeCr)_2O_3$ are formed, growing on the surface in the form of strobiloidal protrusions of 5–10 μm thickness (Figure 5, *b*). Oxide films of hematite alloyed by aluminium $(FeAl)_2O_3$ form on Kh6R3Yu6 and Kh6R3Yu14 coatings with higher aluminium content, which grow on the surface in the form of monolithic film (Figure 5, *c*). Oxide films 0.2–2.0 μm thick form between coating lamels. These films contain particles of matrix metal phase 100–300 μm long, strongly bonded to matrix phase (Figure 5, *d*).

Two-layer oxide film forms on the boundary between coating and base. The part adjacent to the coating has an increased content of aluminium, and the part adjacent to the base has higher iron. Oxide film is embedded into the coating as though by anchors, and strongly binds it to the steel base.

Influence of testing temperature on coating mechanical characteristics. During long-term soaking at testing temperature of 600 °C, hardness of all the coatings decreases and is stabilized on the level of *HV* 500–550, because of coarsening of strengthening phase — $FeCr_2B$ borides. So, as shown by metallographic analysis, after spraying boride size does not exceed 100 nm, and after soaking for 5000 h at 600 °C, their size increases to 300–500 nm (Figure 6, *a*, *b*). Long-term soaking of coatings at testing temperature of 600 °C promotes increase of their cohesion strength (Figure 7).

Such an effect is predetermined by reinforcement of coating structure by thin (less than 1 μm) oxide films (see Figure 5, *d*). Here, the coating acquires a composite structure. The greatest strengthening is observed for a coating from

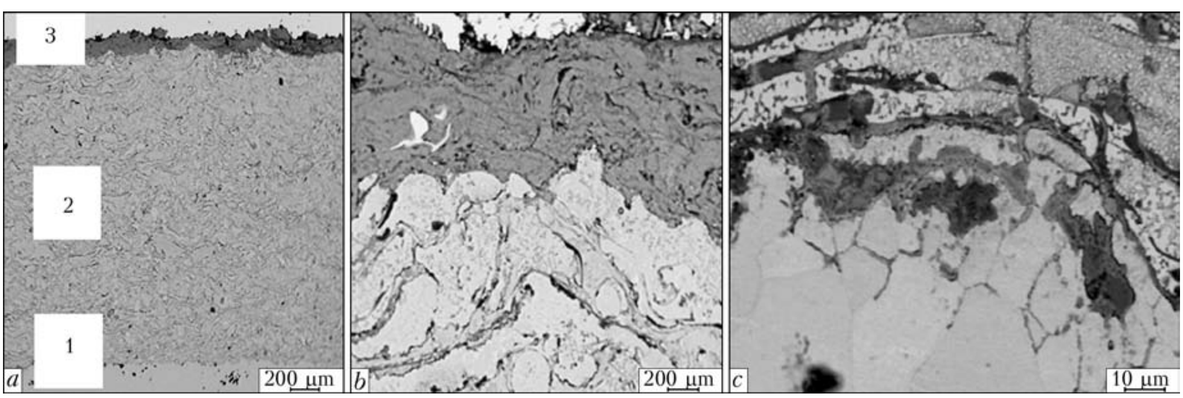

Figure 4. Coating structure after soaking at 600 °C for 2000 h: *a* — total coating structure (*1* — base (12Kh1MF steel); *2* — coating; *3* — oxide film on coating surface); *b* — transition zone between coating and oxide film on coating surface; *c* — transition zone between coating and base metal

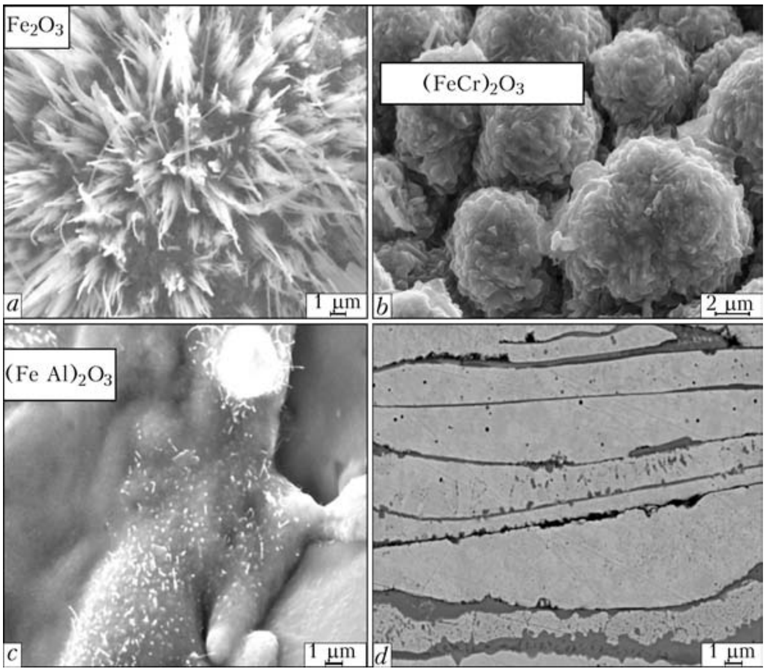

Figure 5. Structure of surface films: *a–c* — see the photoars; *d* — lamels

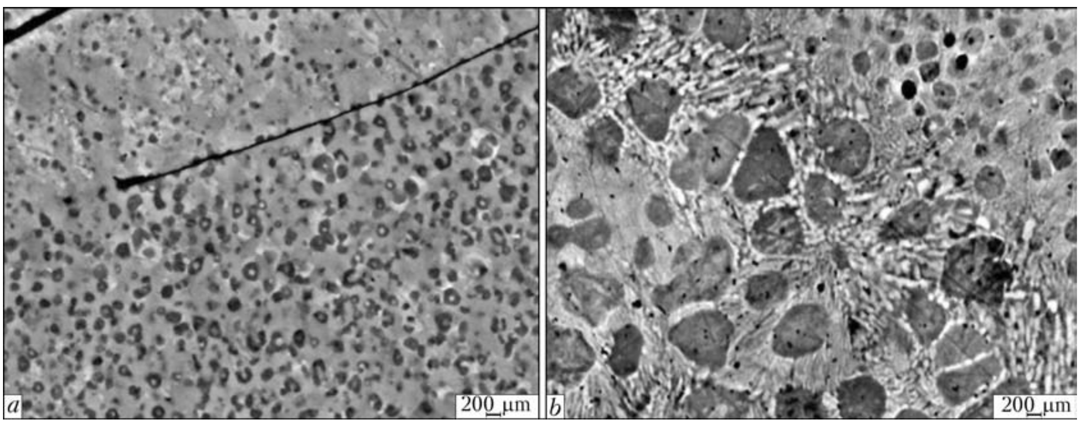

Figure 6. Structure of coatings with borides after spraying (*a*) and after soaking at 600 °C for 5000 h (*b*)

FCW Kh6R3Yu14, that is related to coating reinforcement by aluminium oxide films.

Modulus of elasticity of spray-deposited coatings without heat treatment is in the range of 50,000–70,000 MPa. At increase of testing temperature above 350 °C, the modulus of elasticity of FCW 70V6R3Yu6 coating rises almost 3 times, and for a coating from FCW Kh6R3Yu14 — by 70 % (Figure 8, *a*) [13]. Increase of modulus of elasticity is determined by inner interlamellar oxidation and it is directly proportional to the amount of oxide phase in the coating. So, the modulus of elasticity of 70V6R3Yu6 coating after spraying is equal to 52,000 MPa, and oxide phase amount is 4 wt.%; after soaking for 100 h at 600 °C the value of the modulus of elasticity rises up to 180,000 MPa, and amount of interlamellar oxide phase is 14 wt.% (Figure 8, *b*).

Long-term exposure of samples at the temperature of 600 °C also leads to an essential decrease of tensile stresses in the coating. Two time

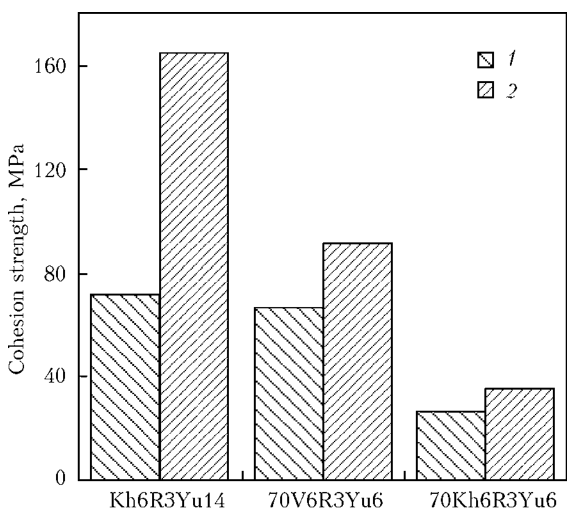

Figure 7. Influence of soaking at 600 °C for 1000 h on cohesion strength of coatings: *1* — initial; *2* — soaking

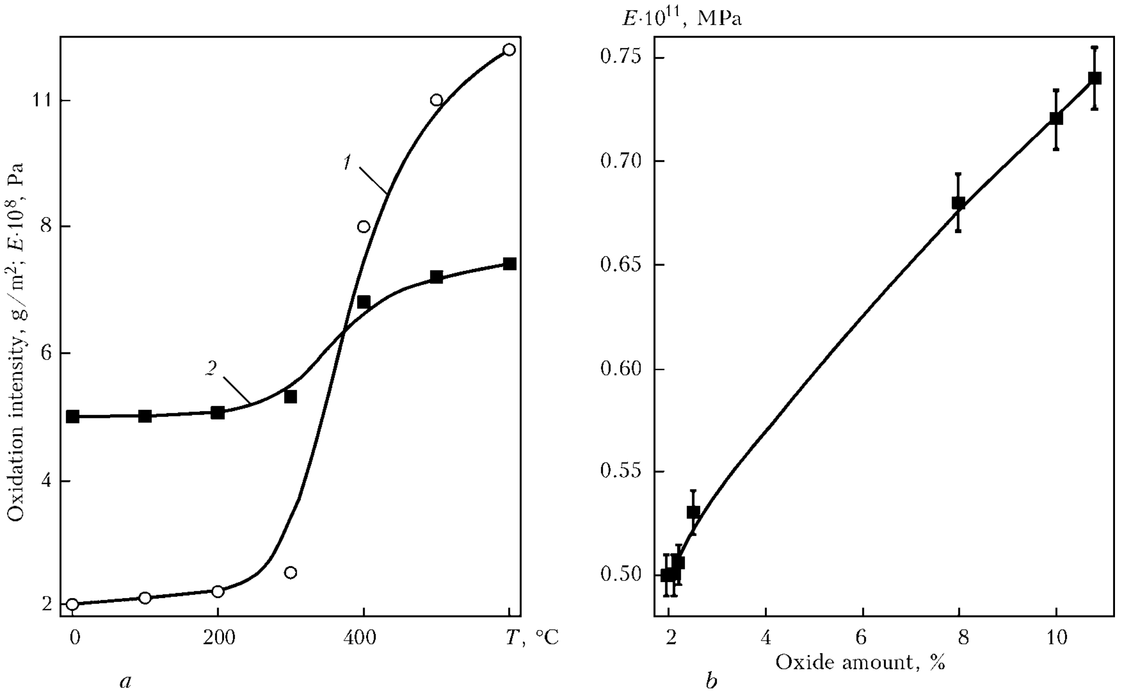

Figure 8. Temperature influence on oxidation intensity (*1*) and modulus of elasticity (*2*) of coatings (*a*), and of amount of interlamellar oxides in the coating on modulus of elasticity (*b*)

stages and two mechanisms are determined, by which lowering of tensile stresses in the coating proceeds (Figure 9).

So, at the first stage which lasts up to 20 h at 600 °C stress lowering occurs due to decomposition of austenite in the coating structure, that is accompanied by increase of coating volume. At the second stage with increase of soaking time above 20 h, compressive stresses rise, because of running of just the process of intralamellar oxidation of the coating

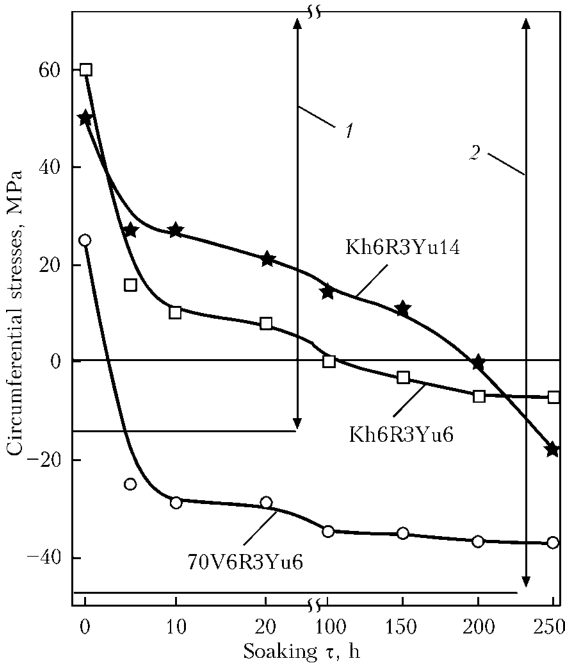

Figure 9. Influence of soaking at 600 °C on stress level in coatings: *1* — first; *2* — second time stage

and increase of the amount of oxide phase, that essentially increases the coating volume.

Gasoabrasive wear resistance of electric arc sprayed coatings. With increase of boron content in the coating up to 2.5 wt.%, gasoabrasive wear resistance of coatings becomes higher. Increased content of boron in the coatings above 2.5 wt.% leads to increase of tensile stresses in the coating and appearance of a net of microcracks in it, that lower coating wear resistance. As the same time, with increase of aluminium content in FCW with 2.5 wt.% B, gasoabrasive wear resistance of coatings rises monotonically (Figure 10, *a*). Replacement of FKhB master alloy by B_4C in FCW charge only slightly, by 15 %, lowers the wear resistance, so that these components can be irreplaceable (Figure 10, *b*).

Investigations for gasoabrasive wear resistance of coatings from FCW with varying content of aluminium of 2, 6, 14 wt.% showed that below 350 °C gasoabrasive wear resistance of coatings and steel rises only slightly (Figure 11), but at lowering of aluminium content in FCW coating wear resistance becomes significantly lower than that of steel.

This is related to the fact that at spraying of coatings from FCW with a low content of aluminium they develop considerable tensile stresses, relaxation of which occurs through formation of a net of microcracks. With increase of aluminium content, a more heterogeneous coating forms, and much lower tensile stresses develop, due to their relaxation by plastic defor-

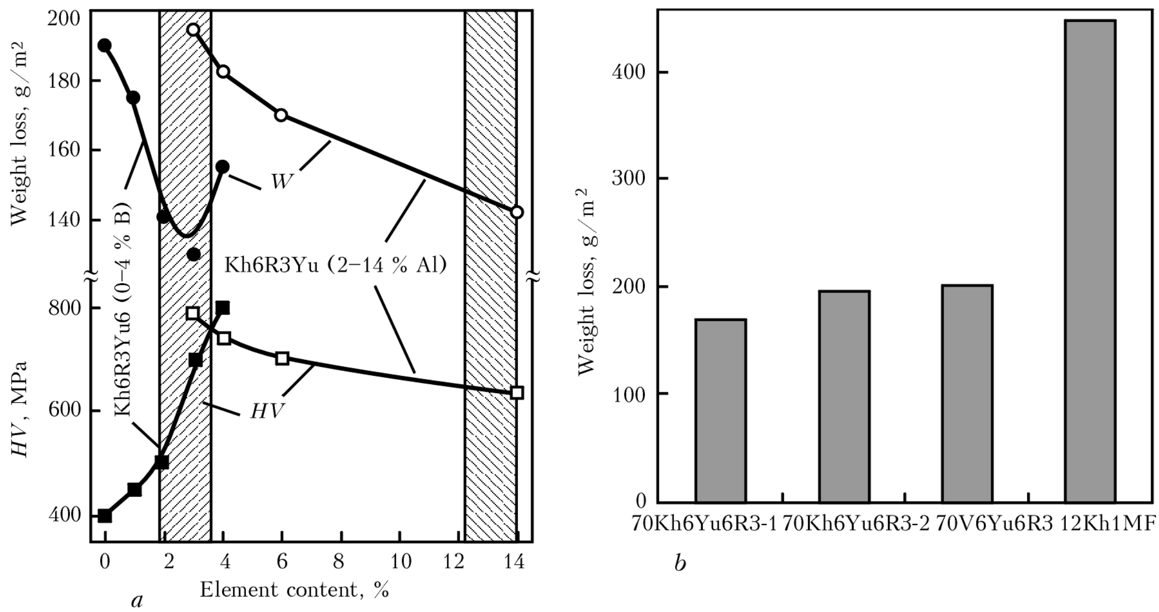

Figure 10. Influence of boron (Kh6R3Yu6 with 0–4 % B) and aluminium (Kh6R3Yu with 2–14 % Al) on hardness and gasoabrasive wear resistance *W* of coatings (*a*), and influence of FKhB (70Kh6Yu6R3-1) and B_4C (70Kh6Yu6R3-2) master alloys in FCW charge on gasoabrasive wear (*b*)

mation in the less hard coating lamels. With increase of testing temperature above 350–400 °C steel wear resistance drops abruptly, and that of the coating rises — to a greater extent for coatings with lower aluminium content. This is related to lowering of tensile stresses in the coatings as a result of interlamellar oxidation of microcracks and their filling by gas corrosion products, which increase the coating volume, leading to lowering of tensile stresses and their transformation into compressive stress. Therefore, a more significant lowering of tensile stresses is observed in coatings with a ramified net of cracks due to additional filling of microcracks by oxides.

However, gasoabrasive wear resistance also depends on morphology of oxide film, which forms on coating surface. Monolithic oxide film $(FeAl)_2O_3$ forms on the surface of coatings with 14 wt.% Al, which ensures 4 times higher wear resistance than in 12Kh1MF steel and 30 % higher value than for coating from FCW Kh6R3Yu2.

Gasoabrasive wear resistance of coating from FCW Kh6R3Yu14 was compared with that of coatings spray-deposited from EndoTec DO 390N, Praxair and TAFA 95MXC FCW alloyed by a large amount of chromium, molybdenum and niobium, which were used for structure protection from gasoabrasive wear (see Figure 11).

Such FCW also have a higher content of boron and carbon, that ensures coating hardness on the level of *HV* 1100–1200. This causes microcracking in the coatings at their spraying. High content of alloying elements (chromium, molybdenum, vanadium) in these coatings essentially slows

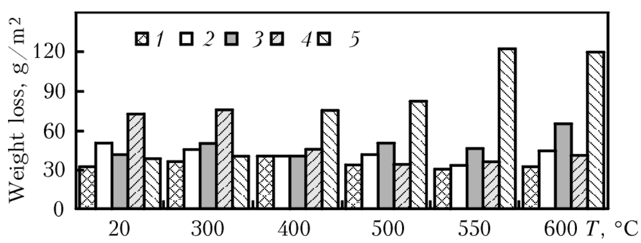

Figure 11. Influence of testing temperature on gasoabrasive wear resistance of various coatings from 12Kh1MF steel: *1* — Kh6R3Yu14; *2* — Kh29R4S2G2; *3* — 500Kh20R5M10 V10B10G5S2; *4* — Kh30M15Yu4; *5* — 12Kh1MF

down their inner interlamellar oxidation. For this reason, tensile stresses in the coating do not essentially decrease with time, as it takes place in the less alloyed coatings, and, therefore, their gasoabrasive wear resistance is much lower than that in the coating from FCW Kh6R3Yu14.

Coatings from FCW ensure a high wear resistance under two conditions. First, FCW charge should contain such alloying elements, which cause dispersion hardening in the coating structure. Secondly, such a content of chromium and aluminium in the coating should be provided as to create the prerequisites for inner interlamellar oxidation at an optimum rate of 0.5 g/(m^2·h) (Figure 12) and, therefore, achieve the transformation of tensile stresses into compressive stresses and formation of a continuous strong oxide film $(FeAl)_2O_3$ on coating surface.

Coatings from FCW studied in this paper, have passed production trials and are applied for protection of economizer and shield pipes from gasoabrasive wear in Burshtin TPS, as well as in Polish thermal power stations.

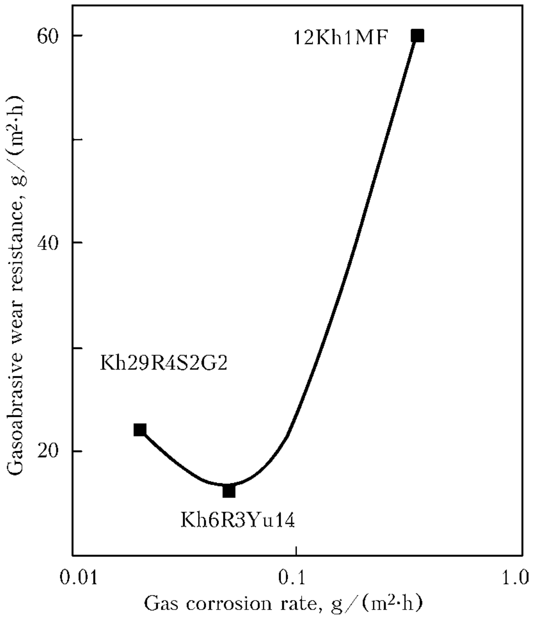

Figure 12. Influence of gas corrosion rate on gasoabrasive wear resistance of coatings and 12Kh1MF steel (testing temperature of 600 °C)

Conclusions

1. Procedure of investigation of gasoabrasvie wear of coatings was improved. It simulates the operation of TPS boilers as close as possible, allows eliminating edge effects, which arise as a result of coating tearing off on the edges of samples by an abrasive jet, and avoiding uncontrolled increment of sample mass due to oxidation of their non-sprayed surfaces at elevated temperatures.

2. To determine the modulus of elasticity of the coating by three-point bending method, a procedure of making beam samples from uncoated material without a substrate was proposed. Dependence of variation of modulus of elasticity of electric arc sprayed coatings of Fe–Cr–B–Al system on temperature and soaking time was established. It is shown that the modulus of elasticity of the coatings is directly proportional to the amount of oxide phase, formed under the conditions of long-term soaking at elevated temperatures.

3. It is also shown that gasoabrasive wear resistance of coatings from FCW depends on coating hardness, stresses of the first kind in the coating and on the type of oxide film, which forms at elevated temperature during testing.

4. High resistance to gasoabrasive wear is demonstrated by coatings, in which tensile stresses are transformed into compressive stresses as a result of the process of inner interlamellar oxidation during isothermal soaking at testing temperatures of 400–600 °C, that leads to increase of coating volume, and of its cohesion strength as a result of its reinforcement by interlamellar films of 100–150 nm thickness.

5. A connection between the morphology of surface oxide films and coating gasoabrasive wear resistance is established and it is found that high resistance to gasoabrasive wear is demonstrated by coatings, forming a dense film of iron oxide alloyed by aluminium.

6. A new composition of FCW Kh6R3Yu14 was developed for deposition of high-temperature coatings capable of dispersion strengthening in operation and improving the wear resistance of 12Kh1MF steel 12 to 14 times, and its gasoabrasive wear resistance by 2.5–4 times.

1. Korobov, Yu.S., Lukanin, V.L., Pryadko, A.S. et al. (2002) Advantage of activated arc metallizing. *Svarshchik*, **2**, 16–17.
2. Borisova, A.L., Mits, I.V., Kajda, T.V. et al. (1991) Structure and properties of electric-arc sprayed ferro-boron-based coatings obtained from flux-cored wires. *Avtomatich. Svarka*, **9**, 66–68.
3. Borisov, Yu.S., Korzhik, V.N. (1995) Amorphous thermal spray coatings: Theory and practice. *Ibid*., **4**, 3–12.
4. Borisov, Yu.S., Koziakov, I.A., Korzhik, V.N. (1996) Structure and properties of thermal spray coatings made using flux-cored wires of Fe–Cr–B, Fe–Cr–B–C system. *Ibid*., **5**, 21–24.
5. Pokhmursky, V.I., Student, M.M., Dovgunyk, V.M. et al. (2005) *Reconditioning and protective electric-arc sprayed coatings*. Lviv: H.V. Karpenka PhMI.
6. Pokhmurska, H., Wielage, B., Grund, T. et al. (2008) Arc-sprayed coatings obtained from iron based cored wires under high-temperature abrasive wear conditions. In: *Proc. of Int. Thermal Spray Conf.*, 338–341.
7. Student, M.M., Pokhmurska, H.V., Hvozdetskyi, V.V. et al. (2009) Effect of high-temperature corrosion on the gas-abrasive resistance of electric-arc coatings. *Materials Sci*., 45(**4**), 481–489.
8. Dallaire, C.S., Levert, H., Legoux, J.-G. (2001) Erosion resistance of arc-sprayed coatings to iron ore at 25 and 315 °C. *J. Thermal Spray Techn.*, **10**, 337–350.
9. Branagan, D.J., Swank, W.D., Haggard, D.C. et al. (2001) Wear resistant amorphous and nanocomposite steel coatings. *Met. and Mater. Trans. A*, 32(**10**), 2615–2621.
10. Branagan, D.J., Alman, D.E., Newrick, J.W. (2001) Devitrified nanocomposite steel powder. In: *Powder metallurgy alloys and particulate materials for industrial application*. Warrendale, PA: Minerals, Metals and Mater. Soc., 111–122.
11. Branagan, D.J., Tang, Y. (2002) Developing extreme hardness (>15 GPa) in iron-based nanocomposites. *Composites*, **6**, 855–859.
12. Badish, E., Katsich, C., Winkelmann, H. et al. (2010) Wear behaviour of hardfaced Fe–Cr–C alloy and austenitic steel under 2-body and 3-body conditions at elevated temperature. *Tribology Int.*, **2**, 214–228.
13. Babichev, M.A. (1955) *Methods for determination of internal stresses in machine parts*. Moscow: AN SSSR.

Received 24.01.2013

APPLICATION OF INDUCTION HEAT TREATMENT TO PROVIDE CORROSION RESISTANCE OF STAINLESS STEEL WELDED PIPES

E.A. PANTELEJMONOV and **L.I. NYRKOVA**
E.O. Paton Electric Welding Institute, NASU
11 Bozhenko Str., 03680, Kiev, Ukraine. E-mail: office@paton.kiev.ua

The effect of induction heat treatment using currents with a frequency of 2.4 kHz on corrosion resistance of ∅85.6 × 0.6 and 142.9 × 0.9 mm welded pipes, made from chrome-nickel stainless steel 1.4301, at different proportions of heat treatment temperatures, heating rate, time of holding at the heat treatment temperature and cooling conditions was investigated. The use was made of specimens of the pipes after heating in single-turn inductors, as well as specimens of the long pipes that passed under current the entire length of the through-type multiple-turn inductors. The heat treatment parameters were chosen on the basis of their possible implementation in lines for production of thin-walled welded pipes at welding speeds of up to 0.063 m/s. It was shown that the heat treatment of the welded pipes in a temperature range of 700–770 °C, at heating rates of up to 47.7 °C/s and cooling rates of up to 12.5 °C/s leads to improvement of their corrosion cracking resistance, and does not deteriorate their intercrystalline and pitting corrosion resistance. 10 Ref., 1 Table, 4 Figures.

Keywords: *welded pipes, corrosion-resistant steel, heat treatment of pipes, corrosion cracking*

Small- and medium-diameter welded pipes made from corrosion-resistant steels of the austenitic grade are widely applied in oil and gas industries, as well as in heating and water supply systems. The low content of carbon in the steels decreases their sensitivity to pitting corrosion (PC) and intercrystalline corrosion (ICC) under the effect of environment [1]. The steels are characterised by satisfactory values of strength and toughness, and by good weldability. However, the technological operations of forming of an initial strip into a tubular billet, local heating of edges in welding and application of stiffeners, which are characteristic of production of welded pipes, lead to a change in structure and properties of the pipe metal. Formation of ferritic and martensitic phases, in addition to austenite, causes the probability of ICC or stress corrosion cracking (CC) [2].

Heat treatment (HT) is applied to provide maximal toughness and corrosion resistance, and to eliminate physical heterogeneity of pipes. The pipes are heated in furnaces with a controlled atmosphere, or in a conventional atmosphere followed by removal of scale. In particular, heating of the 08Kh18N10 steel pipes in a temperature range of 750–900 °C at a low holding and reduction of the heating time does not lead to a marked improvement of the CC resistance [3, 4]. At the same time, to achieve the highest resistance of pipes to ICC it is necessary to avoid the temperature of the beginning of intensive oxidation of steel. For steel 08Kh18N10 this temperature is 800–870 °C [5].

The time of heating of the pipes can be reduced by using the technology for induction heating with high-frequency currents. Generation of energy directly into the pipe metal provides a high heating rate in a range of the phase transformation temperatures that prevent growth of the austenite grain. Conditions for elimination of heterogeneity of volumetric changes can be created at an optimal proportion of the current frequency and pipe wall thickness. One of the advantages of the technology is the possibility of implementing it by the continuous-sequential method in welded pipe production lines [6–8]. A thin layer of oxides forming on the pipe surfaces at high heating rates can be readily removed. The induction equipment and automation means allow the specified HT parameters to be maintained at a high accuracy.

This study was performed to investigate the effect of induction HT using the 2.4 kHz frequency currents on corrosion resistance of welded pipes measuring ∅85.6 × 0.6 and 142.9 × × 0.9 mm, made from chrome-nickel stainless steel 1.4301. The efficiency of HT was estimated from the results of tests of the pipe specimens to the sensitivity to CC, ICC and PC.

Steel 1.4301, which is a close analogue of steel 08Kh18N10, belongs to non-ferromagnetic materials with relative magnetic permeability $\mu = 1$.

Characteristics of inductors and ranges of variations in parameters of HT of pipe specimens

Type of inductor	Parameter	Pipe size, mm	
		∅85.6 × 0.6	∅142.9 × 0.9
Single-turn	Length of current conductor, mm	95	120
	Diameter of current conductor (internal), mm	100	160
	Current frequency, kHz	2.1–2.3	2.0–2.2
	Transformation coefficient of matching transformer	22/1	22/1
	Compensating capacity, μF	85.6	116.0
	HT temperature, °C	440–950	500–1150
	Heating rate, °C/s	20.0–47.5	18.5–32.8
	Cooling rate, °C/s	1.75–4.81	1.54–12.50
	Holding at HT temperature, s	0–60	0–60
	Speed of pipes (expected), m/s	0.026–0.063	0.025–0.043
Through-type multiple-turn	Length of current conductor, mm	640	620
	Diameter of current conductor (internal), mm	120	170
	Quantity of current conductor turns	22	21
	Current frequency, kHz	1.95–2.10	1.92–2.05
	Transformation coefficient of matching transformer	13/4	13/4
	Compensating capacity, μF	66.0	52.3
	HT temperature, °C	540–850	500–780
	Heating rate, °C/s	7.2–10.0	8.1–11.3
	Cooling rate, °C/s	1.59–3.90	1.2–4.8
	Holding at HT temperature, s	10–20	15–20
	Speed of pipes (expected), m/s	0.0092	0.0083–0.014

The recommended current frequency for through heating of hollow cylindrical billets with an external diameter of up to 150 mm and wall thickness of up to 1 mm, made from the materials with $\mu = 1$, ranges from 0.5 to 8.0 kHz [9, 10]. At a current frequency of 2.4 kHz the depth of penetration of the current into the steel exceeds the pipe wall thickness. It can be assumed that the power through the pipe wall thickness is distributed uniformly, this leading to decrease in internal stresses.

Investigated were the pipe specimens after heating in single-turn inductors, as well as the specimens of long pipes that passed under the current along the entire length of through-type multiple-turn inductors. The frequency converter with a power of 160 kW and a rated frequency of 2.4 kHz, fitted with the transformer circuit for matching the converter with a load, was used as an induction heating source. Characteristics of the inductors and ranges of variations in parameters of HT of the pipe specimens are given in the Table. The effect of the HT temperature in a range of 440–750 °C, heating rate, time of holding at the HT temperature, cooling conditions and speed of movement of the pipes in the through-type inductors was evaluated. The working frequency of the heating source ranged from 1.95 to 2.30 kHz. Parameters of HT of the pipe specimens in the single-turn inductors, which are indicated in the Table, allow evaluating the expected parameters of HT of the long pipes in the through-type inductors. In particular, at a temperature of 750 °C, through-type inductor length of 1 m and heating rates of 18.5–47.5 °C/s the expected speed of the ∅85.6 × 0.6 and 142.9 × × 0.9 mm pipes in the through-type inductors will be 1.6–3.8 and 1.5–2.6 m/min, respectively.

Complex resistance of the single-turn inductors changes only insignificantly in heating of short specimens in these inductors. Some difference was observed in the dynamics of heating of specimens in the single-turn and through-type inductors. After the heating source reaches the specified power, the rate of heating of a specimen in the single-turn inductor remained unchanged during the entire heating time (Figure 1). A change in the heating rate was achieved by changing the specified power of the heating source. After switching off of the heating source upon reaching the HT temperature the time of natural holding of the specimens at the HT temperature did not exceed 3–5 s. Adjustment of the power of the heating source was applied to form a longer holding. In heating of the long pipes at their constant movement speed, the rate of heating of the specimens increased as they moved in the through-type inductors. A change in the HT temperature was achieved by changing the proportion of the pipe movement speed and power of the heating source. After the pipe specimens left the inductor-affected zone, the time of natural holding at the HT temperature amounted to 20 s. Forced air cooling of the pipes (fan productivity of 2700 m^3/h) at the exit of the through-type inductors was used to reduce the holding time. In particular, when heating the ∅85.6 × × 0.6 mm pipe to a temperature of 650–660 °C at their speed of 0.0092 m/s, the forced air cooling of the pipes led to reduction of the holding time from 20 to 10 s.

The CC resistance tests of the pipes were carried out in compliance with requirements of GOST 26294–84 «Welded Joints. Corrosion Cracking Test Methods». The pipe specimens in the initial state and after HT were held in 42 % solution of $MgCl_2$ at a boiling temperature of 154 °C. Formation of corrosion cracks was checked every 4–5 h. The CC resistance criterion was the time to formation of the first corrosion crack.

No corrosion cracks formed during the test time of 80 h after HT in the single-turn inductor (Figure 2) of the ∅85.6 × 0.6 mm pipe specimens at a temperature of 770–1070 °C, heating rate of 41.0–56.3 °C/s and natural cooling rate of 3.91–4.96 °C/s. The corrosion cracks appeared 10–66 h after HT of the pipe specimens in a temperature range of 440–640 °C at a heating rate of 20.0–39.2 °C/s, without holding, and at a natural cooling rate of 1.75–2.83 °C/s. No corrosion cracks were detected on the ∅142.9 × × 0.9 mm pipe specimens at the following HT parameters:

- 650–1100 °C temperature, 7.1–27.7 °C/s heating rate, without holding, 2.3–6.6 °C/s natural cooling rate;
- 1000 °C temperature, 6.4 °C/s heating rate, without holding, 9.3–12.5 °C/s forced air cooling rate;
- 960–1050 °C temperature, 6.7 and 29.1 °C/s heating rate, holding for 60 s, 5.36–5.50 °C/s natural cooling rate;
- 1100–1150 °C temperature, 7.1 and 32.8 °C/s heating rate, holding for 60 s, 10.7–12.1 °C/s forced air cooling rate.

It should be noted that no corrosion cracks were detected on the ∅142.9 × 0.9 mm pipe specimens at the heating rates varied within 6.4–7.1 and 18.5–32.8 °C/s, temperature of 960–1150 °C, cooling rates of 2.3–12.5 °C/s and holding for 60 s under the natural or forced air cooling conditions. Parameters of HT of such pipes in the single-turn inductors (960–1000 °C temperature, 23.8–29.1 °C/s heating rate, 5.18–5.50 °C/s natural cooling rate) corresponded to parameters of HT of the long pipes, 650 mm long, in the through-type inductors at their speed of about 0.025 m/s.

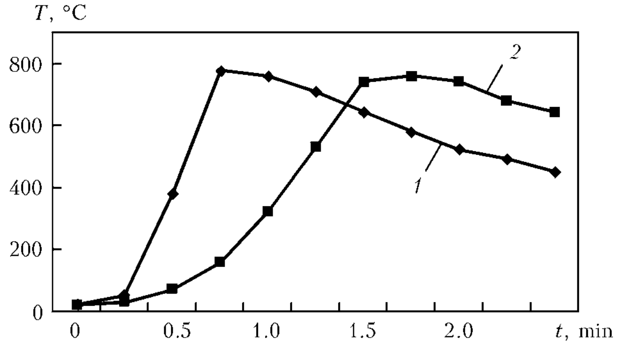

Figure 1. Dynamics of variations in temperature of pipe specimens during heating in single-turn (*1*) and through-type (*2*) inductors

The corrosion cracks formed on the ∅142.9 × × 0.9 mm pipe specimens (see Figure 2) 10–66 h after HT in a temperature range of 500–600 °C, at heating rates of 21.7–25.0 °C/s, without holding, and at natural cooling rates of 1.54–2 °C/s.

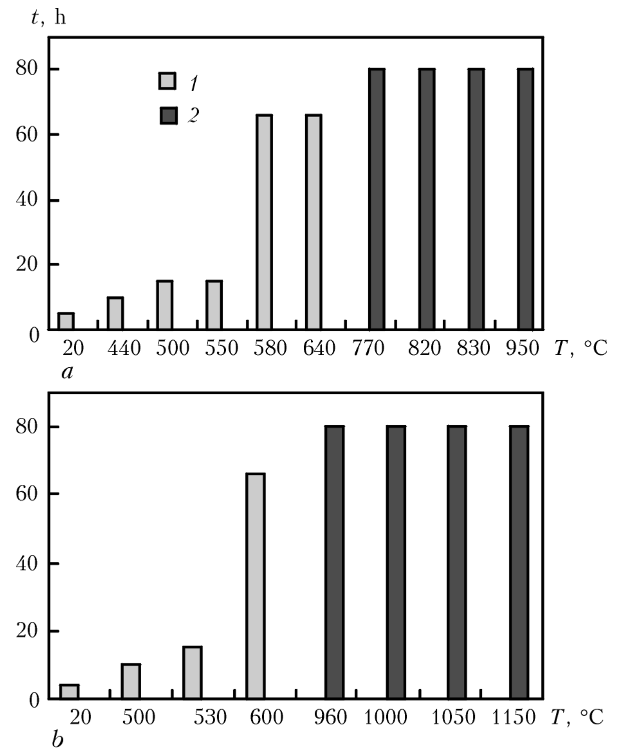

Figure 2. Dependence of time to formation of corrosion cracks on temperature of HT of the ∅85.6 × 0.6 (*a*) and 142.9 × 0.9 (*b*) mm pipe specimens heated in single-turn inductors: *1* — presence of cracks; *2* — absence of cracks

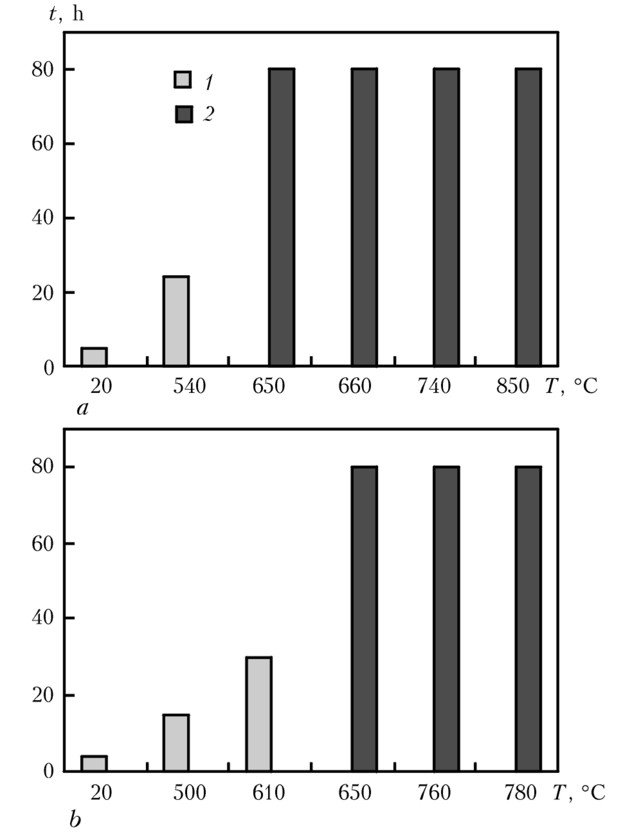

Figure 3. Dependence of time to formation of corrosion cracks on temperature of HT of the ∅85.6 × 0.6 (*a*) and 142.9 × 0.9 (*b*) mm long pipe specimens heated in through-type inductors: *1* — presence of cracks; *2* — absence of cracks

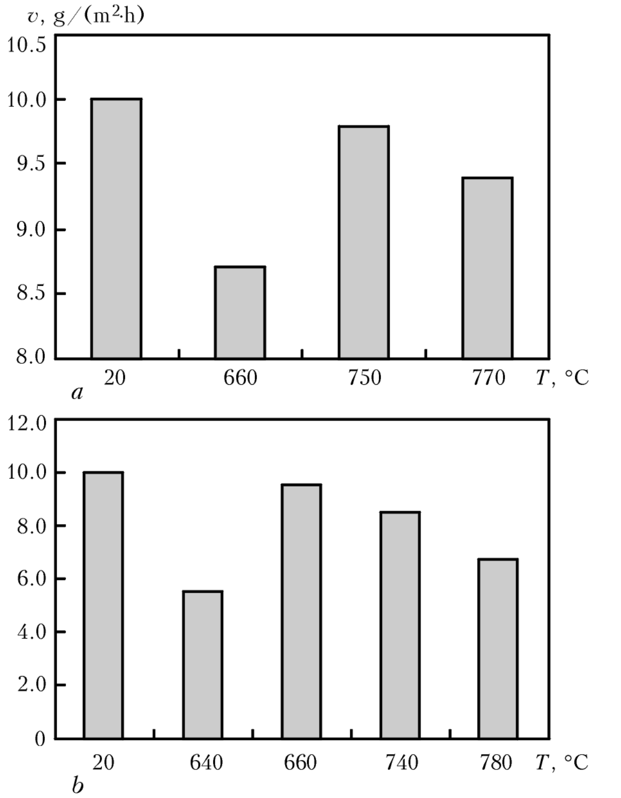

Figure 4. Effect of HT temperature on conditional average rate of PC of the ∅85.6 × 0.6 (*a*) and 142.9 × 0.9 (*b*) mm pipe specimens

On the ∅85.6 × 0.6 and 142.9 × 0.9 mm pipe specimens, which were not subjected to HT, the corrosion cracks appeared after 5 and 4 h, respectively. Therefore, the minimal temperature of HT of the ∅85.6 × 0.6 and 142.9 × 0.9 mm pipe specimens after heating in the single-turn inductors, above which no corrosion cracks formed, is 770 and 650 °C, respectively.

On the ∅85.6 × 0.6 mm, long pipe specimens the corrosion cracks formed 24 h after HT in the through-type inductor at a temperature of 540 °C, heating rate of 7.2 °C/s, natural cooling rate of 1.85 °C/s, and speed of 0.0092 m/s (Figure 3). The corrosion cracks did not form after HT at a temperature above 650 °C. On the ∅142.9 × 0.9 mm, long pipe specimens the corrosion cracks formed 15–30 h after HT at temperatures of 500 and 610 °C, heating rates of 8.7 and 8.1 °C/s, forced air cooling rates of 1.2 and 2.7 °C/s, and speed of 0.014 m/s. As a rule, a crack initiated at the absence of pitting. Therefore, the corrosion cracks did not form after heating of the ∅142.9 × 0.9 mm, long pipe specimens above 650 °C.

The tests to ICC were carried out according to GOST 6032–89 «Corrosion-Resistant Steels and Alloys. Intercrystalline Corrosion Resistance Test Methods» (item 3). The ICC resistance criterion was the absence of fracture at the grain boundaries to a depth of more than 10 μm. The pipe specimens were held in a boiling aqueous solution of 13 % $CuSO_4$ + 12 % H_2SO_4 at the presence of metal copper. The time of holding was 24 ± 0.25 h. No fractures along the grain boundaries were detected on the pipe specimens both in the base metal and in the weld zone after HT in the single-turn and through-type inductors. This is indicative of the ICC resistance of the pipe specimens.

The PC resistance tests of the pipe specimens were carried out in compliance with requirements of GOST 9.912–89 «Corrosion-Resistant Steels and Alloys. Accelerated Pitting Corrosion Resistance Test Methods». Allowing for the total loss of weight of three identical pipe specimens after holding in the 10 % solution of $FeCl_3$ for 24 h, the conditional average rate of PC of the pipe specimens not subjected to HT was v = = 10 g/(m^2·h) (Figure 4). Pittings propagated in the base metal. Isolated pittings had a through character. The welds contained isolated part-through pittings. The pipe specimens after HT in the single-turn and through-type inductors at a temperature of up to 780 °C had v = 5.2–9.8 g/(m^2·h). The quantity of pittings on the base metal and in the weld decreased. Mostly the weld experienced PC. It can be considered that HT did not deteriorate the PC resistance of the investigated pipe specimens.

Conclusions

1. HT of welded pipes with a diameter of up to 150 mm and wall thickness of up to 1 mm, made from chrome-nickel stainless steel 1.4301, in a temperature range of 700–770 °C, at heating rates of up to 47.7 °C/s, cooling rates of up to 12.5 °C/s, and speed of movement of up to 0.063 m/s leads to increase in CC resistance of the pipes, and does not deteriorate their ICC and PC resistance.

2. It is recommended to use induction heating with the 2.4 kHz frequency currents to conduct HT of thin-walled pipes from corrosion-resistant steels in lines for production of pipes by the argon-arc, electron beam and laser welding methods.

1. Semzin, V.N., Shron, R.Z. (1978) *Heat treatment and properties of welded joints*. Leningrad: Mashinostroenie.
2. Gulyaev, G.I., Vojtselenok, S.L. (1978) *Quality of welded pipes*. Moscow: Metallurgiya.
3. Sokol, I.Ya., Ulianin, E.A., Feldgandler, E.G. et al. (1989) *Structure and corrosion of metals and alloys:* Refer. Book-Atlas. Moscow: Metallurgiya.
4. Gulyaev, A.P. (1963) *Metals science*. Moscow: Oborongiz.
5. Borodulin, G.M., Moshkevich, E.I. (1973) *Stainless steel*. Moscow: Metallurgiya.
6. Krotkova, O.V., Chervinsky, V.I., Ratnikova, A.I. et al. (2010) Development of technology and equipment for induction heat treatment of corrugated stainless steel pipes. *Indukts. Nagrev*, **3**, 27–34.
7. Golovin, G.F., Zimin, N.V. (1979) *Technology of heat treatment of metals using induction heating*. Leningrad: Mashinostroenie.
8. Krotkova, O.V., Polyakov, S.G., Pismenny, A.S. et al. (2011) Influence of induction heating on corrosion resistance of thin-walled chrome-nickel steel pipes. *Stal*, **3**, 57–60.
9. Slukhotsky, A.E., Ryskin, S.E. (1974) *Inductors for induction heating*. Leningrad: Energiya.
10. (1980) *Thermal-electric equipment:* Refer. Book. Ed. by A.P. Altgauzen. Moscow: Energiya.

Received 01.04.2013

APPLICATION OF AUTOMATIC ORBITAL WELDING IN MANUFACTURE OF HOUSINGS OF NEUTRON MEASUREMENT CHANNELS OF NUCLEAR REACTORS

N.M. MAKHLIN[1], **V.E. POPOV**[1], **N.S. FEDORENKO**[1], **A.V. BURBA**[1], **V.M. PYSHNY**[2], **V.A. DYUKOV**[3] and **V.B. GONTAREV**[3]

[1]SE REC WCPE of the E.O. Paton Electric Welding Institute, NASU
11 Bozhenko Str., 03680, Kiev, Ukraine. E-mail: techno@paton.kiev.ua
[2]SE NNEGC «Energoatom»
3 Vetrova Str., 01032, Kiev, Ukraine. E-mail: 1.kizmenko@direkcy.atom.gov.ua
[3]SS «Energoeffektivnost» of NNEGC «Energoatom»
59 L. Tolstogo Str., 01032, Kiev, Ukraine. E-mail: ee@eff.atom.gov.ua

Up to present time neutron measurement channels were mainly delivered in Ukraine from abroad. Therefore, problem of improvement of operating characteristics and mastering of domestic production of such channels is highly relevant. Application of automatic non-consumable electrode orbital welding was considered for obtaining of welded joints of elements of housings neutron measurement channel of being one of the most important elements of the system of in-pipe measurements of nuclear power units. Results of working through of technology of automatic GTA welding and optimum modes of performance of these joints using domestic modernized automatic machines for orbital welding ADTs 627 U3.1 and ADTs 625 U3.1 as well as technical characteristics of indicated automatic machines are given. Procedure of assembly for GTA welding of structural elements of housings of neutron measuring channels was described. Results of non-destructive testing, mechanical testing, metallographic investigations and tests to intercrystalline corrosion resistance of welded joints are submitted. It is shown that application of developed technologies and equipment allows mastering the domestic production of neutron measurement channels. 10 Ref., 3 Tables, 3 Figures.

Keywords: *automatic orbital welding, neutron measurement channels, nuclear reactors, spigot-and-socket joint, non-consumable electrode*

One of the main directions of development of modern nuclear power units (NPU) is intensifying of nuclear and heat processes by means of increase of neutron-flux density, temperature and pressure of coolant [1–3]. At the same time, the problems of increase of operating resource of NPU and providing of measures of safety and trouble-free operation are set that causes rise and complication of requirements to functional reliability and life time of systems of measurement, manipulation, protection and control of nuclear reactors being designed, constructed and under operation.

Light-water thermal neutron based reactors (PWR and BWR type), in which water is used as a coolant and moderator, obtained the highest application in world power engineering. Not less than 87 % of power units of nuclear power plants (NPP) of the whole world [1, 2] refers at present time to power units with such reactors. Tank water-water power reactors (WWER) being in operation at all 15 power units of four active NPP of Ukraine can also be related to reactors of PWR type. The same reactors are supposed to be used in future in development of new power units of Ukrainian NPP.

On-line inspection of reactivity and energy-release on height and radius of core in the WWER reactors is carried out by systems of in-pipe measurements, the most important elements of which are the neuron measurement channels (NMC) being immersed in the core (points of immersion are located on cross section). For example, application of 58–64 NMC is provided for the most wide-spread rector WWER-1000.

NMC is a helium-filled long-length (12.14 m) cylinder hollow hosing, inside the immersion part of which 7 neutron and from 1 to 3 (in some modifications of NMC) temperature detectors are installed.

Structurally NMC housing consists of nozzle *1*, penetration *3* and two transition inserts *2* and *4*, forming assembly part, as well as body *5*, pipe (or two pipes) *6*, *7* and tip *8* relating to immersed part of the housing (Figure 1). These elements of NMC housing have different external and internal diameters and being joined into single-

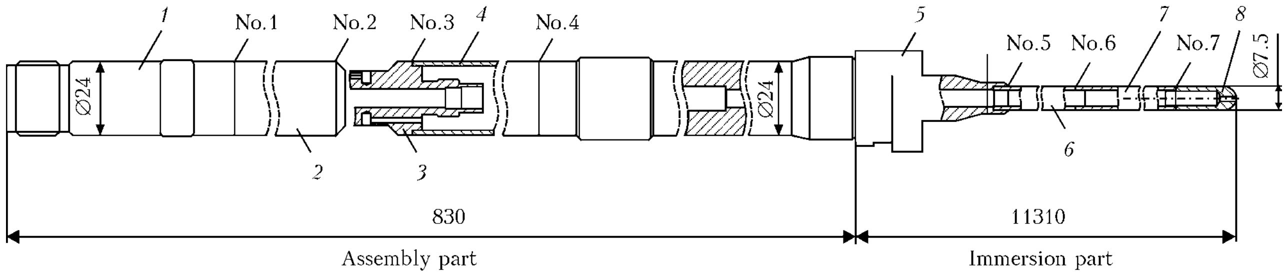

Figure 1. Scheme of NMC housing (for designations see the text)

structure of the housing with the help of welded joints.

Peculiarity of operating conditions of NMC in WWER-1000 reactors is simultaneous effect of neutron irradiation as well as high pressure (15.7–17.7 MPa) and temperature (330–350 °C) of environment. This predetermines the main requirements to NMC housing structure, its elements and welded joints, i.e. resistance to stress-corrosion cracking; vacuum tightness of welded joints and their mechanical strength (breaking force according to the existing requirements of not less than 4905 N or 500 kgf); life time of NMC — not less that 4 years (operating life of not less than 40,000 h). Mentioned requirements provide for application of 08Kh18N10T chromium-nickel steel of austenite grade (0.08C; 18Cr; 9Ni; 0.6Ti) as a structural material of NMC housing and all its structural elements.

Up to present time NMCs were delivered in Ukraine mainly from abroad, therefore, problem of improvement of their service characteristics (first of all safety indices) and mastering of domestic production of such channels is sufficiently relevant.

One of the possible ways of solution of this problem is an industrial application of technology of performance of welded joints of NMC housings by means of non-consumable orbital position butt welding in inert gases (GTAW) and technological fixture for realizing of these processes developed at SE Research-and-Engineer Center of Welding and Control in Power Engineering of Ukraine (REC WCPE) of the E.O. Paton Electric Welding Institute of the NAS of Ukraine together with Separated Subdivision «Energoeffektivnost» of SE NNEGC «Energoatom» (SS «Energoeffektivnost»).

Elaboration of GTAW technology for joints of elements of NMC housing was carried out using serially manufactured modernized automatic machines ADTs 627 U3.1 and ADTs 625 U3.1 for orbital position butt welding of pipelines [4] developed in REC WCPE, the specifications of which are given in Table 1.

Automatic machines ADTs 627 U3.1 and ADTs 625 U3.1 for orbital welding were made on a similar hardware basis, namely specialized multifunctional welding power source ITs 616 U3.1 of chopper type, control system consisting of controller block ITs 616.20.00.000 and remote control panel (operator panel) ITs 616.30.00.000 as well as ADTs 625.07.00.000 collector. The difference between the automatic machines lies only in welding heads of captive type ADTs 627.03.00.000 and ADTs 625.03.00.000, respectively.

Design of these automatic machines in operation mode «Setting» allows performing adjustment operations (regulation of extension of non-consumable electrode and its spatial orientation) before welding, choosing control method («Manual» or «Automatic»), preliminary setting of values of all main parameters of mode and cycle of welding.

In operation mode «Welding» they provide the set parameters of welding cycle in continuous mode, step-pulse or modulated current welding mode.

One of the peculiarities of modernized automatic machines ADTs 627 U3.1 and ADTs 625 U3.1 lies in that a control system of these automatic machines allows carrying out arc passes, following the first circumferential, preliminary continuously adjustment and setting (program) of $(0.5{-}1.0)I_w$ and $(1.0{-}2.0)v_w$ values (where I_w is the welding current, v_w is the welding speed) set after the first circumferential pass, that not only expand the technological capabilities of indicated automatic devices, but also allow efficiently performing the processes of multi-pass welding by means of autoshaping method or subsequent penetration.

Figure 2 shows an example of sequence diagram of GTAW process in continuous mode during performance of two circumferential arc passes (ADTs 625 U3.1 automatic machine was used).

The next peculiarity of modernized automatic machines ADTs 627 U3.1 and ADTs 625 U3.1 is that the control system allows automatic backspacing of direction of movement of face chuck of welding head in completing of each (except for the last one) or first two passes at more than two circumferential arc passes.

Table 1. Main technical characteristics of automatic machines ADTs 625 U3.1 and ADTs 627 U3.1

Parameter	ADTs 627 U3.1	ADTs 625 U3.1
Diameter of pipes being welded, mm	7–24	18–42
Smallest inter-pipe distance, mm	58	72
Ranges of welding current regulation, A:		
lower value	not more than 8	
upper value	not less than 260	
Ranges of arc voltage regulation, V	7–24	
Accuracy of maintaining of set value of welding current in oscillations of supply mains in the range of ±15 % of nominal and disturbances along arc length not more than ±2.5 mm from set value, %	±2	
Accuracy of maintaining of set value of arc voltage, V	±0.20	±0.15
Ranges of regulation of rotation speed of welding head face chuck (welding speed), rpm (m/h)	0.3–10.8 (0.42–15.2; 1.36–48.8)	0.5–10.0 (1.7–33.9; 4–79)
Number of arc circumferential passes	1–4	
Nominal diameter of tungsten electrode (VL, BI or BT type), mm	1.6	2.0; 3.0
Largest radial movement of torch, mm	15	16
Largest movement of torch across the butt, mm	±1	±5
Ranges of duration regulation, s:		
gas blowing	5–25	
smooth rise of welding current	1–5	
«preheating» of welding place	1–5	
smooth drop of welding current	1–5	
Regulation of arc length	Mechanical follower	Automatic arc voltage regulation

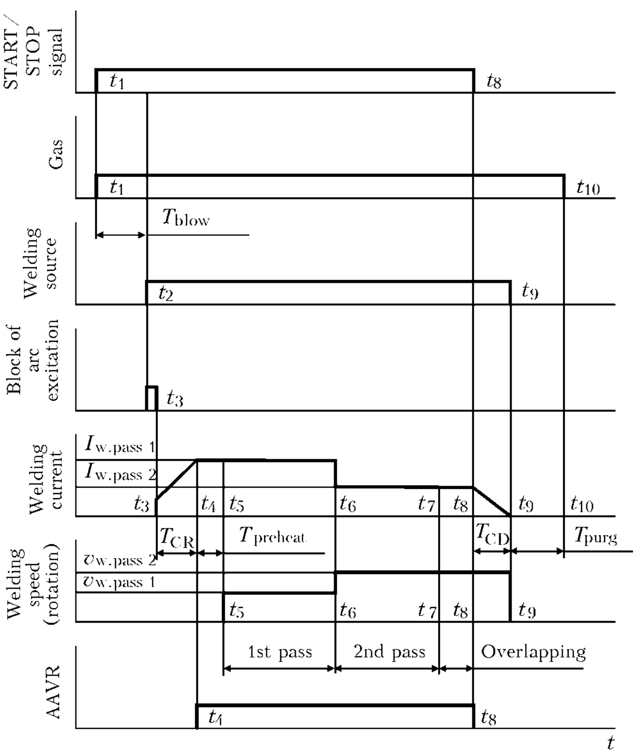

Figure 2. Sequence diagram of GTAW: T_{blow} — interval of time «gas before welding»; T_{CR} — duration of smooth rise of welding current; $T_{preheat}$ — interval of time of «preheating»; T_{CD} — duration of smooth drop of welding current («welding of crater»); T_{purg} — interval of time «gas after welding»

Besides, modernized automatic machines have one more peculiarity, namely capability to maintain the preliminary set values of parameters of welding mode having the most significant effect on quality of welded joints (welding current, arc voltage, speed of welding) in the process of welding with accuracy not worse that ±2.5 %.

Elaboration of technology for GTAW of joints of elements of NMC housing was carried out considering an experience of development of similar processes and their commercial application in manufacture of absorber inserts of containers of spent fuel storages [5] as well as earlier performed investigations in area of physical-chemical fundamentals of GTAW of thin-walled bodies of rotation [6, 7]. As a result the main factors making influence on quality of welded joints were found, determinative parameters of GTAW process of butt joints of thin-walled tubes were stated, ways for determination of ranges of welding modes providing high weld quality [8] were proposed and the most rational types of welded joints were recommended. Analysis of results and recommendations of these investigations, accumulated experience of application of GTAW of thin-walled parts, structural peculiarities of NMC housing and its elements and requirements made to them allowed making a conclusion that

Table 2. Schemes of assemblies of joints of NMC housing elements for GTAW

Joint	Type of joint
Nozzle *1* — insert *1* (weld No.1)	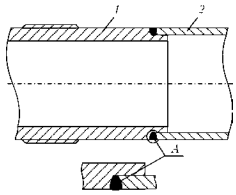
Insert *2* — penetration *3* (weld No.2)	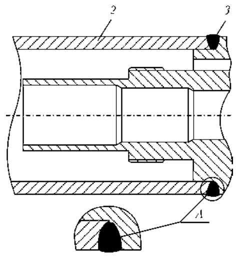
Penetration *3* — insert *4* (weld No.3)	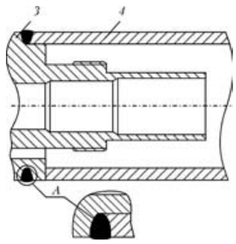
Insert *4* — body *5* (weld No.4)	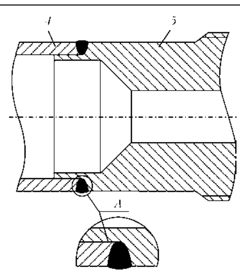
Body *5* — pipe *6* (weld No.5)	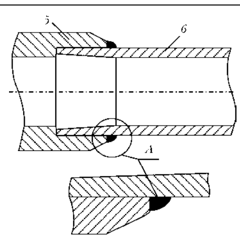
Pipe *6* — pipe *7* (weld No.6)	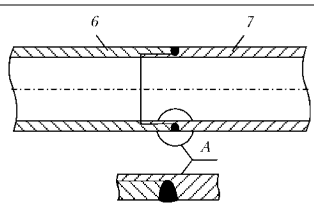
Pipe *7* — tip *8* (weld No.7)	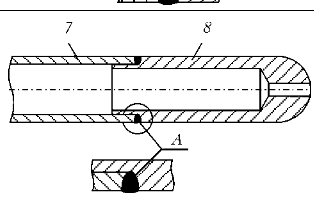

the spigot-and-socket type joints are the most reasonable for manufacture of NMC housing. Considering this, welded joints of NMC housing

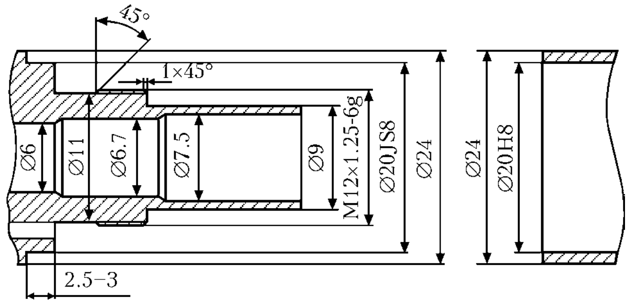

Figure 3. Scheme of joint preparation of NMC housing elements (weld No.3) for GTAW

elements (see Figure 1), i.e. nozzle *1* with insert *2* (weld No.1), penetration *3* with insert *2* (weld No.2) and insert *4* (weld No.3), insert *4* with body *5* (weld No.4), pipe *6* with pipe *7* (weld No.6) and pipe *7* with tip *8* (weld No.7), were worked though as spigot-and-socket ones and joining of pipe *6* with body *5* (weld No.5) as a lap joint of different thickness parts.

Ranges of optimum values of GTAW modes for joints of NMC housing were determined through performance of several series of test welding on full-size specimens (models) of elements of NMC housing. All the specimens were degreased during preparation to welding and joint assembly for welding was carried out in accordance to schemes, given in Table 2 and Figure 3; at that tight fit (class III, accuracy degree 8) of mating parts was provided.

Welding of joints of specimens of NMC housing elements was carried out with variation of main parameters of welding mode (welding current, arc voltage and length, welding speed) and parameters of welding cycle (time intervals «gas before welding», «preheating», «gas after welding»; duration of smooth of rise and drop of welding current), as well as consumption of inert gas (argon), corresponding to GOST 10157.

Test welding was carried out using welding head ADTs 627.03.00.000 in order to determine the ranges of optimum values of parameters of GTAW modes for joints of pipes between themselves (weld No.6), pipe to tip (weld No.7) and pipe to body (weld No.5). At that welding of weld No.6 was performed at normal orientation of axis of non-consumable electrode to longitudinal axis of butt joint, welding of welds Nos. 7 and 5 — at certain shifting (up to 0.5 mm) from the butt axis and electrode incidence at 15° angle (relatively to normal line) in the direction of lager heat sink in accordance to recommendations of [5, 7].

Welding head ADTs 625.03.00.000 with normal orientation of axis of non-consumable electrode to longitudinal axis of butt joint was used

Table 3. Main parameters of modes and cycles of single-pass GTAW of joints of NMC housing elements

Parameter	Joints of NMC housing elements						
	Nozzle–insert (weld No.1)	Insert–penetration (weld No.2)	Penetration–insert (weld No.3)	Insert–body (weld No.4)	Body–pipe (weld No.5)	Pipe–pipe (weld No.6)	Pipe–tip (weld No.7)
Diameter of tungsten electrode, mm	2.0				1.6		
Welding current, A	65–80				25–28	11–15	18–20
Arc voltage, V	9.0–10.5						
Arc length, mm	1.0±0.1						
Welding speed, m/h (rpm)	22.60–31.65 (5.66–7)				12.0–14.3 (8.5–10)	11–15 (7.8–10.6)	12–14.3 (8.5–10)
Duration, s:							
gas blowing	5–10						
smooth rice of welding current	1.0±0.2						
«preheating» of welding place	0.8±0.1				0.70±0.05	0.40±0.05	0.60±0.05
drop of welding current	4.0±0.5						
gas purging	8–18						
Consumption of shielding gas, l/min	6–7						
Note. Grade of tungsten electrode: VT, VI, VL on GOST 23949–80 or Abicor Binzel WT, WR, Wr-2D.							

for test welding of specimens of the rest joints of NMC housing.

Quality of joints obtained as a result of test welding was evaluated by means of non-destructive testing methods (visual-measurement method and leakage tests) as well as with the help of mechanical tests, metallographic investigations and tests to intercrystalline corrosion (ICC) resistance. Visual-measurement testing was carried out in accordance to normative documents [9] currently in force in area of power engineering with the help of micrometer gage, lens, binocular microscope (magnification 8–10) and corresponding templets. Leakage test was performed with the help of mass spectrometer and helium leak detector PTI-10 using method of vacuum chamber in accordance to the requirements and procedure given in [10]. Mechanical tests were carried out based on GOST 1497 on machine of ZDM-10 test type for spigot-and-socket joint of NMC housing with the smallest cross-section over the base metal (weld No.6).

It was determined as a result of the mechanical tests that breaking force for this joint makes not less that 4807 N (490 kgf) at penetration depth 40–50 % and not less than 11380 N (1160 kgf) at 90–100 % penetration depth. Metallographic investigations were carried out on macrosections (cut out from joints obtained by test welding) using metallographic microscope with 50–100 magnification. At that, depth of penetration, presence in metal of such defects as non-metallic inclusions, pores, wormhole and lacks of fusion, structure of weld metal and HAZ, dimensions of austenite grains were determined. Tests to ICC resistance of weld metal and HAZ were carried out on AMU method (GOST 6032).

Performance of several series of test welding of joints of elements of NMC housing, comprehensive quality testing of these joints and system analysis of obtained results allowed determining that constantly high quality of welded joints of elements is achieved in single-pass GTAW (values of the main parameters of welding modes and cycles should correspond to given in Table 3). It was also stated that feeding of inert gas (argon) inside the housing is necessary to be provided in performance of GTAW of any from indicated joints. Method for removal of such visible defects of welds as partial lack of penetration, single pores, unallowable nonuniformity of penetration (caused, mainly, by deviation of requirements on quality of preparation and assembly of parts for welding) was worked as well. It lies in performance of the second pass with the lower (in comparison with the first pass) values of welding current or with the higher welding speed.

Besides, it should be noted that presence of pipe-pipe joint (weld No.6) in NMC housing structure is not necessary. It should be performed only in the case of absence of one-piece pipe delivery.

«Energoeffektivnost» developed a set of technological fixture for providing of possibility of performance of GTAW of joints of NMC housing elements (in determination of ranges of optimum values of welding mode and cycle parameters). Testing of GTAW processes of NMC housing elements developed in REC WCPE on full-size models (experimental specimens) of NMC housings was also carried out in this organization under conditions close to industrial one. It showed that constantly high quality of welded joints is achieved in application of developed technology.

Conclusions

1. Technology of single-pass GTAW of joints of thin-walled different thickness bodies of rotation using ADTs 627 U3.1 and ADTs 625 U3.1 automatic machines for orbital welding was developed. It provides performance of high-quality spigot-and-socket joints of NMC housing elements.

2. Commercial application of developed GTAW technology and means of technological fixture allow manufacturing NMC and similar parts at domestic enterprises in volumes necessary for power engineering.

1. Cameron, I. (1987) *Nuclear reactors*. Moscow: Energoatomizdat.
2. Shirokov, S.V.(1993) *Physics of nuclear reactors*: Manual. Kyiv: Vyshcha Shkola.
3. Trofimov, N.A., Lappo, V.V. (1979) *Measurement of parameters of thermophysical processes in nuclear power engineering*. Moscow: Atomizdat.
4. Makhlin, N.M., Korotynsky, A.E., Bogdanovsky, V.A. et al. (2011) Single- and multioperator systems for automatic welding of position butt joints of nuclear power plant piping. *The Paton Welding J*., **11**, 28–36.
5. Bogdanovsky, V.A., Gavva, V.M., Makhlin, N.M. et al. (2011) Application of automatic orbital welding to fabricate absorbing inserts for spent nuclear fuel storage containers. *Ibid*., **12**, 34–37.
6. Ishchenko, Yu.S. (2002) Physical-technological principles of weld formation in arc welding process. In: *Welding in nuclear industry:* Transact. of NIKIMT. Moscow: IzdAT, Vol. 2, 204–240.
7. Bukarov, V.A. (2002) Technology of automatic shielded arc welding. *Ibid*., Vol. 1, 149–210.
8. Poloskov, S.I., Bukarov, V.A., Ishchenko, Yu.S. (2000) Influence of parameter deviations of argon-arc position butt welding on quality of welded joints. In: *Proc. of All-Russian Sci.-Techn. Conf*. (Moscow, Sept. 2000). Moscow: MEI, 22–25.
9. *PN AE G-7-016–89*: Unified procedure of control of base materials (semi-products) of welded joints and surfacing of equipment and pipelines of nuclear power plant. Visual and measuring control. Moscow: Energoatomizdat.
10. *PN AE G-7-019–89*: Unified procedure of control of base materials (semi-products) of welded joints and surfacing of equipment and pipelines of nuclear power plant. Control of tightness. Gas and liquid method. Moscow: Energoatomizdat.

Received 27.03.2013

AUTOMATIC SUBMERGED ARC SURFACING OF STRUCTURAL STEELS WITH TRANSVERSE HIGH-FREQUENCY MOVEMENTS OF ELECTRODE

Zh.G. GOLOBORODKO, S.V. DRAGAN and **I.V. SIMUTENKOV**
Admiral S.O. Makarov National Shipbuilding University
9, Geroev Stalingrada Ave, 54025, Nikolaev, Ukraine. E-mail: simutenkov@inbox.ru

Transverse oscillations of the electrode in automatic submerged arc surfacing are one of the ways of decrease in penetration depth and share of base metal in deposited one. These oscillations can be created by generating of high-frequency transverse pulsed movements of electrode wire using a specially designed electromechanical generator. The aim of this work is to evaluate the effect of high-frequency low-amplitude transverse pulsed movements of electrode wire on geometry of deposited bead and efficiency of the surfacing process. Deposition of beads was made on plates of low-carbon structural steel with electrode wire Sv-0.8A of 2 mm diameter under flux AN-348A. The pulsed electrode movements at 0.25–5 kHz frequency were generated along the surfacing direction. It was found that with increase in frequency the penetration depth of base metal and bead width are decreased, while the height of bead is increased, in addition the surfacing efficiency is also changed. The nature of change in the mentioned parameters depends on mode of pulsed effect on electrode wire, i.e. the presence or absence of resonance. The most significant change in geometry of the deposited bead is observed in the region of frequencies of the first resonance (0.55–0.75 kHz), namely depth of penetration and share of base metal in deposited one is 3 times decreased. The maximum increase in efficiency is occurred in the region of the second resonance (3.75–3.85 kHz), the coefficient of electrode melting is increased by 10–20 % as compared with surfacing without a pulsed effect. 10 Ref., 1 Table, 4 Figures.

Keywords: *automatic arc surfacing, low-carbon structural steels, high-frequency pulsed movement, mechanical generator, geometry of deposited bead*

The repair of worn-out parts of ship machines and mechanisms is often performed using the automatic submerged arc surfacing (ASAS) which provides, alongside with high efficiency, the required quality and homogeneity of the deposited layer. However, the depth of base metal penetration is increased and its share in deposited one amounts as a rule to 30–50 % [1]. The reduction of the mentioned characteristics of ASAS technology, preserving the high efficiency of the process, is a very urgent problem. To solve this problem, different methods of effect on the processes of electrode metal arc transfer or formation of weld pool are used allowing control the geometric parameters of the deposited bead and, consequently, the share of base metal (SBM) in the deposited layer. The most widely spread are the electric (pulsed-arc welding), mechanical (vibro-arc surfacing) and magnetic methods [2, 3].

It should be noted that the electric method envisages the application of complicated and expensive welding current sources with programming of condition parameters [4], magnetic method has some limitations connected with magnetic properties both of base metal and also electrode metal [5].

The listed drawbacks, in our opinion, are not typical of the mechanical method, characterized by simplicity in realization using the serial welding equipment. It is known that the pulsed feeding of electrode [6] or generation of transverse low-frequency (up to 150 Hz) oscillations of electrode [7] increase the arcing stability, improve the weld geometry and structure. High-frequency (500–1000 Hz) low-amplitude (about 130 μm) transverse pulsed movements of electrode contribute to reduction in penetration depth and SBM at ASAS as well [8]. In the latter case the effect is attained due to periodic forced removal of liquid-metal layer from electrode end at vibration effect allowing control of metal drop mass, transferred through the arc.

The aim of the present paper is to investigate the effect of transverse high-frequency pulsed movement of electrode on geometric characteristics of deposited bead and technological characteristics of process in single-arc ASAS of structural steels.

Generator of transverse high-frequency movements of electrode wire (EW) represents a mechanical drive (Figure 1), easily mounted on welding tractor with a wide range of pulsed effect frequency [8].

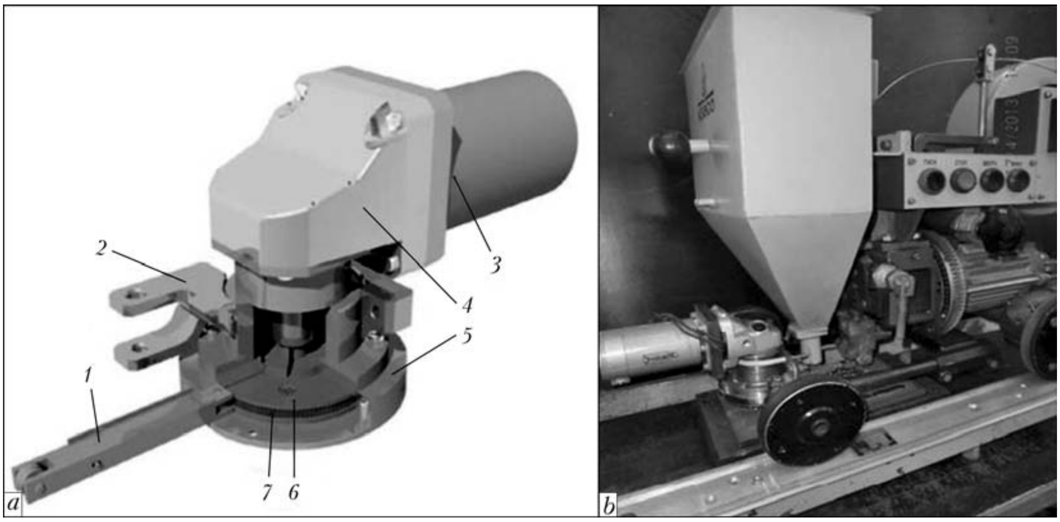

Figure 1. Design of generator of high-frequency pulsed movements of electrode (*a*) and its mounting on welding tractor (*b*): *1* — striker; *2* — fastening bracket; *3* — electric motor; *4* — reduction gear; *5* — body; *6* — driven washer; *7* — set-up rollers

The pulsed effect on EW leads to transverse oscillations of its end in two modes: interresonance and resonance. Within the region of frequencies close to resonance, the amplitude of oscillations is abruptly increased, due to which the geometry of deposited bead can significantly change. The resonance frequency, at which the frequencies of pulsed effect and natural oscillations of EW coincide, can be presented in the form of [9]

$$f_{oi} = \frac{d_e}{8\pi}\left(\frac{E}{\gamma}\right)^{0.5}\left(\frac{p_i}{l_s}\right)^2,$$

where d_e, E, γ are the diameter, elasticity modulus and density of EW metal, respectively; $p_i = kl_s$ are the roots of frequency equation determined by nature of fixation of rod end subjected to oscillations, i.e. by scheme of EW fixation in current conductor; l_s is the stickout length; is the Krylov function.

The current conductors, mostly widely used in serial tractors for ASAS, can be conditionally combined into two calculation schemes, realizing hinged (Figure 2, *a*) or rigid (Figure 2, *b*) fixation of electrode. The values of the first two roots of the frequency equation, respectively for the scheme presented in Figure 2, *a* are equal $p_1 = 3.9266$ and $p_2 = 7.0685$, and for scheme in Figure 2, *k*, $p_1 = 1.8751$ and $p_2 = 4.6941$ [10].

It is possible to control the resonance frequency according to above-given equation by change in stickout length or nature of electrode fixation in current conductors. Thus, in the range of 100–1000 Hz frequencies the resonance oscillations for electrode diameter $d_e = 2$ mm take place at stickout length $l_s = 25$–80 mm, and for $d_e = 5$ mm, respectively, at $l_s = 40$–150 mm. In this case the increase in stickout length and rigidity of electrode fixation in current conductor leads to reduction in resonance frequency.

The drawback of method of metal arc transfer process control with applying the resonance phenomenon is the discrete change in resonance frequencies.

In the interresonance mode of pulsed effect it is possible to control smoothly the amplitude of electrode end oscillations in narrow range (1–3 mm) either by increase in stickout length l_s or by decrease in arm h_f of force applying $F(t)_p$. However, the length of electrode stickout is determined, as a rule, in selection of parameters of surfacing conditions and cannot be freely changed, and arm h_f is limited by value of bending moment, causing the plastic deforming of EW [8].

It is sufficiently simply to control the amplitude of EW end oscillation by changing the frequency of pulsed effect. With increase in frequency the speed and acceleration of transmission link (generator striker) are increased, thus lead-

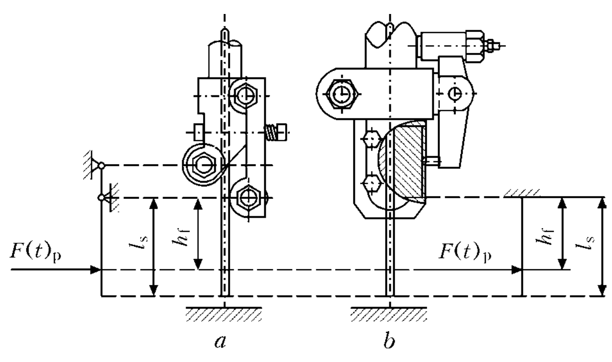

Figure 2. Designs of current conductor and appropriate calculation schemes of applying the force of pulsed effect $F(t)_p$ with continuous (*a*) and discrete (*b*) compensation of wear: h_f — arm of $F(t)_p$ force applying

Effect of frequency of pulsed movements of electrode at ASAS on formation of bead, SBM and coefficient of melting

Frequency f, Hz	Macrosection of deposited bead	SBM	K_m, g/(A·h)
0	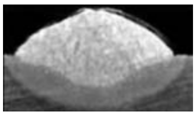	0.36	15.4
680 (f_{r1})	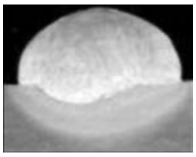	0.13	16.9
1295	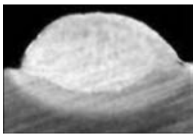	0.30	15.0
3820 (f_{r2})	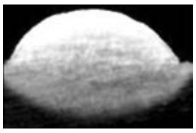	0.22	18.6
5800	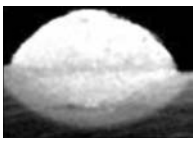	0.25	16.1

ing to increase in inertial component of force $F(t)_p$.

This assumption was confirmed by the results of a special experimental investigation. During experiments the length of trace, remained on the sample of plastic material, was measured by oscillating sharpened end of EW. It was found (Figure 3) that with increase in frequency of pulsed effect the amplitude of oscillations is increased by parabolic law (see dashed line in Figure). Moreover, at frequencies close to resonance for the given stickout of EW, the abrupt increase in amplitude of oscillations is observed.

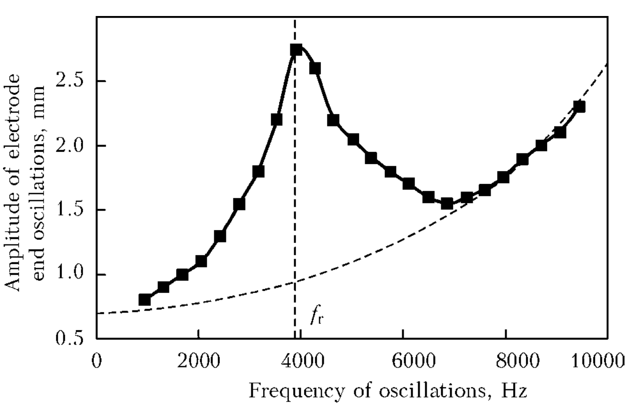

Figure 3. Effect of frequency on amplitude of oscillations of 2 mm diameter EW end: f_r — resonance frequency

The amplitude of oscillations of electrode end can be adjusted by two methods: step-wise by change in mass of generator striker or value of its movement in a pulse, as well as smoothly by varying the frequency of rotation of driven electric motor shaft.

The effect of transverse high-frequency pulsed movements of electrode on geometric characteristics of deposited bead was evaluated from results of investigations made on experimental stand (see Figure 1, *b*), equipped by welding tractor KA-001 with a generator of high-frequency pulsed movements of electrode and power source KIU-501.

Bead depositing was made by EW Sv-08A of 2 mm diameter under flux AN-348A on 10 mm thick plate of low-carbon structural steel St3sp (killed). In experiments only frequency of pulsed effect was varied, remaining other parameters of welding conditions unchanged. Stability of welding process, recorded by electron USB-oscillograph IRIS, was evaluated from oscillograms of arc voltage. Geometric parameters of deposited beads, area of penetration and surfacing, and SBM were determined from macrosections.

Below the results are presented, corresponding to pulsed effect on EW along the surfacing direction. It was found that with increase in frequency of pulses the bead width and depth of penetration of base metal are decreased, and bead height is increased (Figure 4).

The nature of the above-mentioned parameters depends on mode of pulsed effect on EW, i.e. the presence or absence of resonance. At the resonance condition the «extremal» change in bead geometry with appropriate change in SBM is observed (Table).

Maximum effect was attained at main tone (first resonance) of oscillating system within the

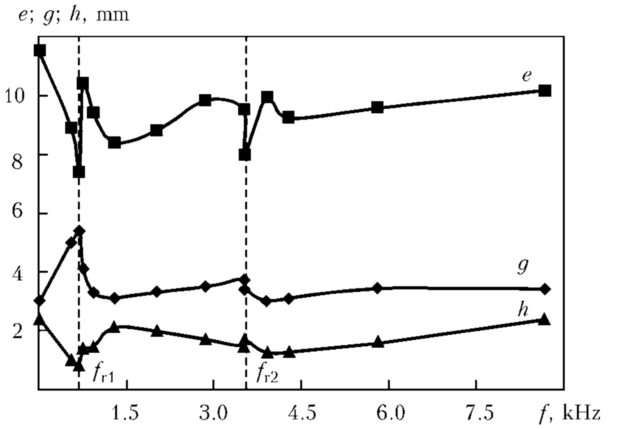

Figure 4. Effect of frequency of pulsed movements of electrode on geometric parameters e, g and h of deposited bead at d_e = 2 mm, I = 200 A, v_w = 19 m/h, l_s = 48 mm: e — bead width; g — height; h — depth of penetration of base metal

range of frequencies f_{r1} = 560–750 Hz. This is well correlated with resonance frequency f_r = = 630 Hz, calculated using equation above-given.

The interresonance mode of oscillations leads to a smooth change in bead geometry. With increase in frequency the force effect of electrode metal drops on weld pool is increased. The depth of penetration and SBM due to it are increased logically.

The high-frequency pulsed movements of electrode have an effect also on the surfacing efficiency. Increase in frequency and amplitude promotes the decrease in thickness of liquid-metal layer at the EW end, increase both in heat transfer from arc to electrode and also in coefficient of electrode melting. Thus, at 3820 Hz frequency of the first overtone the coefficient of melting exceeds the initial value by more than 20 % (see the Table).

Conclusions

1. Applying the high-frequency mechanical pulsed effect on EW allows control the metal transfer process, sizes of deposited bead and efficiency of ASAS process.

2. Transverse mechanical oscillations of EW have the highest effect in the region of resonance frequencies of the first tone — on the geometric parameters of deposited bead, and of the second tone — on the efficiency of electrode melting.

3. ASAS of structural steels the mechanical pulsed effect on EW within ranges of frequencies of 600–4000 Hz allows 3 times decreasing the depth of penetration and SBM, and increasing the coefficient of electrode melting by 10–20 %.

1. (1974) *Technology of fusion electric welding of metals and alloys*. Ed. by B.E. Paton. Moscow: Mashinostroenie.
2. Najdenov, A.M. (1998) Calculation of electrode wire melting rate in mechanized methods of arc welding. *Svarochn. Proizvodstvo*, **6**, 10–14.
3. Tarasov, N.M. (1984) Energy calculation of electrode metal drop detachment under action of pulse of external electromagnetic field. *Avtomatich. Svarka*, **6**, 21–25.
4. Lebedev, V.A. (2008) Aspects of choice of electric arc and automatic welding equipment with pulsed feed of electrode wire. *Svarochn. Proizvodstvo*, **5**, 45–49.
5. Razmyshlyaev, A.D., Mironova, M.V. (2011) Efficiency of electrode wire melting in submerged arc surfacing under action of transversal magnetic field. *Visnyk Donbas. Derzh. Mashynobud. Akademii*, **1**, 142–147.
6. Lebedev, V.A., Kuzmin, I.S., Novgorodsky, V.G. et al. (2002) Control of mechanized CO_2 welding process using parameters of electrode metal transfer. *Svarochn. Proizvodstvo*, **5**, 6–14.
7. Alov, A.A., Vinogradov, V.S. (1958) Effect of electrode vibration on arc welding process and properties of welds. *Ibid*., **9**, 19–22.
8. Dragan, S.V., Simutenkov, I.V. (2011) Development of device for control of weld geometric parameters in automatic submerged arc surfacing. *Zbirnyk Nauk. Prats NUK*, **3**, 59–64.
9. (1970) *Physics and technique of power ultrasound*. Vol. 3: Physical principles of ultrasonic technology. Ed. by L.D. Rozenberg. Moscow: Nauka.
10. (1970) *Physics and technique of power ultrasound*. Vol. 1: Supplies of power ultrasound. Ed. by L.D. Rozenberg. Moscow: Nauka.

Received 04.02.2013

WELDS FORMATION IN EBW OF HEAT-RESISTANT STEELS OF THE GRADES 10Kh9MFBA AND 10Kh12M

V.M. NESTERENKOV, L.A. KRAVCHUK, Yu.A. ARKHANGELSKY and **A.A. BONDAREV**
E.O. Paton Electric Welding Institute, NASU
11 Bozhenko Str., 03680, Kiev, Ukraine. E-mail: office@paton.kiev.ua

The influence of both the conditions of electron beam welding of heat-resistant steels 10Kh12M and 10Kh9MFBA 30 mm thick without preheating and also the spatial arrangement of electron beam relatively to the part being welded on weld formation and tendency to crack formation was investigated. It was established that in EBW of the mentioned heat-resistant steels without preheating the elimination of cracks and elongated cavities is achieved at the speed of welding of not more than 3 mm/s. The reproducibility of quality welds and formation of narrow and deep welds with parallel walls of cast zone is possible by application of technological scanning of electron beam around the circle and elliptic trajectory, and also arrangement of electron beam focus at the level of 2/3 of the specimen thickness. In the development of EBW technology of heat-resistant steels the non-destructive method of ultrasonic testing can be recommended for application. 6 Ref., 1 Table, 6 Figures.

Keywords: *electron beam welding, heat-resistant steels, electron beam, welding scheme, energy input, welding speed, focusing, defects, middle cracks, face and reverse weld beads*

In manufacture of such critical assemblies in machine building as bodies of drums, steam lines, diaphragms, rotors, discs, turbine blades and other high-loaded parts the heat-resistant steels of martensite-ferrite class are widely applied. Relating to the category of steels with a limited weldability, they require obligatory preheating in arc welding as they are susceptible to partial hardening with formation of martensite structures and cracks, and postweld tempering. These steels obtain the optimal properties as a result of double heat treatment by normalization + tempering or hardening + tempering, and are usually supplied for welding after final heat treatment.

EBW, the thermal cycle of which is featured by high rates of heating and cooling due to low value of energy input and also metal short-time duration at high temperatures, begins to occupy strong positions in power machine building. As compared to the arc welding, in ESW the sizes of near-weld zone and HAZ are decreased and also development of structure changes and deformations is delayed, which allows improving the mechanical characteristics of welded joints. The use of vacuum in EBW perfectly protects the molten metal from interaction with environment, which facilitates the improvement of quality of welded joints.

In this work the influence of conditions of EBW of heat-resistant steels of the grades 10Kh12M and 10Kh9MFBA of thickness $\delta = 30$ mm without preheating and also spatial location of electron beam relatively to the part being welded on welds formation and their tendency to cracks formation was investigated. It should be noted that investigated steels (Table) were supplied for welding under different heat conditions to obtain moderate levels of strength of base metal:

- 10Kh9MFBA alloy was subjected to the procedure of normalization + tempering: at normalization the specimens were heated to 1040–1095 °C, then the holding for 72 min and air cooling were followed; in tempering the specimens were heated to 770±10 °C, then the holding for 72 min and air cooling were followed;
- 10Kh12M alloy was subjected to the procedure of hardening + tempering: in hardening the specimens were heated to 1050 °C with subsequent cooing in oil; in tempering the specimens were heated to 720 °C with subsequent air cooling.

The welding of specimens was performed in the installation UL-209M with the power unit ELA-60/30 composed of EB gun with metal cathode and short-focus optics with electron beam current I_b = 0–500 mA. The tendency to cracks formation was determined on 200 × 100 mm size butt specimens of $\delta = 30$ mm. The control of electrode beam focusing on the surface of specimen was carried out according to the sharpness of image on the monitor of RASTR monitoring system [1], and at the same time according to the brightness of illumination of cir-

Chemical compositions of investigated heat-resistant steels, wt.%*

Grade of steel	C	Si	Mn	Cr	Mo	V	Nb	Cu	Ni	Other
10Kh9MFBA	0.07–0.13	0.15–0.55	0.27–0.63	7.9–9.6	0.8–1.1	0.16–0.27	0.05–0.11	≤ 0.25	≤ 0.43	S ≤ 0.01 P ≤ 0.02
10Kh12M	0.10–0.15	≤ 0.50	≤0.60	11.5–13.0	0.3–0.6	–	–	≤ 0.30	0.30–0.60	S ≤ 0.03 P ≤ 0.03

*Additional investigations on spectral analysis revealed gases in 10Kh9MFBA alloy: $[O_2] \le 0.0037$, $[N_2] \le 0.0386$, $[H_2] \le 0.0009$; in 10Kh12M alloy: $[O_2] \le 0.0033$, $[N_2] \le 0.0310$, $[H_2] \le 0.0008$ wt.%.

cular beam scanning of d_{circ} = 5 mm with $I_b \cong$ $\cong$ 10 mA on the copper massive plate. The narrow deep welds with parallel walls of cast zone were produced by deepening of electron beam focus inside the specimen, and also beam scanning around the circle or ellipsis, which provided the $\le 5\cdot 10^{-2}$ rad convergence angle of beam at the working distance from lower end of gun to the specimen l_{work} = 200–250 mm [2, 3]. The presence of defects of welded joint formation was detected by non-destructive method of ultrasonic testing and further metallographic examinations. To eliminate the residual magnetization, all the specimens of investigated heat-resistant steels were subjected to additional demagnetization on a special stand and supplied for welding with the magnetization level of not more than 0.5 Gs.

At first, to produce the guaranteed weld formation on the investigated heat-resistant steels of δ = 30 mm, the through penetrations along the solid metal according to the scheme in flat position (vertical electron beam) at movement of EB gun along the coordinates X–X or Y–Y were performed. As a result, during change of beam current I_b in a wide range, focusing current I_f and welding speed v_w the defect-free weld could not be formed as far as on the face bead the non-regular depressions and undercuts of weld and wavy non-regular sagging of weld metal on reverse bead were formed.

To eliminate the defects of weld formation at through penetration of specimens of δ = 30 mm according to the scheme in flat position, the technological backing 8 mm thick from material to b welded was applied. The I_b value was selected so that in welding process the single spot penetrations (peens) could be made. As the results of through penetrations showed, in welding with technological backing the face bead is formed regularly without depressions and undercuts on the both investigated steels.

Tendency of steels 10Kh12M and 10Kh9MFBA to cracks formation was investigated after a number of through penetrations on solid metal of δ = 30 mm made according to the scheme in flat position with technological backing at v_w = 3, 6, 9 and 12 mm/s. The mode of penetration of specimens for both investigated steels at each selected speed of weldiand was not changed. The focusing current was preset so that electron beam focus was positioned below the surface of specimen at the level of 2/3 of thickness of specimen; for this case the value of partial focusing of electron beam from the value of focusing current on the surface of specimen corresponds to $-\Delta I_f$ = 15 mA. At l_{work} = 200 mm the technological electron beam scanning around circle of f_r = 500 Hz frequency amounted to d_{circ} = = 1.5 mm.

Ultrasonic testing and metallographic examinations of welded joints on the specimens of δ = = 30 mm showed that steel 10Kh12M has no tendency to cracks formation at v_w = 3–6 mm/s; only at v_w = 9 and 12 mm/s the macrodefect in the form of a middle crack of about 3 mm length and 0.05 mm width was detected approximately at the half of penetration depth. As is seen from Figure 1, with increase in speed of welding the weld configuration is changed: the width of face bead decreases, transverse section from conical one is approaching the cylindrical one. The face bead is formed at all speeds with reinforcement, undercuts on the edges of weld are absent. The detected middle crack of the sizes mentioned above was detected using ultrasonic testing.

Unlike steel 10Kh12M, in EBW of specimens of steel 10Kh9MFBA of δ = 30 mm the quite different results on tendency to cracks formation according to the scheme in flat position with technological backing were obtained. As metallographic examinations of welded joints showed, the cracks are absent at v_w = 3 mm/s (Figure 2, *a*); at v_w = 6, 9 and 12 mm/s the defects as middle cracks are detected, propagating in vertical direction along the weld axis from reinforcement to the root (Figure 2, *b–d*). The geometric sizes of middle cracks in upper and root part of a weld are practically similar to the defects on steel 10Kh12M.

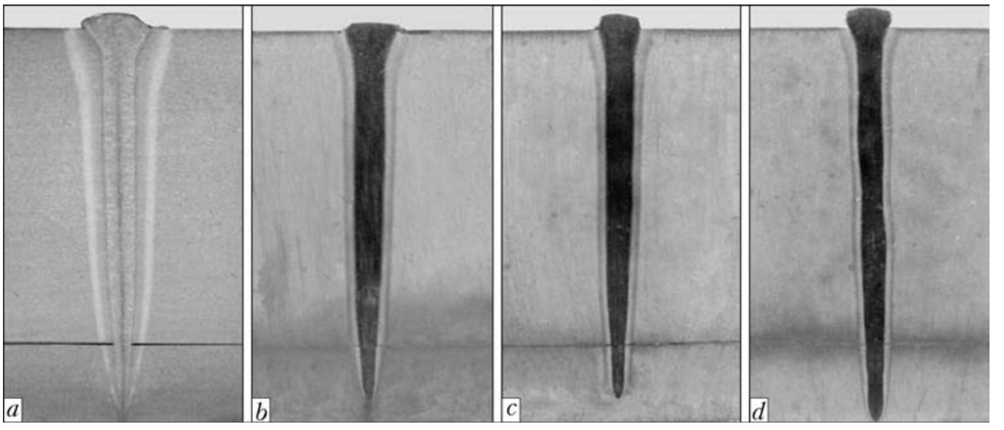

Figure 1. Macrostructure (×1.5) of welded joints on 10Kh12M alloy of δ = 30 mm in flat position at U_{acc} = 60 kV, I_f = = 630 mA, $-\Delta I_f$ = 15 mA, d_{circ} = 1.5 mm, l_{work} = 200 mm: *a* — v_w = 3 mm/s, I_b = 128 mA; *b* — v_w = 6 mm/s, I_b = = 184 mA; *c* — v_w = 9 mm/s, I_b = 236 mA; *d* — v_w = 12 mm/s, I_b = 310 mA

Thus, basing on the obtained results of through penetration of specimens of δ = 30 mm it can be concluded that with increase of welding speed the tendency to cracks formation on the investigated steels 10Kh9MFBA and 10Kh12M is increased, and this proves, in its turn, the fact that with increase of welding speed the increase of both welding stresses and also rate of growing of inner strains in welding occur. In other words, with increase of welding speed the quicker solidification of weld metal occurs, which leads to a higher rate of deformations growing [4, 5]. Therefore, the welding speed of not more than 3 mm/s can be more rational to be recommended for practical use of steels 10Kh12M and 10Kh9MFBA 30 mm thick in EBW.

According to the results of through penetrations of the specimens of heat-resistant steels 10Kh12M and 10Kh9MFBA 30 mm thick according to the scheme in flat position with technological backing (see Figures 1 and 2) the dependencies of energy input in EBW and width of face bead on the speed of welding were plotted. As is shown in Figure 3, with increase of welding speed in the range 3–12 mm/s the values of energy input q/v and width of face weld bead B are decreased in non-linear way according to hyperbolic law $(1/v_w)^{1/3}$: q/v = 2.56 kJ/mm and B = 5.8 mm at v_w = 3 mm/s up to q/v = = 1.55 kJ/mm and B = 3.5 mm at v_w = 12 mm/s, i.e. by 1.66 times. At v_w = 6 mm/s the value of energy input amounted to 1.84 kJ/mm and width of face weld bead B = 4.5 mm.

One can refuse from technological backings, having provided defect-free weld formation with through penetration, by transition to the scheme of EBW using horizontal electron beam and movement of EB gun in horizontal plane along the coordinate X–X or Y–Y. This method turned to be the most reliable and efficient, allowing elimination of root defects, reducing the angular deformations to minimum, decreasing the probability of pores formation and longitudinal cavities due to improvement of conditions of degassing of weld pool metal.

The first through penetrations of the specimens of steels 10Kh12M and 10Kh9MFBA of δ = = 30 mm using horizontal electron beam showed

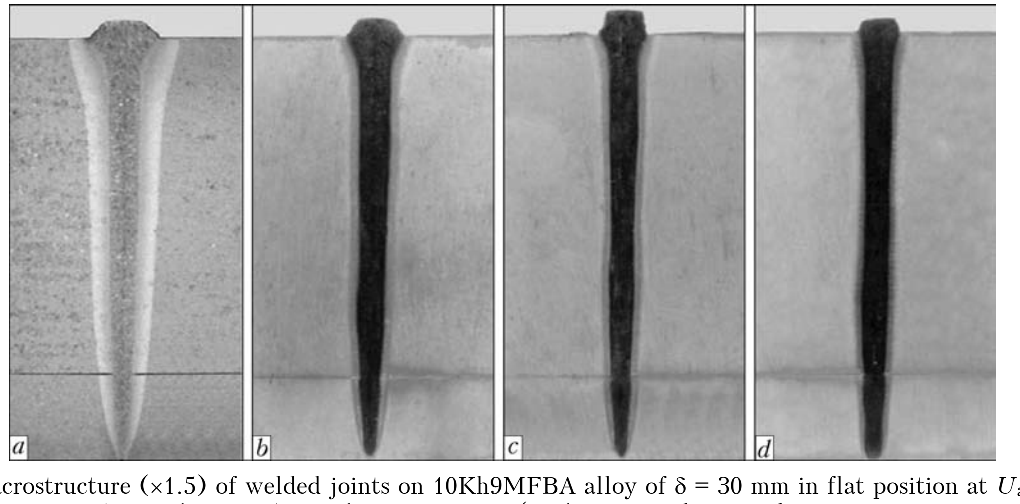

Figure 2. Macrostructure (×1.5) of welded joints on 10Kh9MFBA alloy of δ = 30 mm in flat position at U_{acc} = 60 kV, I_f = 630 mA, $-\Delta I_f$ = 15 mA, d_{circ} = 1.5 mm, l_{work} = 200 mm (*a*–*d* — v_w and I_b are the same as in Figure 1)

that direction of gravity force of liquid metal of weld pool has no considerable influence on selection of electron beam power, as compared to the similar welding conditions in flat position. In this connection and considering the recommendations [6], the through penetrations of specimens of investigated heat-resistant steels 30 mm thick with guaranteed face and reverse bead formation at different positions of electron beam focus relatively to the surface of specimen were carried out. As is shown in Figures 4 and 5, the face and reverse beads on the both steels are formed stably and regularly without depressions and flowing out of weld metal in the whole range of partial focusing $-\Delta I_f$ = 13–25 mA (electron beam focus is deepened inside the specimen), undercuts and visible defects are not observed. It should be noted that in welding of steel 10Kh12M the intensive spattering of weld metal from the face side occurs, unlike that of steel 10Kh9MFBA where EBW process is running much more smoothly.

According to the results of through penetrations of specimens of steels 10Kh12M and 10Kh9MFBA of δ = 30 mm using horizontal electron beam and basing on the analysis of transverse

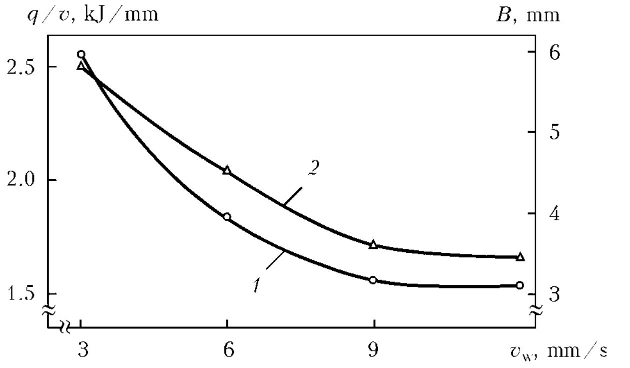

Figure 3. Dependence of energy input (*1*) and width of face weld bead (*2*) on speed of welding of steels 10Kh12M and 10Kh9MFBA of δ = 30 mm in flat position at U_{acc} = 60 kV, $-\Delta I_f$ = 15 mA, d_{circ} = 1.5 mm and l_{work} = 200 mm

macrosections of welded joints given in Figures 4 and 5, the dependencies of width of face and reverse beads on deepening of electron beam focus inside the specimen at q/v = 1.98 kJ/mm were plotted. As is shown in Figure 6, the width of reverse weld bead b in the whole range $-\Delta I_f$ = = 13–25 mA remains practically constant and amounts to $b \cong 2$ mm, whereas width of face weld bead B with increase of deepening of electron beam focus inside the specimen is decreased in non-linear way: to $-\Delta I_f$ = 17 mA, where B is

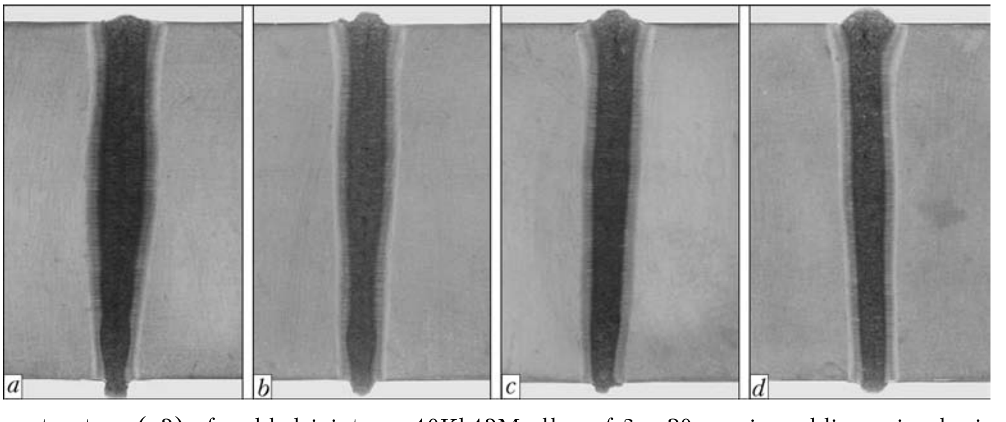

Figure 4. Macrostructure (×2) of welded joints on 10Kh12M alloy of δ = 30 mm in welding using horizontal beam at U_{acc} = 60 kV, I_b = 198 mA, v_w = 6 mm/s, d_{circ} = 1.5 mm and l_{work} = 200 mm: *a–d* — respectively, $-\Delta I_f$ = 25, 21, 17 and 13 mA

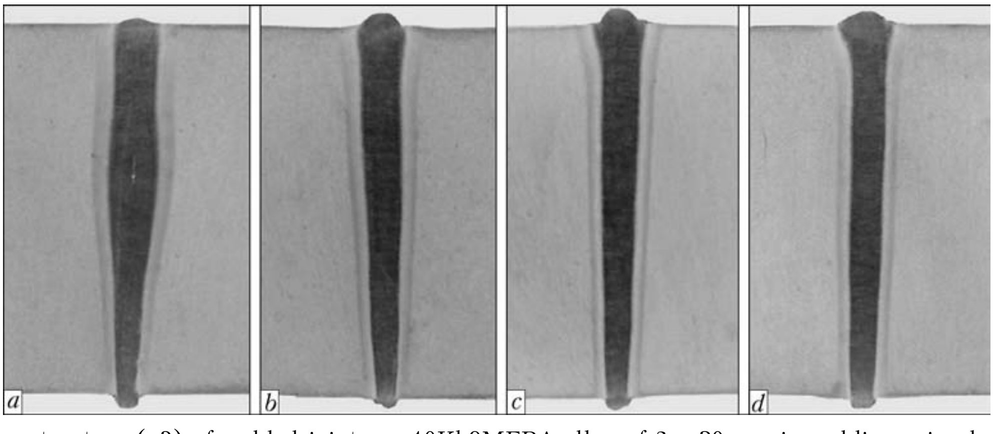

Figure 5. Macrostructure (×2) of welded joints on 10Kh9MFBA alloy of δ = 30 mm in welding using horizontal beam (U_{acc}, I_b, v_w, d_{circl}, l_{work} and *a–d* are the same as in Figure 4)

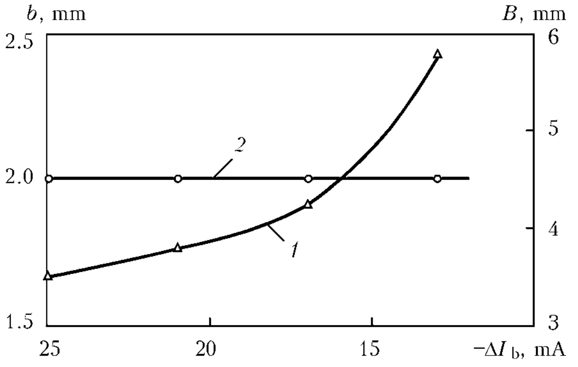

Figure 6. Dependence of width of face (*1*) and reverse (*2*) weld beads on deepening of electron beam focus in EBW of heat-resistant steels 10Kh12M and 10Kh9MFBA 30 mm thick using horizontal beam at U_{acc} = 60 kV, I_b = 198 mA, v_w = 6 mm/s, d_{circ} = 1.5 mm and l_{work} = 200 mm

sharply decreased, then to $-\Delta I_f$ = 25 mA, where the decrease of B parameter is delayed.

Metallographic examinations carried out on the welded joints of steels 10Kh12M and 10Kh9MFBA of δ = 30 mm after EBW using horizontal electron beam allowed establishing that position of electron beam focus relatively to the surface of specimen influences not only the shape of weld but also can result in cracks formation. As is shown in Figures 4, *a* and 5, *a*, at a large deepening of electron beam focus inside the specimen in the area of half of penetration depth on the both steels, the local widening of weld and middle cracks in them of up to 10 mm length are formed. With reduction of partial focusing current $-\Delta I_f$, local widening of weld is eliminated, and at $-\Delta I_f$ = 13–17 mA the weld shape from conical one is approaching the cylindrical one.

Conclusions

1. Welds formation with through penetration on heat-resistant steels 10Kh12M and 10Kh9MFBA of δ = 30 mm is achieved in transition to the scheme of EBW using horizontal electron beam and movement of EB gun in horizontal plane.

2. In EBW of these steels without preheating the elimination of cracks is achieved at the speed of welding of not more than 3 mm/s.

3. The application of technological scans of electron beam around the circular and elliptical trajectory and location of electron beam focus at the level of 2/3 of thickness of the specimen provides reproducibility of quality welds and also formation of narrow and deep welds with parallel walls of cast zone.

1. Nazarenko, O.K., Shapoval, V.I., Loskutov, G.A. et al. (1993) Observation of electron beam welding process and automatic seam tracking. *Avtomatich. Svarka*, **5**, 35–38.
2. Sayegh, G. (1986) *State of the art of high energy density beam welding*: Houdremont Lecture. Tokyo: IIW.
3. Fritz, D. (1988) Electron beam welding of today. In: *Proc. of 2nd Int. Conf. on Electron Beam Technologies* (Varna, 31 May–4 June 1988), 1048–1063.
4. Morochko, V.P., Sorokin, L.I., Zorin, N.Ya. (1975) Influence of electron beam welding mode on weld shape and properties of heat-resistant alloy welded joints 10–15 mm thick. *Svarochn. Proizvodstvo*, **6**, 32–36.
5. Shida, T., Kita, H., Okamura, H. et al. (1978) Effects of welding parameters and prevention of defects in deep penetration EBW of heavy section steel. *IIW Doc. IV-239–78*.
6. Petrenko, V.R., Olshansky, N.A., Lopatko, A.P. et al. (1985) Study of influence of beam focus deepening in titanium specimens on weld formation stability in EBW. In: *Proc. of 2nd All-Union Conf. on Current Problems of Welding of Non-Ferrous Metals*. Kiev: Naukova Dumka, 223–226.

Received 25.03.2013

WEAR RESISTANCE OF DEPOSITED METAL OF THE TYPE OF CARBON AND CHROMIUM-MANGANESE STEELS UNDER THE CONDITIONS OF DRY SLIDING FRICTION OF METAL OVER METAL

V.D. KUZNETSOV[1], **D.V. STEPANOV**[1], **V.A. MAKOVEJ**[1] and **Ya.P. CHERNYAK**[2]
[1]NTUU «Kiev Polytechnic Institute»
6/2 Dashavskaya Str., 03056, Kiev, Ukraine. E-mail: v.kuznetsov@kpi.ua
[2]E.O. Paton Electric Welding Institute, NASU
11 Bozhenko Str., 03680, Kiev, Ukraine. E-mail: office@paton, kiev.ua

Parts subjected to intensive wear are made from medium- and high-carbon unalloyed or low-alloyed structural steels. Increased carbon content ensures a high hardness and strength of materials. Because of low-alloying, however, their wear resistance is on a relatively low level. High carbon content considerably complicates the technology of reconditioning the above parts, because of the risk of cold cracking in arc surfacing. To recondition this type of parts it is rational to apply consumables producing deposited metal with the structure of metastable austenite. Such a structure can be produced at application of consumables alloyed by chromium and manganese for surfacing. Preliminary work hardening or work hardening directly during service leads to decomposition of metastable austenite and increase of hardness and wear resistance of the deposited metal. The objective of the work was investigation of wear resistance of deposited metal of chromium-manganese class under the conditions of dry sliding friction of metal over metal. Wear resistance of deposited metal of various alloying systems was studied. It is shown that the correlation between hardness and wear resistance is manifested not in all the cases, both for carbon and for austenitic materials. It is found that materials with the structure of metastable austenite are superior to carbon steels as to wear resistance and are preferable at reconditioning of parts from structural medium- and high-carbon steels. 6 Ref., 1 Table, 3 Figures.

Keywords: *arc surfacing, surfacing consumables, sliding friction, wear resistance, structure, hardness*

A considerable number of parts of machines and mechanisms, used in various industries, wears as a result of dry friction of metal over metal. Many of them are reconditioned by various surfacing processes [1–4].

Such parts are usually made from medium- and high-carbon unalloyed or low-alloyed structural steels. Increased carbon content ensures high hardness and strength of materials. However, because of low alloying their wear resistance is on a relatively low level. In addition, at more than 0.5 % C, technology of reconditioning the parts from above-mentioned steels by surfacing becomes much more complicated that is related to formation of quenching structures and cold cracking in the HAZ metal.

Cracking can be avoided through application of special technological measures, such as heating of the surfaced part up to 300–400 °C with subsequent delayed cooling after surfacing.

Application of consumables, providing deposited metal with austenitic structure, has a good effect in terms of crack resistance. However, wear resistance of deposited metal of this type under the conditions of dry sliding friction of metal over metal is on a low level, while the price of consumables for this type of surfacing is quite high and their application is not always cost-effective.

For reconditioning parts of this type, it is more rational to apply consumables, which provide deposited metal with the structure of metastable austenite. Such a structure can be obtained at application of surfacing consumables alloyed by chromium and manganese. Preliminary work hardening or in-service hardening lead to decomposition of metastable austenite, as well as increase of hardness and wear resistance of the deposited metal.

The objective of this work is investigation of wear resistance of the deposited metal with different content of chromium and manganese under the conditions of dry sliding friction of metal over metal. Composition of the studied types of deposited metal is given in the Table. Samples of

Composition of deposited metal, wt.%

Deposited metal type	C	Cr	Mn	Ni	Si	Mo	V	Ti	Cu
U7	0.70	–	0.89	–	0.25	–	–	–	–
30Kh5G5	0.27	4.5	5.0	–	0.20	–	–	–	–
10Kh10G10	0.11	11.0	10.0	–	–	–	–	0.8	–
60Kh20G9N2MD	0.62	20.8	9.0	2.0	0.55	0.5	–	–	0.17
20Kh13G6N6MFD	0.22	13.0	5.8	6.0	0.60	1.4	0.4	–	0.90
50G11M	0.50	0.2	11.0	–	0.80	0.3	–	–	–

deposited metal of the type of high-carbon steel U7 were used as a reference. For comparison, deposited metal alloyed practically by manganese alone was studied, alongside chromium-manganese deposited metal of various compositions.

Investigation of wear resistance of deposited metal was performed in friction machine of M-22 type in «shaft–block» configuration. Samples of 20 mm length and 10 mm thickness with a cylindrical slot in the form of a segment of 20 mm radius and 20 mm chord were used.

A disc of 40 mm diameter made from U7 steel with *HB* 300–350 hardness was used as a counterbody.

Testing conditions were as follows: pressure on the sample $p = 0.5 \pm 0.1$ MPa; friction speed $v = 3 \pm 0.25$ m/s; temperature $T = 60 \pm 20$ °C; duration $t = 1$ h.

Samples were weighed on laboratory scales with 0.0001 g error. Wear by weight Δm was determined as difference of values of sample weight before and after testing. Deposited metal hardness was also measured. Investigation results are given in Figure 1.

Deposited metal structure was identified by the results of metallographic analysis (Figure 2). Producing structures of specified type was ensured by selection of chemical composition of surfacing consumables and surfacing heat inputs.

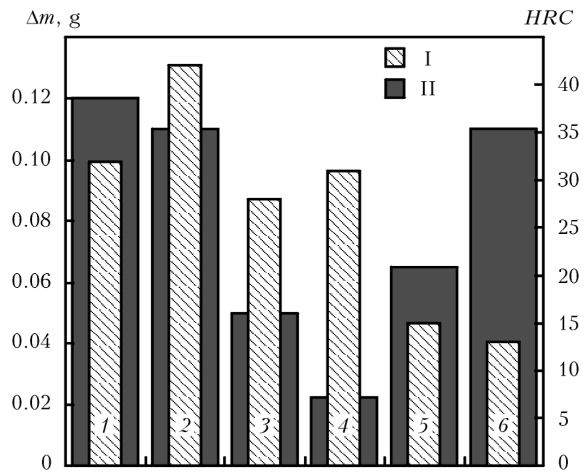

Figure 1. Wear by weight (I) and hardness (II) of deposited metal: *1* – U7; *2* – 30Kh5G5; *3* – 10Kh10G10; *4* – 60Kh20G9N2MD; *5* – 20Kh13G6N6MFD; *6* – 50G11M

Recommendations given in [5] were used in surfacing of austenitic materials.

Testing results showed (see Figure 1) the absence of a direct link between hardness and wear resistance of the studied types of deposited metal.

So, for instance, types of deposited metal U7, 30Kh5G5 and 50G11M have approximately the same wear parameters ($\Delta m = 0.11$–0.12 g), but differ considerably by hardness: 50G11M – *HB* 180; U7 – *HRC* 35; 30Kh5G5 – *HRC* 42. On the other hand, types of deposited metal 20Kh13G6N6MFD and 50G11M have approximately the same hardness – *HB* 150–180, but differ considerably as to wear – $\Delta m = 0.062$ and 0.115 g, respectively.

Deposited metal structure has apparently significant influence on wear resistance. High-alloyed 60Kh20G9N2MD deposited metal with austenitic-martensitic structure had minimum wear (see Figure 2, *d*) and sufficiently high hardness *HRC* 30. Deposited metal 10Kh10G10, as well as 20Kh13G6N6MFD and 50G11M, having metastable austenitic structure (Figure 2, *c*, *e*, *f*), had somewhat inferior wear resistance compared to it. It is obvious that the conditions of wear testing (at relatively small load) did not allow full realization of the possibility of work hardening of these materials. Nonetheless, wear resistance of deposited metal 10Kh10G10 and 20Kh13G6N6MFD is quite high and is much superior to that of hard materials U7 and 30Kh5G5.

From the studied materials having maximum wear resistance (10Kh10G10, 60Kh20G9N2MD, 20Kh13G6N6MFD) preference, in our opinion, should be given to the first of them, not containing any expensive alloying elements, and having sufficiently high wear resistance.

It should be noted that the obtained data are in good agreement with those of [6] as to investigation of wear resistance of steel U7 and deposited metal of ferritic and austenitic classes.

After wear resistance testing, fractograms of friction surfaces of deposited metal samples were studied (see Figure 3), and it was found that in 10Kh10G10 sample with the structure of metastable austenite (Figure 2, *c*) friction surface has uniform relief without any traces of spalling or characteristic furrowed structure (Figure 3, *a*).

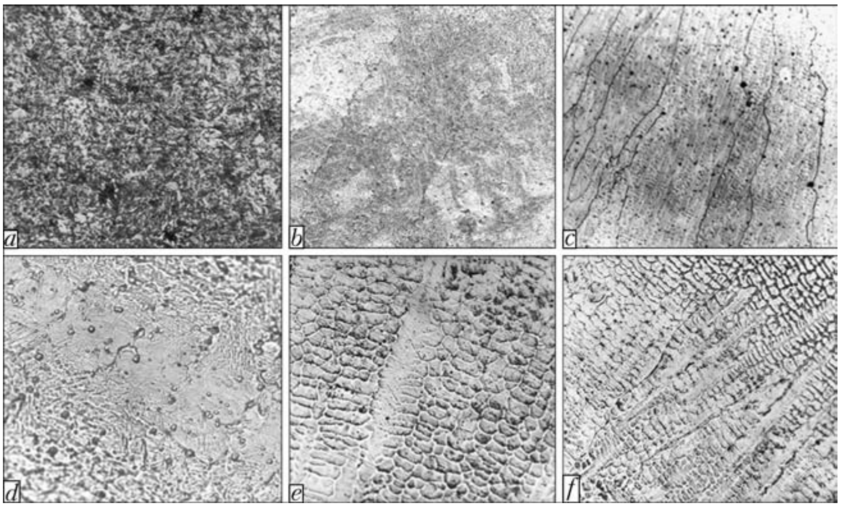

Figure 2. Microstructures (×500) of deposited metal: *a* — U7; *b* — 30Kh5G5; *c* — 10Kh10G10; *d* — 60Kh20G9N2MD; *e* — 20Kh13G6N6MFD; *f* — 50G11M

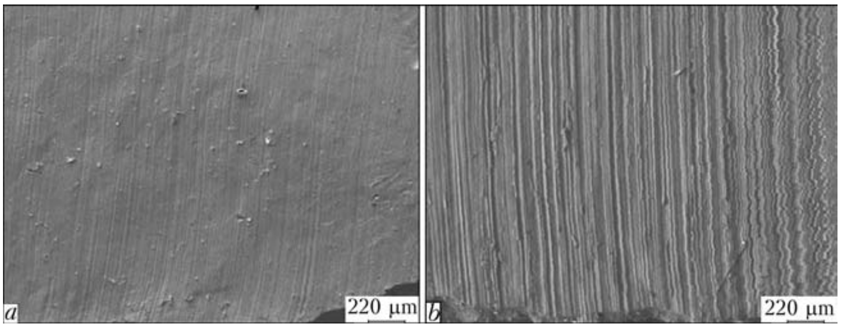

Figure 3. Fractograms of friction surfaces after wearing of deposited metal of the samples: *a* — 10Kh10G10; *b* — 30Kh5G5

In 30Kh5G5 sample with martensitic-sorbitic structure with residual austenite (see Figure 2, *b*), contrarily, the characteristic morphological feature of friction surface is the furrowed structure (Figure 3, *b*), which forms as a result of plastic driving of material from friction surface by wear product particles. Geometrical dimensions of the grooves change in a wide range that is indicative of structural inhomogeneity, and of different wear resistance of structural components of the considered type of deposited metal, respectively.

Conclusions

1. Wear resistance and microstructure of deposited metal of various types was studied. It is shown that the best wear resistance is found in deposited metal with the structure of metastable austenite. Preliminary work hardening or in-service work hardening with increased mechanical loads leads to decomposition of metastable austenite and increase of deposited metal hardness and wear resistance.

2. From the studied types of deposited metal of various alloying systems, deposited metal 10Kh10G10 has an optimum combination of properties.

1. Frumin, I.I. (1961) *Automatic electric arc surfacing*. Kharkov: Metallurgizdat.
2. Ryabtsev, I.A., Kondratiev, I.A. (1999) *Mechanized electric arc surfacing of metallurgical equipment parts*. Kiev: Ekotekhnologiya.
3. Ryabtsev, I.A. (2004) *Surfacing of machine and mechanism parts*. Kiev: Ekotekhnologiya.
4. Kuskov, Yu.M., Skorokhodov, V.N., Ryabtsev, I.A. et al. (2001) *Electroslag cladding*. Moscow: Nauka i Tekhnologiya.
5. Kalensky, V.K., Chernyak, Ya.P., Vasiliev, V.G. et al. (2001) Heat input influence on formation of tears in high-carbon steel building-up with austenitic wires. *The Paton Welding J.*, **11**, 9–12.
6. Chernyak, Ya.P. (2007) Comparative evaluation of wear resistance of electrode materials applied for reconditioning tram rails. *Ibid.*, **12**, 33–35.

Received 21.03.2013

DISTRIBUTION OF CHEMICAL ELEMENTS IN THE ZONE OF ALUMINIUM ALLOY AMg6 TO TITANIUM ALLOY VT6 JOINTS PRODUCED BY DIFFUSION WELDING IN VACUUM

Yu.V. FALCHENKO, E.V. POLOVETSKY and **L.M. KAPITANCHUK**
E.O. Paton Electric Welding Institute, NASU
11 Bozhenko Str., 03680, Kiev, Ukraine. E-mail: office@paton.kiev.ua

The possibility of a combined use of titanium and aluminium alloys in the form of permanent joints is of high interest to many industries. However, no investigations involving evaluation of the effect of the diffusion welding process on distribution of chemical elements and microstructure of the welded joints have been conducted so far. As revealed by the metallographic examinations carried out in this study, magnesium during the welding process diffuses from alloy AMg6 to the zone of joining with alloy VT6 and accumulates in the contact region. An interlayer of aluminium AD1 was used to eliminate the negative effect of magnesium. A gradual decrease in the concentration of magnesium from AMg6 to AD1 was observed in the joining zone when using the aluminium interlayer. A region of diffusion interaction, in which titanium and vanadium diffused from VT6 to AD1, was detected in the AD1 + VT6 joining zone. It can be concluded from the investigation results that in vacuum diffusion welding of titanium alloys to aluminium alloys containing magnesium the use of the interlayer of pure aluminium provides the sound welded joints with a gradual distribution of magnesium in the joint. The main role in formation of the titanium alloy to interlayer joint is played by the processes of diffusion of titanium and vanadium in a direction of the interlayer. 7 Ref., 3 Figures.

Keywords: *diffusion welding in vacuum, welded joint structure, distribution of chemical elements, diffusion, diffusion interaction zone*

The progress in modern machine building, aerospace, chemical and other engineering fields is related to the application of components made from aluminium and titanium alloys. Of the highest interest to designers is the possibility of the combined use of titanium and aluminium alloys in the form of permanent joints.

The problem of producing components from such materials can be solved by using vacuum diffusion welding (VDW) [1–3]. Analysis of literature data shows that no detailed investigations of the effect of distribution of chemical elements in the welded joint on its microstructure have been conducted up to now for this pair of alloys [4–6].

Welding of alloy AMg6 to alloy VT6 was performed both without interlayers and with an interlayer of aluminium AD1. Welding parameters were as follows: pressure P = 20 MPa, time t = 20 min, and welding temperature T = 540 °C. Investigations were conducted on the sections made from the investigated welded joints with their subsequent ion etching using the JEOL unit JFC-1100 (Japan) under the conditions specially selected and optimised for the investigated bimetal pairs. Investigations of distribution of chemical elements were carried out by using the JEOL Auger microanalyser JAMP 9500F equipped with the «Oxford Instruments» energy-dispersive X-ray spectrometer of the INCA system (Great Britain).

During welding the alloys are subjected to the thermal-deformation effect. This causes occurrence of the recrystallisation and diffusion processes in the joints, thus influencing the metal structure and properties.

As shown by the investigations, it is impossible to produce the welded joints between titanium alloy VT6 and aluminium alloy AMg6 by the VDW method using no technological approaches. Fracture of the resulting joints occurs directly in the joint.

According to the Mg–Ti equilibrium constitutional diagram [7], magnesium is insoluble in titanium. In the course of the welding process magnesium diffuses from AMg6 to the zone of joining with VT6, and accumulates there to form the 15–17 μm wide region with a content of up to 11 wt.% (Figure 1, *a*). Titanium at a content of up to 15 wt.% and vanadium of up to 1 wt.% were also detected in this region. The 3–4 μm deep zones with an increased content of oxygen (up to 9 wt.%) were revealed on the contact

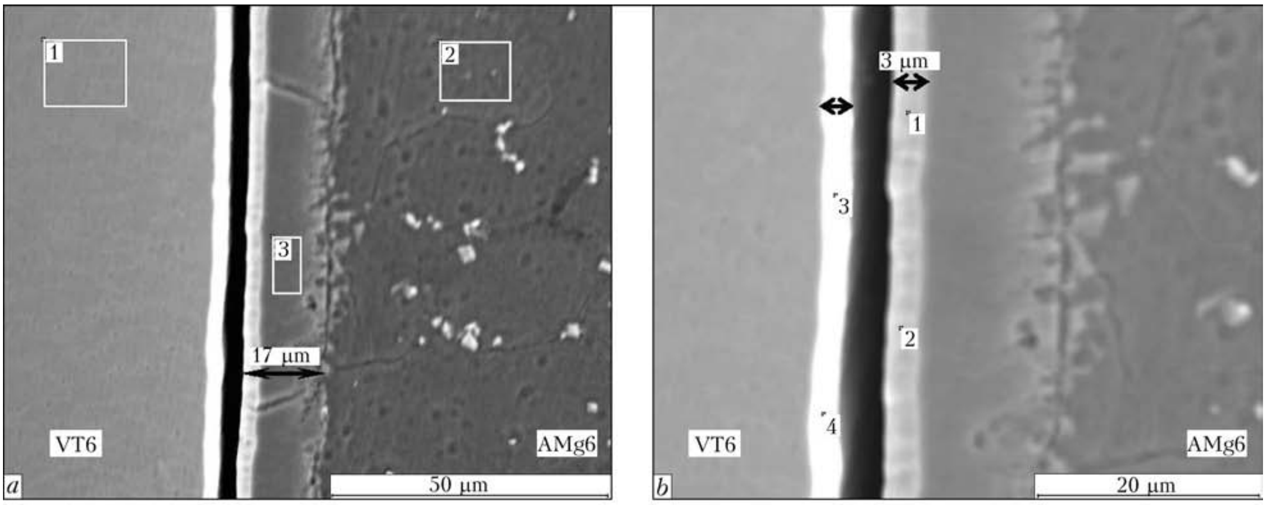

Spectrum	O	Mg	Al	Ti	V	Mn
1	0	0	6.63	89.58	3.80	0
2	2.21	5.23	91.70	0.18	0	0.66
3	0	10.63	73.19	14.81	0.94	0.43

Spectrum	O	Mg	Al	Ti	V
1	8.49	7.32	43.12	34.07	1.99
2	4.81	8.77	58.10	23.95	1.62
3	3.03	1.91	12.78	77.76	3.72
4	4.54	2.42	14.30	74.18	3.97

Figure 1. Microstructure and distribution of chemical elements in the AMg6 + VT6 welded joint produced by the VDW method without interlayers at t_w = 20 min, T_w = 540 °C, P_w = 20 MPa: *a* — in an area of the layer with increased content of magnesium, and in the base metals; *b* — in layers at the near-contact surfaces

surfaces of both alloys. The zone on AMg6 contained also (wt.%) up to 30 Ti, up to 2 V and up to 9 Mg, while the zone on VT6 contained up to 4.5 Mg (Figure 1, *b*).

It is the formation of all these zones that prevents production of the welded joint. Therefore, the 150 µm thick interlayer of commercially pure aluminium AD1 was used to avoid the negative

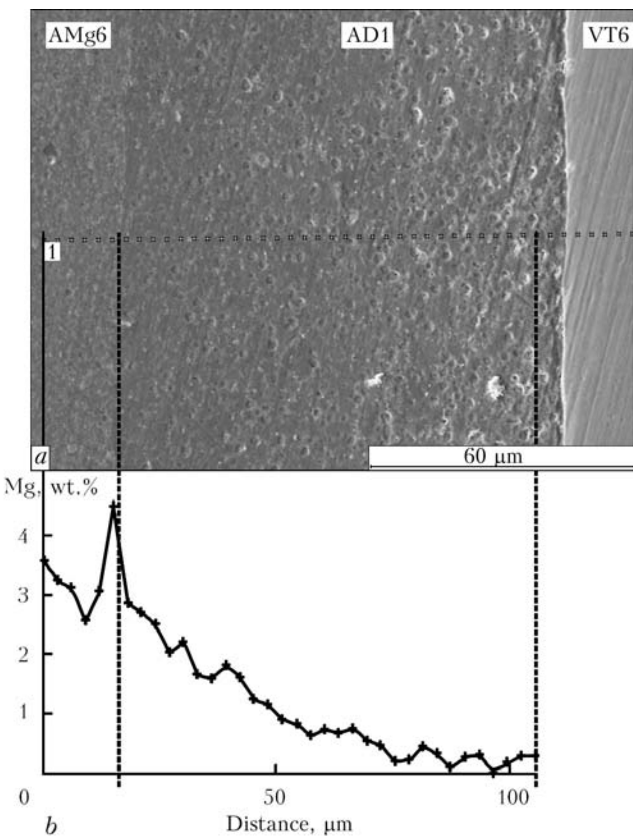

Figure 2. Microstructure of the AMg6 + AD1 + VT6 joint (*a*), and distribution of magnesium in the AMg6 + AD1 joining zone (*b*)

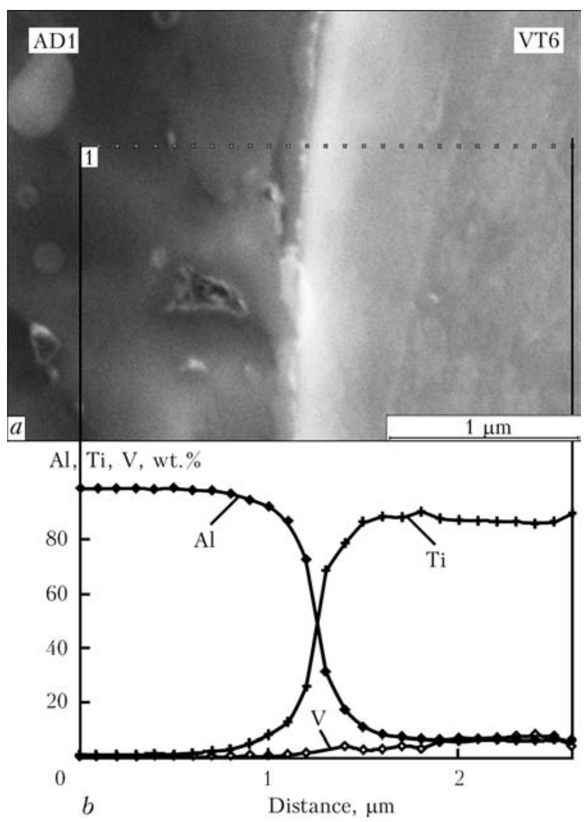

Figure 3. Microstructure of the region of contact of titanium alloy with the interlayer (*a*), and distribution of the concentration of titanium, vanadium and aluminium along the normal to the AD1 + VT6 joining line (*b*)

effect of alloying elements of alloy AMg6. The main goal of the interlayer is to block diffusion of magnesium as the most active chemical element. The thickness of the interlayer, i.e. 150 μm, was chosen in accordance with the literature data and our earlier experimental studies.

Analysis of the welded joints produced by the VDW method using the AD1 interlayer showed that during the welding process magnesium diffused from AMg6 to AD1 to a depth of 60–65 μm. In this case no accumulation of magnesium near the AD1 + VT6 joining zone was fixed (Figure 2). A region with the decreased magnesium content, down to 150 μm deep, formed in the near-contact zone of AMg6. The 1.5–2.0 μm wide region of diffusion interaction was detected in the AD1 + VT6 joining zone (Figure 3). Titanium and vanadium in this zone diffused from VT6 to AD1 to a depth of 0.5–0.8 μm, and aluminium — to VT6. In our opinion, formation of the detected region of diffusion interaction is the main condition for producing the sound welded joint.

Conclusions

1. It was established that diffusion welding of AMg6 to VT6 alloys using no aluminium interlayer fails to provide the welded joints due to the negative effect of magnesium.

2. Application of the aluminium interlayer leads to formation of two diffusion zones in the joint: AMg6 + AD1 and AD1 + VT6.

3. In the joining zone adjoining alloy AMg6, magnesium during the welding process diffuses in a direction to the AD1 interlayer. The zone with a decreased magnesium content forms in this case in aluminium alloy AMg6.

4. Diffusion of vanadium and titanium in a direction of the AD1 interlayer is observed in the joining zone adjoining alloy VT6.

1. Karakozov, E.S. (1976) *Joining of metals in solid phase*. Moscow: Metallurgiya.
2. Kazakov, N.F. (1976) *Diffusion welding of metals*. Moscow: Mashinostroenie.
3. Rabkin, D.M., Ryabov, V.R., Gurevich, S.M. (1976) *Welding of dissimilar metals*. Kiev: Tekhnika.
4. (1996) *Constitutional diagrams of binary metal systems*: Refer. Book. Vol. 1. Ed. by P. Lyakishev. Moscow: Mashinostroenie.
5. Grigorievsky, V.I. (1991) Diffusion welding of aluminium alloy AMg6 to titanium alloy OT4 through a composite titanium–aluminium interlayer. *Svarochn. Proizvodstvo*, **8**, 2–4.
6. Toshio, E., Kenji, I., Toshiharu, M. (1978) Influence of intermediate inserts on properties of diffusion welded Al–Ti joints. *J. JILM*, 16(**3**), 107–114, 127.
7. Akiomi, K., Akihika, Y., Tashihiro, Y. et al. (1985) Diffusion welding of Ti–6Al–4V alloy with intermediate aluminium insert. *J. JWS*, 3(**1**), 145–151.

Received 07.05.2013